Aberrant CDK1 Activity in S Phase Induces Chromosomal Instability by Increasing Mitotic Microtubule Polymerisation Rates in Colorectal Cancer Cells

Dissertation

for the award of the degree
“Doctor rerum naturalium”
of the Georg-August-Universität Göttingen

within the doctoral program “Molecular Medicine”
of the Georg-August University School of Science (GAUSS)

submitted by
Ann-Kathrin Schmidt

from Fulda, Germany

Göttingen, January 2021

Members of the Thesis Committee

Prof. Dr. Holger Bastians
Institute for Molecular Oncology
Section of Cellular Oncology
University Medical Center Göttingen

Dr. Ruth Geiss-Friedlander
Institute of Molecular Medicine and Cell Research
Center of Biochemistry and Molecular Cell Research (ZBMZ)
Albert-Ludwigs-University Freiburg

Prof. Dr. Heidi Hahn
Institute of Human Genetics
Section for Molecular Developmental Genetics
University Medical Center Göttingen

Members of the Examination Board

Referee: Prof. Dr. Holger Bastians
Institute for Molecular Oncology
Section of Cellular Oncology
University Medical Center Göttingen

2nd Referee: Dr. Ruth Geiss-Friedlander
Institute of Molecular Medicine and Cell Research
Center of Biochemistry and Molecular Cell Research (ZBMZ)
Albert-Ludwigs-University Freiburg

Further Members of the Examination Board

Prof. Dr. Heidi Hahn
Institute of Human Genetics
Section for Molecular Developmental Genetics
University Medical Center Göttingen

Prof. Dr. Dieter Kube
Department of Haematology and Oncology
University Medical Center Göttingen

Prof. Dr. Peter Burfeind
Institute of Human Genetics
University Medical Center Göttingen

Prof. Dr. Sigrid Hoyer-Fender
Johann-Friedrich-Blumenbach Institute for Zoology and Anthropology
Department of Developmental Biology
Georg-August-University Göttingen

Date of Oral Examination

13.04.2021

AFFIDAVIT

Hereby I declare that my doctoral thesis entitled "Aberrant CDK1 Activity in S Phase Induces Chromosomal Instability by Increasing Mitotic Microtubule Polymerisation Rates in Colorectal Cancer Cells" has been written independently with no other sources and aids than quoted.

Göttingen, January 2021

Ann-Kathrin Schmidt

CONTENTS

LIST OF FIGURES

LIST OF TABLES

ABBREVIATIONS

+TIP	Microtubule plus-end tracking protein
And-1	Acidic nucleoplasmic DNA-binding protein 1
APC	Adenomatous polyposis coli protein
APC/C	Anaphase-promoting complex/cyclosome
ATM	Ataxia telangiectasia mutated
ATP	Adenosine triphosphate
ATR	ATM-Rad3-related
BRCA1	Breast cancer type 1 susceptibility protein
BSA	Bovine serum albumin
Bub3	Budding uninhibited by benzimidazole 3
BubR1	Bub-related 1
CAK	CDK activating kinase
CDC	Cell division cycle
CDK	Cyclin-dependent kinase
CDT1	Chromatin licensing and DNA replication factor 1
CENP-C	Centromere protein C
CEP72	Centrosomal protein 72
CFS	Common fragile site
CHK1/2	Checkpoint kinase 1/2
ch-TOG	Colonic and hepatic tumour overexpressed gene
CIN	Chromosomal instability
CKI	CDK inhibitor
CRC	Colorectal cancer
DDK	DBF4-dependent kinase
DME	Dimethylenastrone
DMSO	Dimethylsufoxide
DNA	Deoxyribonucleic acid
EB	End binding protein
EDTA	Ethylenediaminetetraacetic acid
EGTA	Ethyleneglycoltetraacetic acid
FBS	Fetal bovine serum
GDP	Guanosine diphosphate
GFP	Green fluorescent protein
GTP	Guanosine triphosphate
h	Hour(s)

HPV	Human papillomavirus
HRP	Horseradish peroxidase
Kif2B	Kinesin family member 2B
LUC	*LUCIFERASE*
mAb	Monoclonal antibody
Mad2	mitotic arrest deficient 2
MAP	Microtubule associated protein
MAPK	Mitogen-activated protein kinase
MAT1	Ménage à trois 1
MCAK	Mitotic centromere-associated kinesin
MCC	Mitotic checkpoint complex
MCM	Mini-chromosome maintenance
MDM2	Mouse double-minute 2
MIN/MSI	Microsatellite instability
Mps1	Monopolar spindle 1
MTOC	Microtubule-organising centre
OD	Oligomerisation domain
ORC	Origin recognition complex
pAb	Polyclonal antibody
PBS	Phosphate-buffered saline
PCM	Pericentriolar material
PCNA	Proliferating cell nuclear antigen
PI	Propidium iodide
PLK1	Polo-like kinase 1
PP1	Protein phosphatase 1
pRb	Retinoblastoma protein
Pro	Proline
RFC	Replication factor C
RIF1	Replication timing regulatory factor 1
RNA	Ribonucleic acid
RPA	Replication protein A
SAC	Spindle assembly checkpoint
SAM	Sterile alpha motif
S-CIN	Structural chromosomal instability
SD	standard deviation
SDS	Sodium dodecyl sulfate
SDS-PAGE	Sodium dodecyl sulfate polyacrylamide gel electrophoresis

Ser	Serine
shRNA	Small hairpin RNA
siRNA	Small interfering RNA
TAD	Transactivation domain
TBS	Tris-buffered saline
Thr	Threonine
TID	Transactivation inhibitory domain
TIPIN	TIMELESS interacting protein
Tris	Tris(hydroxymethyl)aminomethane
Tyr	Tyrosine
W-CIN	Whole chromosomal instability
γ-TuRC	γ-tubulin ring complex

ABSTRACT

Whole chromosomal instability (W-CIN), one of the major hallmarks of human cancer, is defined as the perpetual gain or loss of whole chromosomes during mitosis leading to the development of heterogeneous karyotypes. W-CIN is associated with tumourigenesis, tumour progression, therapy resistance, and poor prognosis. Therefore, it is of great interest to elucidate the molecular mechanisms underlying W-CIN in order to understand genome instability driven tumorigenesis and tumour progression.

Recently, our lab has shown that W-CIN is triggered by increased microtubule polymerisation rates during mitosis which promote the formation of lagging chromosomes in anaphase, a mitotic error frequently observed in cancer cells. The results presented in this study show that the concomitant loss of the transcription factors p53 and p73 increases mitotic microtubule polymerisation rates and, consequently, induces W-CIN. Reduced expression of *CDKN1A*, a target gene of p53 and p73 encoding for the CDK inhibitor $p21^{CIP1}$, causes the mitotic defects observed upon p53/p73 depletion. Importantly, increased CDK1 activity, which is the result of loss of the p73/p53-$p21^{CIP1}$ pathway, is responsible for the observed chromosome missegregation. Unexpectedly, increased microtubule polymerisation rates and W-CIN are the result of elevated CDK1 activity specifically during S phase and not during mitosis. This suggests that increased CDK1 activity might interfere with DNA replication which leads to subsequent mitotic chromosome missegregation. Accordingly, normal mitotic microtubule growth rates and chromosome segregation were restored by nucleoside supplementation or inhibition of CDC7, a kinase involved in the firing of DNA replication origins. These results indicate that replication stress and increased origin firing are indeed triggered by increased CDK1 activity. In line with this, inhibition of the kinase ATR, a negative regulator of CDK1 in S phase, also increases mitotic microtubule growth rates and the incidence of lagging chromosomes.

In summary, this study shows that loss of the p73/p53-$p21^{CIP1}$ tumour suppressor pathway in colorectal cancer cells causes abnormal microtubule polymerisation rates in mitosis and W-CIN by unleashing CDK1 activity during S phase of the cell cycle, which might trigger increased origin firing during DNA replication. Thus, the present study provides new insights into the mechanisms promoting the generation of chromosomal instability in human cancer cells.

1 INTRODUCTION

1.1 The eukaryotic cell cycle and its regulation

The cell cycle describes the recurring phases of growth and division in proliferating cells.

1.1.1 Cell cycle phases

The eukaryotic cell cycle can be divided into interphase and mitosis. The interphase consists of a first gap (G1) phase, the DNA synthesis (S) phase, and a second gap (G2) phase (Figure 1.1). During G1 phase, cells grow and prepare for the following S phase. In S phase, the centrosome, the major microtubule organising centre, duplicates and DNA replication takes place. Cells prepare for the upcoming cell division during G2 phase. During mitosis, the DNA is equally distributed to two emerging daughter cells. In the absence of growth stimuli, cells can remain in a quiescent state (G0). The cells in G0 are metabolically active and do not proliferate until they re-enter the cell cycle upon proliferative signalling (Cooper, 2000).

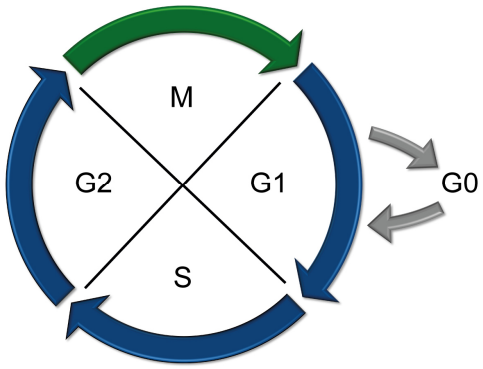

Figure 1.1: The eukaryotic cell cycle.
The eukaryotic cell cycle consists of interphase and mitosis (M). Interphase is divided into a first gap (G1) phase, the DNA synthesis (S) phase, and a second gap (G2) phase. Without proliferative signalling, cells can enter a quiescent state (G0).

Mitosis requires the activity of several kinases including cyclin-dependent kinase 1 (CDK1) in complex with the cyclins A and B, Aurora kinases A and B, and polo-like kinase 1 (PLK1) (Nigg, 2001). Mitosis is subdivided into several phases which are illustrated in Figure 1.2. During prophase, chromosome condensation starts and most of the cohesin protein complexes, which connect the two sister chromatids after DNA replication, are removed (Antonin and Neumann, 2016; Sumara *et al.*, 2000). Only at the centromere, cohesin complexes are still intact to prevent premature segregation of the sister chromatids (Waizenegger *et al.*, 2000). Moreover, the formation of the

mitotic spindle is initialised by the separation of the two centrosomes (Tanenbaum and Medema, 2010). In prometaphase, the kinetochores, the binding sites for microtubules, are assembled at the centromeric region of each sister chromatid. After the breakdown of the nuclear membrane, the highly dynamic microtubules emanating from the centrosomes gain access to the chromosomes (Cheeseman and Desai, 2008; Gascoigne and Cheeseman, 2011). Microtubules quickly polymerise and depolymerise until they are stabilised by attachment to a kinetochore, a process described as “search-and-capture” mechanism (Heald and Khodjakov, 2015; Kirschner and Mitchison, 1986).

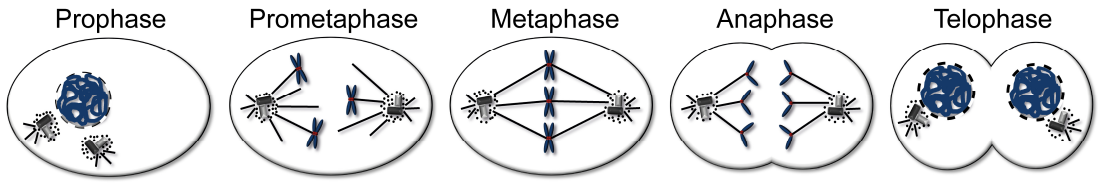

Figure 1.2: Mitosis can be divided into five different phases.
In prophase, chromosome condensation starts and centrosomes begin to separate to establish a bipolar mitotic spindle. After nuclear envelope breakdown, microtubules emanating from the two centrosomes attach to the kinetochores of the chromosomes (prometaphase). After correct alignment at the equator of the cell (metaphase), chromosomes are segregated (anaphase). In telophase, chromosomes decondense and nuclear envelopes are re-established.

In metaphase, all kinetochores are bound to microtubules from opposing spindle poles and are aligned at the equator of the cell (metaphase plate) which is required for symmetric cell division (Tan *et al*., 2015). After satisfaction of the spindle assembly checkpoint (SAC), the remaining centromere-bound cohesin complexes are cleaved and the chromatids are equally distributed to the two spindle poles during anaphase (Musacchio, 2015; Waizenegger *et al*., 2000). At first, sister chromatids are transported to the spindle poles because kinetochore-bound microtubules shorten (anaphase A) (Asbury, 2017). Afterwards, the two centrosomes move away from each other (anaphase B) (Scholey *et al*., 2016). Additionally, a contractile actomyosin ring is built at the cell equator perpendicular to the spindle axis beneath the plasma membrane (Cheffings *et al*., 2016; O’Shaughnessy and Thiyagarajan, 2018). In telophase, nuclear membranes assemble around the separated DNA to form new nuclei and chromosomes decondense (Antonin and Neumann, 2016). A cleavage furrow appears upon contraction of the actomyosin ring. The cytoplasm and cellular organelles of the parental cell are divided into two daughter cells during cytokinesis, which completes the cell cycle (Glotzer, 2005; Green *et al*., 2012).

1.1.2 Cell cycle regulation by CDK-cyclin complexes in mammals

The correct duplication of the DNA and its error-free distribution to the daughter cells is essential to maintain chromosomal stability in proliferating cells. Therefore, the cell cycle is strictly regulated. Important components of the regulatory machinery are cyclin-dependent kinases (CDKs), a family of Ser/Thr kinases, together with their cyclin subunits (Figure 1.3) (Malumbres and Barbacid, 2009). The expression of cyclins is cell cycle dependent, whereas the concentration of CDK hardly changes during the cell cycle. Mitogenic signals promote the expression of D-type cyclins which form complexes with CDK4 and CDK6 in G1 phase (Malumbres and Barbacid, 2005). CDK4/6-cyclin D phosphorylates pocket proteins, a protein family including Retinoblastoma protein (pRb), p107, and p130. Phosphorylated pocket proteins release and thus activate transcription factors of the E2F family, which results in the expression of E2F target genes, including *CCNE* (encoding for cyclin E) and genes encoding for factors of the replication machinery. CDK2 in complex with cyclin E promotes the transition from G1 to S phase. CDK2-cyclin E is also involved in the hyperphosphorylation of pocket proteins and, consequently, the transcription of further E2F responsive genes, like *CCNA* (encoding for cyclin A), is induced (Harbour *et al*., 1999; Lundberg and Weinberg, 1998; Malumbres and Barbacid, 2005).

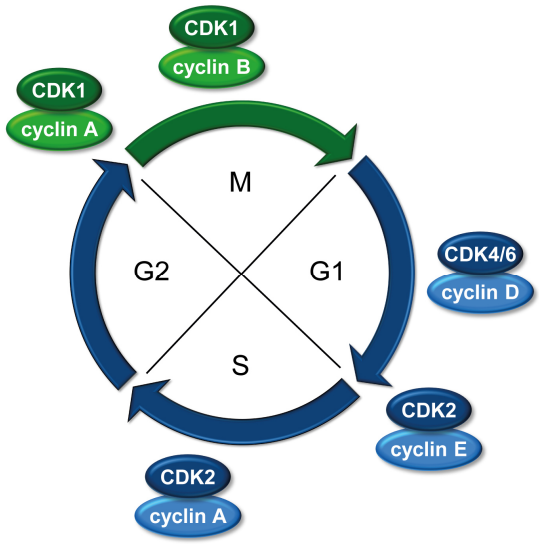

Figure 1.3: The cell cycle is regulated by CDK-cyclin complexes.
CDK4/6-cyclin D complexes are activated during G1 phase. CDK2 in complex with cyclin E promotes the transition from G1 to S phase. CDK2-cyclin A complexes ensure proper S phase progression. In late G2 phase, CDK1-cyclin A complexes are activated to promote G2/M transition and during mitosis, the activity of CDK1-cyclin B is necessary.

Subsequently, cyclin A forms a complex with CDK2 which is active throughout S phase and G2 phase. The activity of CDK1-cyclin A is required for the transition from G2 phase to mitosis. After nuclear envelope breakdown, cyclin A is degraded and

CDK1 in complex with cyclin B regulates further progression through mitosis (Vermeulen *et al*., 2003). The inactivation of CDK1 upon degradation of cyclin B and the activation of phosphatases which remove CDK1-mediated phosphorylations lead to mitotic exit (Musacchio, 2015; Queralt and Uhlmann, 2008).

CDKs are not only regulated by the complex formation with cyclin subunits, but also by various inhibitory and activating phosphorylations. For example, the CDK activating kinase (CAK), a complex consisting of ménage à trois 1 (MAT1), CDK7 and cyclin H, phosphorylates CDK1 at Thr161 (Fisher and Morgan, 1994; Tassan *et al*., 1995). However, this activating phosphorylation is counteracted by Myt1- and Wee1-mediated inhibitory phosphorylations at Thr14 and Tyr15, respectively (Booher *et al*., 1997; Heald *et al*., 1993). To fully activate CDK1, these inhibitory phosphorylations have to be removed by the phosphatase cell division cycle 25 (CDC25) (Millar *et al*., 1991; Strausfeld *et al*., 1991). Furthermore, CDK inhibitors (CKIs) can bind to CDKs or CDK-cyclin complexes. The INK family of CKIs includes $p16^{INK4a}$, $p15^{INK4b}$, $p18^{INK4c}$, and $p19^{INK4d}$ which bind to and inhibit CDK4 and CDK6 by preventing complex formation with D-type cyclins (Vermeulen *et al*., 2003). The Cip/Kip family of CKIs consists of $p21^{Cip1}$, $p27^{Kip1}$, and $p57^{Kip2}$ which limit the activity of CDK1 and CDK2 in complex with E-, A-, or B-type cyclins (Satyanarayana and Kaldis, 2009). Activating mutations, amplifications, or overexpression of CDKs and cyclin subunits or the loss of CKI activity have been described in various cancer entities which might contribute to the upregulated growth and cell cycle progression in cancer cells (Li *et al*., 2020; Malumbres and Barbacid, 2001; Nam and Van Deursen, 2014).

1.1.3 Cell cycle checkpoints

Several cell cycle checkpoints ensure the integrity of the DNA and the proper progression through the cell cycle. DNA damage checkpoints during G1, S, and G2 phase prevent cell cycle progression in the presence of DNA damage. DNA damage checkpoints are activated by the kinases ataxia telangiectasia mutated (ATM) and ATM-Rad3-related (ATR). ATM is recruited to DNA double strand breaks whereas ATR is recruited to single stranded DNA which occurs at impaired replication forks or after resection of double strand breaks. ATR and ATM phosphorylate and activate the checkpoint kinases CHK1 and CHK2, respectively. The subsequent signal transduction leads to cell cycle arrest and the activation of DNA repair mechanisms. Cells with severe DNA damage can be eliminated by induction of apoptosis (Shaltiel *et al*., 2015).

During mitosis, the spindle assembly checkpoint (SAC) ensures that the kinetochores of sister chromatids are properly bound by microtubules from opposing spindle poles before anaphase onset. When all kinetochores are correctly attached to microtubules, CDC20 can activate the anaphase-promoting complex/cyclosome (APC/C). APC/C has ubiquitin ligase activity and ubiquitinates securin. After ubiquitination, securin is degraded which leads to the activation of the protease separase. Separase can now cleave cohesin complexes which allows the separation of sister chromatids and, thus, the progression from metaphase to anaphase. Another target of APC/C is cyclin B. The ubiquitination and subsequent degradation of cyclin B leads to the inactivation of CDK1 and is required to complete and exit from mitosis (Musacchio, 2015). In the presence of unattached or incorrectly attached kinetochores, mitotic arrest deficient 2 (Mad2), budding uninhibited by benzimidazole 3 (Bub3), and Bub-related 1 (BubR1) form the mitotic checkpoint complex (MCC). For the recruitment and activation of MCC components, the activity of the kinase monopolar spindle 1 (Mps1) and several other factors are necessary. The MCC stops the activation of APC/C by sequestering CDC20. Consequently, cells cannot proceed to anaphase before all kinetochores are correctly bound by microtubules (Grieco and Serpico, 2020).

1.2 DNA replication and replication stress

The exact and complete replication of the genome during S phase of the cell cycle is essential for the maintenance of genomic integrity.

1.2.1 DNA replication

The “licensing” of origins of DNA replication constitutes the loading of the replicative helicase onto DNA (Figure 1.4a). It is the first step of DNA replication and takes place during G1 phase. Origins of DNA replication are recognised by the origin recognition complex (ORC). With the help of the ATPase cell division cycle 6 (CDC6) and chromatin licensing and DNA replication factor 1 (CDT1), two mini-chromosome maintenance (MCM) complexes are recruited. The MCM complex consists of the subunits MCM2-7 and is the major component of the replicative helicase (Bell and Kaguni, 2013). Origin firing describes the activation of licensed origins and requires the activity of CDKs and the DBF4-dependent kinase (DDK), a complex consisting of the kinase cell division cycle 7 (CDC7) and the regulatory subunit DBF4 (Figure 1.4b). Phosphorylation targets are for example members of the MCM and GINS complexes, cell division cycle 45 (CDC45), and DNA polymerases (Labib, 2010).

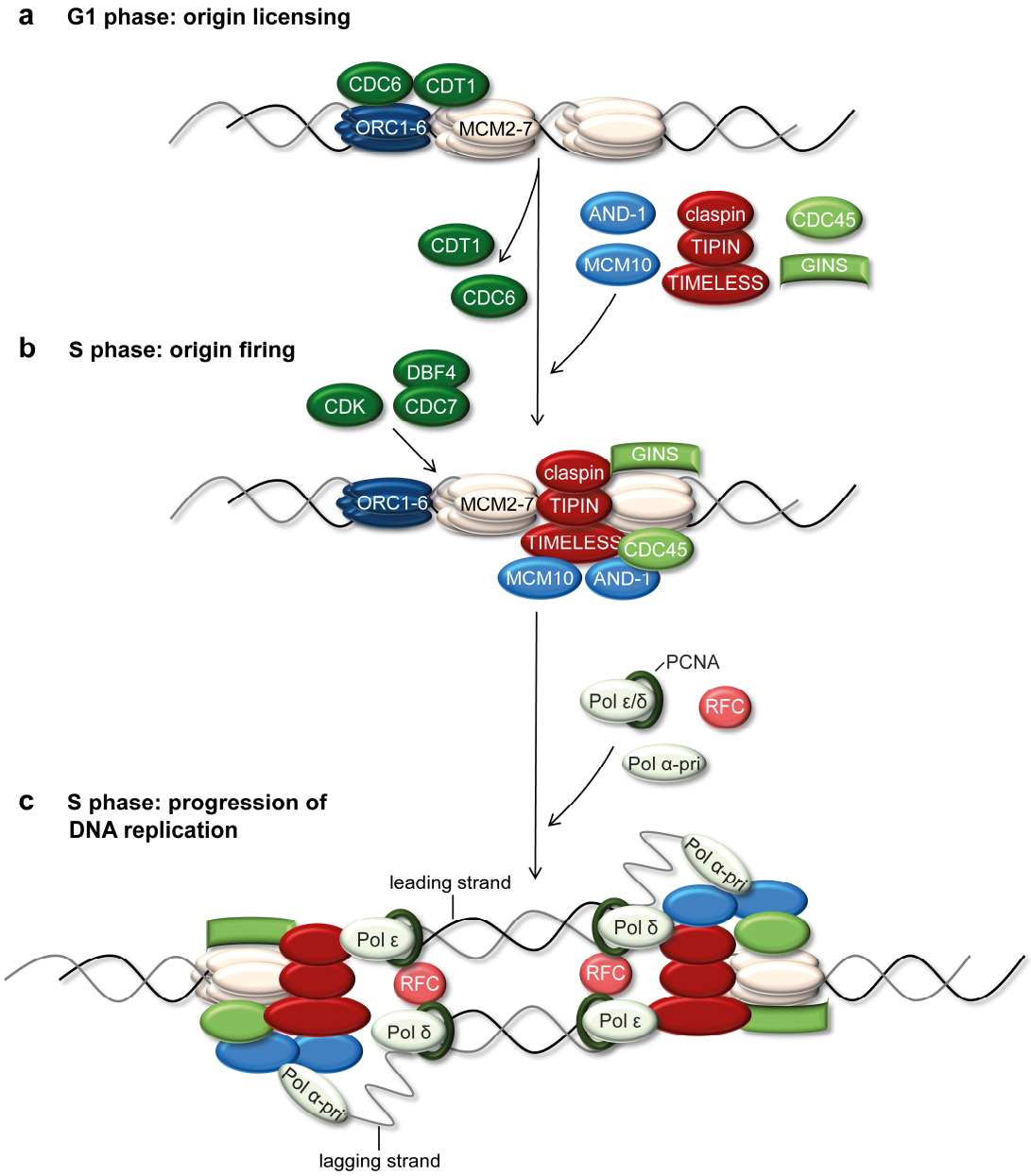

Figure 1.4: The initiation of eukaryotic DNA replication.
(a) In G1 phase, the ORC binds to origins of replication. With the help of CDC6 and CDT1, two MCM2-7 complexes are loaded onto the DNA. **(b)** Origin firing during S phase requires the activity of CDKs and DBF4-CDC7. The replicative helicase consisting of MCM2-7, GINS, and CDC45, is activated. Additional stabilising factors are recruited. **(c)** The replicative helicases unwind the double stranded DNA and move into opposite directions. RFC recruits PCNA, which serves as a scaffold for the DNA polymerases. The polymerase α-primase complex (Pol α-pri) initiates DNA synthesis and the polymerases ε and δ (Pol ε/δ) elongate the leading and lagging strand, respectively. Scheme adapted from Gaillard *et al.*, 2015.

The GINS complex and CDC45 are recruited to form the active CMG helicase together with MCM2-7 (Moyer *et al.*, 2006). Additional factors, like MCM10 and acidic nucleoplasmic DNA-binding protein 1 (And-1), are involved in the stable assembly of the helicase (Im *et al.*, 2009). The activation of the helicase complexes and their movement in opposite directions forms two sister replication forks. After unwinding

the DNA double strands, single stranded DNA is protected against degradation by binding of replication protein A (RPA). The polymerase α-primase complex starts DNA synthesis and the polymerases ε and δ perform elongation on the leading and lagging strand, respectively (Figure 1.4c) (Burgers and Kunkel, 2017). Proliferating cell nuclear antigen (PCNA) serves as a scaffold for the DNA polymerases and is loaded onto DNA strands by replication factor C (RFC) (O'Donnell and Kuriyan, 2006). Additionally, a protein complex consisting of TIMELESS, TIMELESS interacting protein (TIPIN), and claspin is involved in the coordination of DNA unwinding and DNA synthesis, stabilises replication forks, and supports checkpoint signalling (Leman and Noguchi, 2012).

The temporal separation of origin licensing in G1 phase and origin firing in S phase ensures that DNA replication takes place only once during the cell cycle (Siddiqui *et al*., 2013). It is of note that approximately $5x10^5$ origins are licensed in a human genome but only a small proportion (approximately 10 %) is sequentially activated during normal DNA replication in S phase (Moiseeva and Bakkenist, 2019). The so-called dormant origins are passively replicated by replisomes emerging from adjacent active origins and remain as a backup mechanism which allows the completion of DNA replication in case of replication stress (Ge *et al*., 2007; Woodward *et al*., 2006).

1.2.2 Causes of replication stress

Replication stress is defined as the impaired progression or stalling of replication forks which might even result in the collapse of the replication forks. Several causes of replication stress have been described so far. Exposure to chemical mutagens, ultraviolet light, or reactive oxygen species can cause DNA damage, for example thymidine dimers, which impairs replication fork progression. Furthermore, the interference of the replisome with the transcription machinery has been described as a cause for replication stress (Magdalou *et al*., 2014; Zeman and Cimprich, 2014). In addition, oncogene activation can interfere with normal DNA replication (Gaillard *et al*., 2015). For instance, nucleotide deficiency due to oncogene activation (for example *CCNE*, HPV-16 genes *E6*/*E7*) decelerates replication fork progression. In this case, replication stress and resulting DNA damage can be rescued by supplementation with nucleosides (Bester *et al*., 2011). Depletion of nucleotide pools and factors required for DNA synthesis was also observed after excessive origin firing as a consequence of overexpression or constitutive activation of oncogenes (for example *MYC*, *CCNE*) (Jones *et al*., 2013; Srinivasan *et al*., 2013). Additionally,

collisions with the replication machinery have been described under these circumstances jones (Jones *et al*., 2013).

1.2.3 Consequences of replication stress

At stalled replication forks, the uncoupling of DNA unwinding and DNA synthesis leads to the excessive formation of single stranded DNA which induces the replication stress response. Consequently, ATR, one of the central kinases mediating replication stress response, is activated (Byun *et al*., 2005; Nam and Cortez, 2011). ATR activates its downstream target CHK1 which phosphorylates and thus inhibits CDC25, a phosphatase essential for the activation of CDK2. The lack of CDK2 activity leads to cell cycle arrest. In addition, firing of late-replicating origins is inhibited to prevent the consumption of nucleotides and other replication factors. These global effects of ATR-CHK1-mediated signalling provide additional time to react to the cause of replication stress and resources are maintained to complete DNA synthesis in the proximity to stalled replisomes. Moreover, ATR-mediated signalling is required for the stabilisation of impaired replication forks and the induction of repair processes (Cimprich and Cortez, 2008). It is of note that the activation of dormant origins near stalled replication forks is not inhibited by ATR-CHK1 signalling (Ge and Blow, 2010). Thus, dormant origin firing contributes to the completion of DNA replication when global replication is slowed down (Ge *et al*., 2007; Woodward *et al*., 2006).

Importantly, very mild replication stress might not induce a replication stress response allowing cell cycle progression even in the presence of short stretches of under-replicated DNA. DNA damage and chromosomal rearrangements can occur if cells cannot finish DNA replication before the onset of mitosis (Gelot *et al*., 2015). This phenomenon is especially observed at so-called common fragile sites (CFSs). CFSs have a reduced number of licensed origins and often contain sequence motives which favour the formation of secondary structures impairing DNA replication. They frequently include large late-replicating genes which complicates the coordination of replication and transcription. These characteristics of CFSs explain their hypersensitivity to replication stress. The instability of CFSs upon replication stress is associated with cancer development and chromosomal instability (Debatisse and Rosselli, 2019).

1.2.4 ATR-CHK1 signalling in unperturbed cells

ATR-CHK1 signalling is one of the central signalling pathways in the replication stress response. Recently, Moiseeva *et al.* (2019) have proposed that low-level ATR-CHK1

signalling is also essential for the orderly replication in unperturbed cells. During unperturbed DNA replication, basal ATR-CHK1 signalling limits CDK1 activity. The result is a balanced activity of the kinase CDC7 and the phosphatase complex RIF1-PP1. CDC7 promotes origin firing by phosphorylation of components of the replicative helicase and can be counteracted by the phosphatase RIF1-PP1 (Figure 1.5a). It was shown that inhibition of ATR-CHK1 signalling leads to increased CDK1 activity. CDK1, in turn, phosphorylates RIF1, which promotes the dissociation of the phosphatase complex RIF1-PP1 and, thus, allows additional CDC7-mediated activation of dormant origins (Figure 1.5b) (Moiseeva *et al.*, 2019).

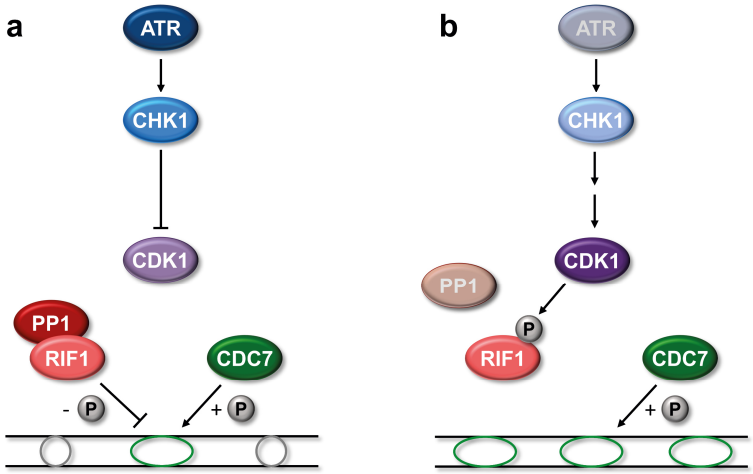

Figure 1.5: ATR inhibition induces dormant origin firing in a CDK1-dependent manner. **(a)** During unimpeded DNA replication, basal ATR-CHK1 signalling inhibits CDK1. The phosphatase complex RIF1-PP1 remains active and opposes the kinase CDC7, which is involved in origin firing. **(b)** Loss of ATR-CHK1 signalling results in increased activity of CDK1. CDK1 phosphorylates RIF1 which leads to the dissociation of the phosphatase complex RIF1-PP1. CDC7-mediated phosphorylation of the replicative helicase contributes to firing of dormant origins. Scheme based on Moiseeva *et al.*, 2019.

1.3 The transcription factors p53 and p73 and their target $p21^{CIP1}$

The gene *TP53* encodes for the transcription factor p53 which is also known as “guardian of the genome”. Cellular stresses like DNA damage lead to the stabilisation and activation of p53. p53 assembles to tetramers and activates the expression of genes involved in the induction of cell cycle arrest, DNA repair, and induction of apoptosis to protect genomic integrity (Levine and Oren, 2009). The transcription factor p53 contains several conserved domains, namely the transactivation domain (TAD) at its amino-terminus, a DNA binding domain (DBD), and a carboxy-terminal oligomerisation domain (OD) (Figure 1.6) (Levrero *et al.*, 2000). In addition to p53, the p53 family of transcription factors includes the homologues p63 and p73 which have

a similar domain structure (Figure 1.6) (Kaghad *et al*., 1997; Levrero *et al*., 2000; Yang *et al*., 1998).

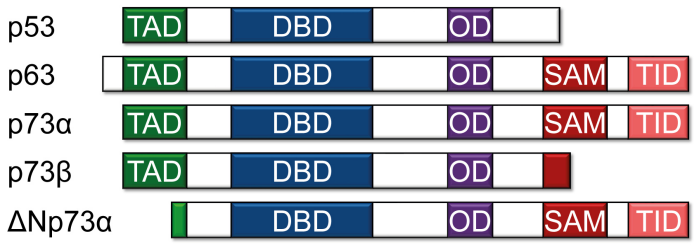

Figure 1.6: The homologous transcription factors p53, p63, and p73 share a similar domain structure.
The transcription factor p53 contains a transactivation domain (TAD), a DNA binding domain (DBD), and an oligomerisation domain (OD). The transcription factors p63 and p73 share these domains and contain an additional sterile alpha motif (SAM) and a transactivation inhibitory domain (TID). Activation of different promotors and alternative splicing sites allows the generation of various isoforms, for example p73α, p73β, or ΔNp73. N-terminally truncated isoforms like ΔNp73 can act as dominant-negative regulators of transcription factors with an intact TAD.

It has been shown that p63 and p73 can also activate the expression of p53-responsive genes, including genes relevant for cell cycle regulation (for example *CDKN1A*) or apoptosis (for example *BAX*) (Gressner *et al*., 2005; Guo *et al*., 2009; Jost *et al*., 1997; Zhu *et al*., 1998). Additionally, p63 and p73 have some functions which are not shared with p53. For example, p63 is crucial for craniofacial, limb, and skin development whereas p73 is important for neurogenesis (Yang *et al*., 1999, 2000). Various isoforms of the p53 family members can be generated by activation of different promotors or alternative splicing (Pflaum *et al*., 2014). Examples for p73 isoforms are given in Figure 1.6. Isoforms with a truncated amino-terminus (ΔN) were shown to antagonise the tumour suppressive function of isoforms with an intact TAD (Grob *et al*., 2001; Yang *et al*., 1998).

1.3.1 p53 and p73 in cancer

The most common alterations in cancer, which can be detected in approximately 50 % of human malignancies, are mutations of the gene *TP53* (Kandoth *et al*., 2013). Nonsense or frameshift mutations which lead to a loss of p53 have been described. Missense mutations which result in the generation of defective p53 protein are even more common. The presence of a single mutated p53 oligopeptide in a p53 tetramer is sufficient to impair its function. Several hotspot mutations have been identified in the DNA binding domain of p53 which can alter both its DNA binding ability and protein folding. Consequently, these mutations compromise the tumour suppressive function due to impaired activation of p53-responsive genes. Additionally, mutant p53 can act

as an oncogenic transcription factor. This gain of function can be mediated by direct binding to DNA sequences, which are not bound by wildtype p53, or by modulation of the activity of other transcription factors (Muller and Vousden, 2014).

In contrast to *TP53* mutations, *TP73* mutations are rarely described in cancer. However, *TP73* is located on the chromosome arm 1p36 which is frequently lost in various cancer entities, for example neuroblastoma and pancreatic adenocarcinoma (Kaghad *et al*., 1997; Loukopoulos *et al*., 2007). Additionally, the tumour suppressive function of both p53 and p73 can be inhibited by ΔNp73, a truncated variant of p73 (Figure 1.6). ΔNp73 is still able to bind to DNA and can either initiate gene transcription or suppress gene expression by blocking p53- or p73-responsive promotors. In addition, it has been suggested that ΔNp73 can form hetero-tetramers with p53 or p73 and, thus, inhibit their function (Bailey *et al*., 2011). However, hetero-tetramer formation of p53 and p73 isoforms could not be confirmed *in vitro* suggesting that competition for DNA binding is the main mechanism of action (Joerger *et al*., 2009). The expression of ΔNp73 has been documented for colorectal, lung, and breast cancer, among others, suggesting a tumour-promoting function (Di *et al*., 2013).

1.3.2 The cell cycle regulator p21^{CIP1} in cancer

The gene *CDKN1A* encodes for the cell cycle inhibitor p21^{CIP1} which induces cell cycle arrest in G1 and G2 phase by inhibiting CDK2 and CDK1 (Medema *et al*., 1998). Additionally, p21^{CIP1} can impair DNA replication by inhibiting PCNA (Luo *et al*., 1995). It is well established that the expression of *CDKN1A* can be induced by p53 and also by the homologous transcription factor p73 upon DNA damage (Jost *et al*., 1997; Kaghad *et al*., 1997). Therefore, p21^{CIP1} might be an important protein which mediates the tumour suppressive function of the transcription factors of the p53 family. A role of p21^{CIP1} in preserving chromosomal stability has also been described previously (Barboza *et al*., 2006; Shen *et al*., 2005). Actually, loss of *CDKN1A* and its gene product p21^{CIP1} leads to late onset tumours in mouse models (Martín-Caballero *et al*., 2001). A reduced expression of *CDKN1A* was described for several cancers, including colorectal cancer and non-small cell lung cancer (Kreis *et al*., 2019). In addition, loss of *CDKN1A* leads to several mitotic defects. Analyses in HCT116-*CDKN1A*$^{-/-}$ cells revealed prolonged mitosis and chromosome missegregation (Kreis *et al*., 2014). Together, these findings indicate that loss of p21^{CIP1}-mediated cell cycle regulation is associated with chromosomal instability and tumourigenesis. However,

overexpression in cancer and an oncogenic function of $p21^{CIP1}$ have also been described (Kreis *et al*., 2019).

1.4 Microtubules and mitotic spindle assembly

Actin filaments, intermediate filaments, and microtubules form the cytoskeleton. Microtubules are important for the cellular shape, are involved in cell migration, are essential for the transport of vesicles and the arrangement of organelles, and form the mitotic spindle (Hohmann and Dehghani, 2019).

1.4.1 Characteristics of microtubules

α- and β-tubulin subunits form dimers which associate to linear protofilaments and 13 protofilaments assemble to hollow cylindrical fibres, the microtubules. The αβ-tubulin dimers are all oriented in the same direction which leads to a defined polarity of the microtubules. The end exposing α-tubulin is referred to as minus-end, whereas the end exposing β-tubulin represents the plus-end (Figure 1.7). Microtubule growth is possible at both ends, but the growth rate is higher at the plus-end (Desai and Mitchison, 1997).

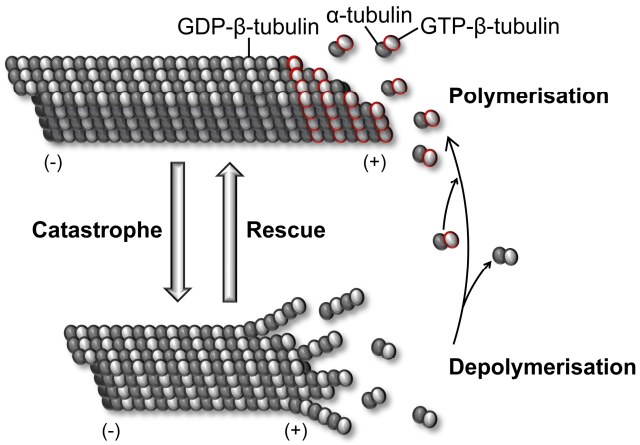

Figure 1.7: The dynamic instability of microtubules.
Microtubule polymerisation results from the incorporation of GTP-bound αβ-tubulin dimers at the plus-end. After GTP hydrolysis, the affinity to adjacent tubulin molecules decreases which leads to microtubule depolymerisation. The transition from polymerisation to depolymerisation is called catastrophe, whereas the switch from depolymerisation to polymerisation is called rescue.

Tubulin dimers have GTPase activity. After incorporation at the microtubule plus-end, the GTP bound to β-tubulin is hydrolysed to GDP which induces conformational changes and reduces the affinity to adjacent tubulin molecules. In growing microtubules, the incorporation of new αβ-tubulin dimers is faster than GTP hydrolysis, resulting in a “GTP-cap” which protects the αβ-tubulin dimers from rapid

dissociation (Dimitrov *et al*., 2008). In contrast, microtubules shrink if the GTP hydrolysis is faster than the recruitment of new αβ-tubulin dimers. The switch from growth to shrinkage of microtubules due to depolymerisation is called catastrophe, whereas the transition from shortening to growth is described as rescue (Figure 1.7). If dissociation and association of αβ-tubulin dimers are equal, the length of the microtubule does not change despite the continuous rearrangements. This process is called treadmilling (Desai and Mitchison, 1997). Microtubules can quickly change from growth to shrinkage, which has been described as dynamic instability (Mitchison and Kirschner, 1984). The dynamic instability of microtubules is essential for their function, especially for the formation of correct microtubule-kinetochore attachments during mitosis (Kirschner and Mitchison, 1986; Mitchison and Kirschner, 1984).

1.4.2 Microtubule associated proteins

In vitro, the formation of microtubules is possible in the presence of only α-and β-tubulin, GTP, and magnesium ions (Voter and Erickson, 1984). However, the formation, growth and shrinkage, as well as the function of microtubules is modulated by various microtubule associated proteins (MAPs) in living cells. Depending on their function, MAPs can be divided into several classes: microtubule nucleators (Roostalu and Surrey, 2017), end-binding proteins attaching to plus- or minus-ends of microtubules including enzymes promoting microtubule polymerisation and depolymerisation (Akhmanova and Steinmetz, 2015), motor proteins generating forces and movement (Bhabha *et al*., 2016; Hirokawa *et al*., 2009), and microtubule stabilising MAPs (Bodakuntla *et al*., 2019). Several examples are presented below.

In mammalian cells, the centrosome represents the major microtubule-organising centre (MTOC). It consists of two centrioles which are surrounded by pericentriolar material (PCM). The γ-tubulin ring complex (γ-TuRC) is associated with the centrosomes and forms the basis for microtubule nucleation (Kollman *et al*., 2011). Polymerases like colonic and hepatic tumour-overexpressed gene (ch-TOG, encoded by the gene *CKAP5*) support the polymerisation of microtubules (Brouhard *et al*., 2008). Additionally, ch-TOG can act as a microtubule nucleator (Thawani *et al*., 2018). *CKAP5* is frequently overexpressed in cancer (Charrasse *et al*., 1995). In contrast, the kinesins mitotic centromere-associated kinesin (MCAK) and kinesin family member 2B (Kif2B) have microtubule depolymerase activity and are involved in the correction of erroneous microtubule-kinetochore attachments (Bakhoum *et al*., 2009a; Hunter *et al*., 2003; Knowlton *et al*., 2006). Microtubule plus-end tracking proteins (+TIPs) bind to the plus-ends of microtubules and can recruit additional MAPs. End

binding proteins (EBs) belong to the group of +TIPs (Akhmanova and Steinmetz, 2015). End binding proteins fused to fluorescent proteins can be used to track microtubule plus-tips in cell biological experiments (Stepanova *et al*., 2003). Motor proteins including kinesins and dynein consist of a motor domain and a cargo-binding domain. Due to this structure, they are able to “walk” on microtubules and can transport vesicles or arrange cellular organelles. If the cargo-binding domain is replaced by another motor domain, motor proteins can move microtubules along microtubules. Kinesins are directed to the microtubule plus-ends, whereas dynein molecules move to the minus-ends of microtubules (Bhabha *et al*., 2016; Hirokawa *et al*., 2009).

1.4.3 The mitotic spindle

In proliferating cells, the centrosome as major MTOC is duplicated during S phase. After maturation, centrosomes are separated at the onset of mitosis to start the formation of a bipolar mitotic spindle which is essential for the equal distribution of the DNA. Bipolar kinesin complexes with two motor domains, for example Eg5, can move microtubules in opposite directions which promotes the separation of the centrosomes (Tanenbaum and Medema, 2010). Different classes of microtubules are present in mitotic spindles. Interpolar microtubules form a network of overlapping and antiparallelly arranged microtubules emanating from the two opposing spindle poles. Astral microtubules interact with the cellular cortex and are involved in the correct positioning of the mitotic spindle in the cell. Kinetochore microtubules, which are also called k-fibres, bind to the kinetochores of chromosomes. For this process, the activity of several kinetochore proteins and MAPs is necessary (Petry, 2016).

The increased proliferative capacity of cancer cells can be targeted by microtubule modulating drugs. Taxol belongs to the taxanes, a group of microtubule-targeting drugs. Taxol stabilises microtubule dynamics especially at their plus-ends or, if applied in higher concentrations, promotes microtubule polymerisation (Derry *et al*., 1995; Jordan *et al*., 1993). This interference with microtubule dynamics prevents the formation of correct microtubule-kinetochore attachments during mitosis. Consequently, cells cannot progress from metaphase to anaphase leading to mitotic slippage and, ultimately, apoptosis (Jordan *et al*., 1996). In addition, our lab has shown that sub-nanomolar concentrations of Taxol can be used to specifically reduce abnormally increased microtubule polymerisation rates (Ertych *et al*., 2014).

1.5 Chromosomal instability

The correct duplication of the DNA during S phase and its faithful segregation during mitosis are essential to generate euploid progeny and to maintain chromosomal stability in a cell population. In contrast, chromosomal instability (CIN) is one of the central hallmarks of cancer cells (Hanahan and Weinberg, 2011).

1.5.1 Types of chromosomal instability

Chromosomal instability can be divided into two major forms, namely structural chromosomal instability (S-CIN) and whole chromosomal instability (W-CIN). S-CIN describes a high rate of structural chromosomal rearrangements like deletions, insertions, and amplifications (Sansregret *et al*., 2018). Replication stress and impaired DNA repair processes are possible causes for S-CIN (Gelot *et al*., 2015). W-CIN describes the perpetual gain or loss of whole chromosomes. It is of note that W-CIN is a dynamic process whereas aneuploidy characterises the current state of a karyotype, in detail an aberrant karyotype with a chromosome number differing from the modal number of 46 chromosomes in human somatic cells (Sansregret *et al*., 2018). The analyses of colorectal cancer (CRC) samples revealed that up to 85 % of CRC cells show a W-CIN phenotype which is associated with poor prognosis. In contrast, only 15 % of CRC cells exhibit microsatellite instability (MIN/MSI) which is caused by mutations in the DNA mismatch repair system and associated with an increased rate of point mutations (Cisyk *et al*., 2015; Dunican *et al*., 2002).

1.5.2 Causes of whole chromosomal instability

W-CIN is associated with various mitotic defects which are illustrated in Figure 1.9. Analyses in cell lines revealed that defects in the spindle assembly checkpoint (SAC) are sufficient to induce W-CIN and aneuploidy (Michel *et al*., 2001). The tumour incidence was higher in mice with a reduced expression of SAC components in comparison with their wildtype litter mates (Kops *et al*., 2005). However, mutations in known SAC genes are only rarely present in human tumours (Thompson *et al*., 2010).

Mutations or loss of cohesin subunits lead to the untimely separation of sister chromatids and, thus, chromosome missegregation. Cohesion defects associated with aneuploidy and W-CIN were detected in colorectal and bladder cancer (Barber *et al*., 2008; Solomon *et al*., 2013).

In early mitosis, the formation of incorrect microtubule-kinetochore attachments is common due to the search-and-capture mechanism. In contrast to correct amphitelic attachments, only one kinetochore or both kinetochores from sister chromatids can be bound by microtubules from only one spindle pole. These errors are referred to as monotelic or syntelic attachments, respectively (Figure 1.8a) (Godek *et al.*, 2015).

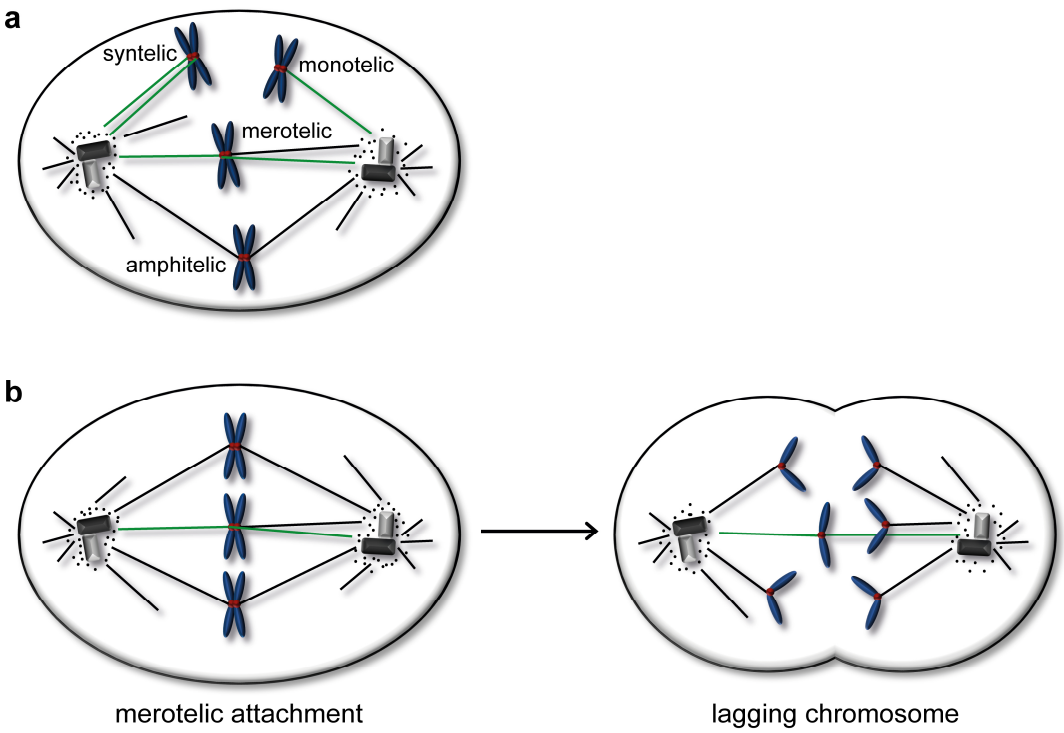

Figure 1.8: Microtubule-kinetochore attachments.
(a) Monotelic or syntelic attachments occur when one or both sister kinetochores are bound by microtubules emanating from only one spindle pole. Merotelic attachments occur when one kinetochore is bound by microtubules originating from both centromeres. A correct bipolar attachment is referred to as amphitelic. **(b)** Lagging chromosomes are generated when cells proceed from metaphase to anaphase in the presence of merotelic microtubule-kinetochore attachments.

In the presence of monotelic attachments and, thus, unattached kinetochores, SAC signalling is active. Consequently, the progression of mitosis is delayed until the monotelic attachments are corrected. In the presence of syntelic attachments, the inter-kinetochore tension is reduced because both sister kinetochores are bound by microtubules emanating from the same spindle pole. The lack of tension induces an Aurora B-dependent signalling pathway which leads to the destabilisation of erroneous microtubule-kinetochore attachments and active SAC signalling until correct amphitelic attachments are established (Musacchio, 2015). In addition to monotelic and syntelic attachments, a third type of erroneous microtubule-kinetochore attachments has been described: A merotelic attachment occurs when a single kinetochore is bound by microtubules emanating from both spindle poles (Figure

1.8a). Significantly, the SAC is satisfied despite the persistence of merotelic attachments allowing the onset of anaphase in the presence of these erroneous microtubule-kinetochore attachments. If the error correction machinery is impaired or simply overrun by the increased formation of merotelic attachments, cells enter anaphase and the affected chromatid is not correctly transported to one of the two spindle poles and remains as a “lagging chromosome” (Figure 1.8b). Merotelic attachments and lagging chromosomes are frequently associated with W-CIN in cancer cells (Cimini, 2008; Cimini *et al*., 2001).

The possible causes for the generation of lagging chromosomes in cancer cells are diverse. Supernumerary centrosomes have been detected in various tumour entities and cancer cell lines. To avoid lethal multipolar cell divisions, cells cluster the centrosomes to form a pseudo-bipolar spindle. However, multipolar spindle intermediates favour the formation and persistence of merotelic microtubule-kinetochore attachments which is associated with W-CIN (Ganem *et al*., 2009).

Additionally, hyperstability of microtubule-kinetochore attachments has been described as a cause for the increased formation and persistence of merotelic attachments and subsequent chromosome missegregation in cells exhibiting W-CIN (Bakhoum *et al*., 2009b). Faithful chromosome segregation could be restored by increasing microtubule turnover upon overexpression of the microtubule depolymerising kinesins MCAK and Kif2B (Bakhoum *et al*., 2009a). These results indicate that impaired correction of erroneous microtubule-kinetochore attachments might underlie W-CIN. However, mutations in the genes encoding for MCAK, Kif2B, or Aurora B, which is involved in the regulation of MCAK and Kif2B localisation and activity (Bakhoum *et al*., 2009a; Knowlton *et al*., 2006), are rarely found in human malignancies (Thompson *et al*., 2010). Nonetheless, alterations in genes encoding for other proteins, which modulate microtubule-kinetochore attachment stability, might be cancer-relevant. One example is the tumour suppressor gene adenomatous polyposis coli (*APC*) which is often mutated in chromosomally instable colorectal tumours (Fodde *et al*., 2001; Green and Kaplan, 2003). Loss of APC leads to hyperstability of microtubule-kinetochore attachments, lagging chromosomes, and chromosome missegregation (Bakhoum *et al*., 2009b).

Recently, our lab has described that increased mitotic microtubule polymerisation rates lead to transient mispositioning of the mitotic spindle, merotelic microtubule-kinetochore attachments, chromosome missegregation, and W-CIN (Ertych *et al*., 2014). The correction of microtubule polymerisation rates by the microtubule-binding

drug Taxol or by depletion of the microtubule polymerase ch-TOG was sufficient to restore chromosome segregation and chromosomal stability, which indicates a causal relationship between elevated microtubule growth rates and whole chromosome missegregation (Ertych *et al*., 2014).

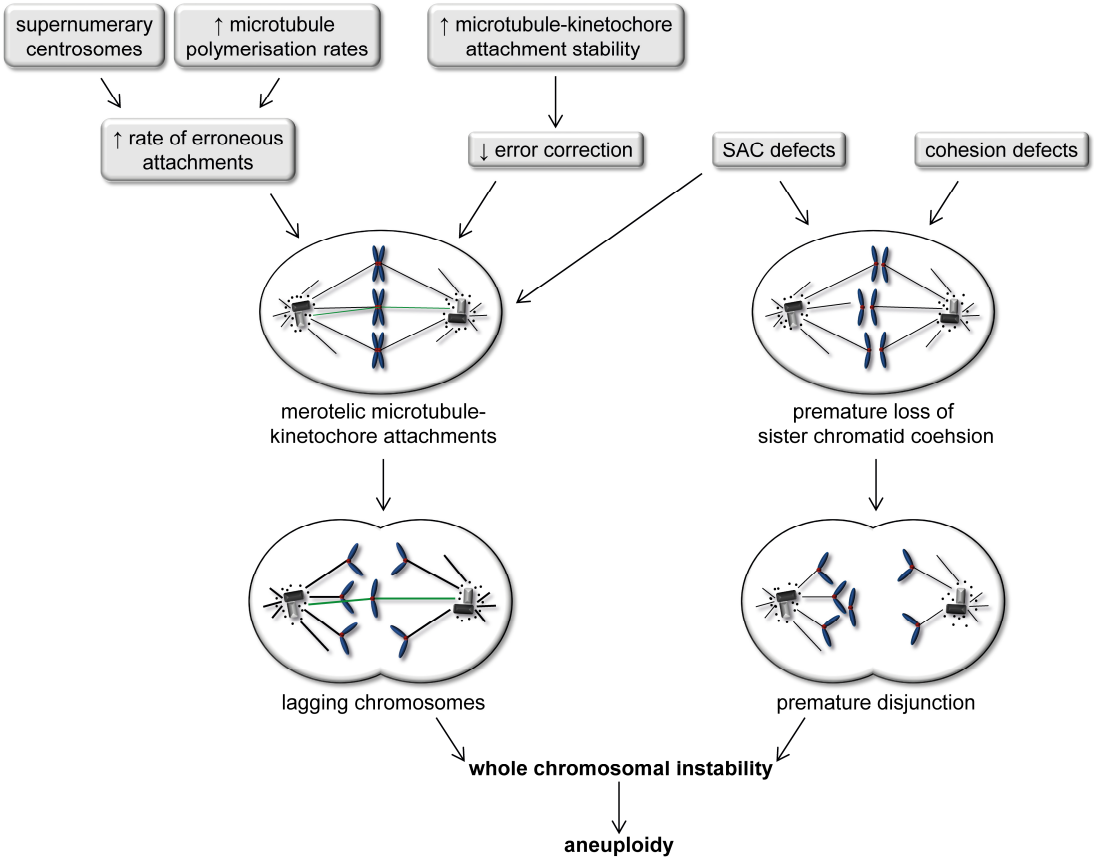

Figure 1.9: Possible causes of whole chromosomal instability (W-CIN).
Increased formation and persistence of merotelic microtubule-kinetochore attachments and premature loss of sister chromatid cohesion are well-established mechanisms leading to chromosome missegregation and W-CIN in human cancer cells. Possible underlying defects are, for instance, cohesion defects, impaired SAC function, supernumerary centrosomes, hyperstable microtubule-kinetochore attachments, and increased microtubule polymerisation rates. Scheme adapted from Bastians, 2015.

The underlying causes for increased microtubule growth rates are only incompletely understood. Our lab showed that the loss of BRCA1, a tumour suppressor involved in DNA repair by homologous recombination, results in elevated microtubule polymerisation rates and W-CIN. The kinase CHK2 phosphorylates BRCA1 at Ser988 which leads to its activation. The loss of the positive regulator CHK2 mimics the phenotype of BRCA1 loss regarding microtubule growth rates and chromosome missegregation (Ertych *et al*., 2014; Stolz *et al*., 2010). The kinase Aurora A, whose activity is important for the progression of mitosis, is often overexpressed in cancer. Our lab found out that overexpression of *AURKA* (gene encoding for Aurora A) also leads to higher microtubule polymerisation rates and W-CIN. Aurora A phosphorylates

BRCA1 at Ser308, which is an inhibitory phosphorylation regarding the mitotic function of BRCA1 (Ertych *et al*., 2016). In addition, overexpression of *CEP72*, the gene encoding for the centrosomal protein 72 (Cep72), induces abnormal microtubule growth rates and W-CIN. Cep72 interacts with BRCA1 and seems to be a negative regulator of BRCA1 (Lüddecke *et al*., 2016). Together, these previous results strongly indicate that a BRCA1-centred signalling network is required for the maintenance of proper microtubule growth rates in mitosis. However, the underlying mechanisms remain to be investigated. More recently, we have shown that overexpression of oncogenic *ΔNp73* or the concomitant loss of the tumour suppressor genes *TP53* and *TP73* result in increased microtubule polymerisation rates and chromosome missegregation (Berger, 2016; Schmidt *et al*., 2021).

Interestingly, the induction of mild replication stress is sufficient to induce higher microtubule growth rates, chromosome missegregation, and W-CIN (Böhly *et al*., 2019). This is in line with previous findings showing that replication stress does not only induce structural chromosome aberrations but also triggers W-CIN (Burrell *et al*., 2013a).

1.5.3 Consequences of chromosomal instability

Chromosomal instability is the major mechanism leading to the development of genetic heterogeneity in tumours (Burrell *et al*., 2013b). It is of note that excessive chromosome missegregation often results in the formation of unviable karyotypes (Sansregret *et al*., 2018). In this case, severe gene dosage imbalances and the resulting metabolic changes and proteotoxic stress have detrimental effects (Tang and Amon, 2013). Additionally, it has been shown that cells with complex aneuploid karyotypes induce an immune response leading to their clearance (Santaguida *et al*., 2017). However, loss or amplifications of genes acquired by moderate levels of CIN favour tumour adaptability under selective pressure occurring during tumour evolution and cancer therapy which is associated with poor prognosis (Sansregret *et al*., 2018).

Considering the importance of CIN in tumourigenesis, tumour progression, and development of therapy resistance, it is of utmost interest to target CIN in therapeutic approaches. Aneuploid cells suffer from proteotoxic and metabolic stress. Induction of additional stress by the protein folding inhibitor 17-AAG or the energy stress-inducing compound AICAR inhibit the growth of aneuploid cancer cells (Tang *et al*., 2011). Inhibitors of Mps1, a central kinase of the spindle assembly checkpoint, have been developed to increase the rate of chromosome missegregation to support the generation of unviable karyotypes. These compounds have been shown to improve

the efficacy of Taxol treatment in cellular assays and in mouse models (Janssen *et al*., 2009; Wengner *et al*., 2016). Another approach is the reactivation of p53 in chromosomally instable tumour cells to abrogate cellular tolerance to CIN (Sansregret *et al*., 2018).

It is of note that the vast majority of human cancer cells displays both structural and numerical chromosomal aberrations. Hence, it is not surprising that an interplay of W-CIN and S-CIN has been described (Sansregret *et al*., 2018). Replication stress, an established cause for S-CIN, also contributes to the missegregation of whole chromosomes (Burrell *et al*., 2013a). *Vice versa*, missegregated chromosomes are prone to DNA damage and structural aberrations (Crasta *et al*., 2012; Janssen *et al*., 2011; Passerini *et al*., 2016).

2 SCOPE OF THE STUDY

Whole chromosomal instability (W-CIN) is defined as the continuous gain or loss of whole chromosomes during mitosis and is a major hallmark of cancer. W-CIN contributes to the genetic heterogeneity of tumour cell populations and is associated with tumourigenesis, tumour progression, development of therapy resistance, and poor prognosis (Sansregret *et al*., 2018). Therefore, it is of great interest to elucidate the mechanisms leading to W-CIN to understand tumour development and progression, which might result in new approaches in cancer treatment (Sansregret *et al*., 2018). Our lab established a causal relationship between increased microtubule polymerisation rates in mitotic spindles and the induction of W-CIN (Ertych *et al*., 2014). However, the underlying mechanisms are hardly understood. Thus, the aim of this study is to identify further cancer-relevant alterations leading to increased mitotic microtubule polymerisation rates and W-CIN. Since recent results of our lab revealed that overexpression of *ΔNp73* or the concomitant loss of the transcription factors p53 and p73 induce abnormal microtubule growth rates and chromosome missegregation (Berger, 2016; Schmidt *et al*., 2021), the focus of this study is to unravel the mechanisms leading from *TP53/TP73*-deficiency to aberrant microtubule polymerisation rates.

3 MATERIAL AND METHODS

3.1 Material

Materials including cell culture dishes, centrifuge tubes, coverslips, disposable syringes, microscopy dishes and slides, pipette (filter) tips, reaction tubes, and repeat dispenser tips were purchased from Becton, Dickinson and Company (Franklin Lakes, NJ, USA), Greiner Bio-One International GmbH (Kremsmünster, Österreich), ibidi GmbH (Gräfelfing, Germany), Sarstedt AG & Co. KG (Nümbrecht, Germany), Starlab GmbH (Hamburg, Germany), Thermo Fisher Scientific (Waltham, MA, USA), and Th. Geyer GmbH & Co. KG (Renningen, Germany).

3.1.1 Equipment

The equipment, which was used for this study, is listed in Table 3.1.

Table 3.1: Equipment used in this study.

Equipment	Model	Company
Centrifuge, cooling	Heraeus Multifuge X3R	Thermo Fisher Scientific, Waltham, MA, USA
Centrifuge, tabletop	Heraeus Pico 17 Centrifuge	Thermo Fisher Scientific, Waltham, MA, USA
Centrifuge, tabletop cooling	Heraeus Fresco 21 Centrifuge	Thermo Fisher Scientific, Waltham, MA, USA
Chemiluminescence imaging system	Fusion-SL-3500.WL	Vilber Lourmat, Collégien, France
CO_2 incubator	HERAcell 240i CO_2 Incubator	Thermo Fisher Scientific, Waltham, MA, USA
Electrophoresis power supply	Consort Power Supply EV231	Consort, Turnhout, Belgium
Electroporation device	Gene Pulser Xcell©	Bio-Rad Laboratories, Inc., Hercules, CA, USA
Flow cytometer	BD FACSCanto© II	Becton, Dickinson and Company, Franklin Lakes, NJ, USA
Heating block	TDB-120 Dry Block Thermostat	Biosan, Riga, Latvia
		Own manufacturing
Incubator	New Brunswick™ Innova®42 Shaker	Eppendorf AG, Hamburg, Germany
Laboratory scale	Sartorius Research R200D	Sartorius AG, Göttingen, Germany

Equipment	Model	Company
Magnetic Mixer	IKAMAG© RCT	IKA Werke GmbH & Co. KG, Staufen, Germany
Microscope	Delta Vision Elite©	GE Healthcare, Chicago, IL, USA
	Leica DMI6000B	Leica, Wetzlar, Germany
	Zeiss Axioscope FS	Zeiss, Oberkochen, Germany
Microscope camera	PCO Edge sCMOS camera	PCO AG, Kelheim, Germany
	Leica DFC360 FX camera	Leica, Wetzlar, Germany
	Hamamatsu digital camera C4742-95	Hamamatsu Photonics, Hamamatsu, Japan
Microscope camera adapter	A3474-07	Hamamatsu Photonics, Hamamatsu, Japan
Mounting medium	Euparal	Carl Roth, Karlsruhe, Germany
	VECTASHIELD®	Vector Laboratories, Inc., Burlingame, CA, USA
Multilabel plate reader	Victor© X3	PerkinElmer, Waltham, MA, USA
Nitrocellulose membrane	Amersham™ Protran™ 0.45 µm NC	GE Healthcare Life Sciences, Chalfont St. Giles, UK
pH meter	Portamess® 911 pH	Knick Elektronische Messgeräte GmbH & Co. KG, Berlin, Germany
Pipettes	PIPETMAN Classic	Gilson Incorporated, Middleton, WI, USA
Pipettor	Pipetboy acu 2	Integra Biosciences GmbH, Zizers, Switzerland
	pipetus® standard	Hirschmann Laborgeräte GmbH & Co. KG, Eberstadt, Germany
Rocker	SLG® Rocking platform	Süd-Laborbedarf GmbH, Gauting, Germany
Spectrophotometer	NanoDrop 2000	Thermo Fisher Scientific, Waltham, MA, USA
Sterile workbench	HERAsafeM	Thermo Fisher Scientific, Waltham, MA, USA
Vertical gel electrophoresis system		Own manufacturing
Vortex mixer	VORTEX-GENIE© 2	Scientific Industries, Inc., Bohemia, NY, USA
Wet blotting system	Mini Trans-Blot® Cell	Bio-Rad Laboratories, Inc., Hercules, CA, USA
		Own manufacturing

3.1.2 Software

The software, which was used for data analysis, is listed in Table 3.2.

Table 3.2: Software used in this study.

Software	Company
BD FACSDiva	Becton, Dickinson and Company, Franklin Lakes, NJ, USA
Fusion 15.12	Vilber Lourmat, Collégien, France
GraphPad Prism 5.0	GraphPad Software, San Diego, CA, USA
Hokawo Launcher 2.1	Hamamatsu Photonics, Hamamatsu, Japan
ImageJ	NIH Image, Bethesda, MD, USA
Leica LAS AF 2.7.3.9723	Leica, Wetzlar, Germany
softWoRx© 6.0 Software Suite	GE Healthcare, Chicago, IL, USA
softWoRx© Explorer 1.3.0	GE Healthcare, Chicago, IL, USA

3.1.3 Chemicals

Standard chemicals were obtained from AppliChem GmbH (Darmstadt, Germany), Bio-Techne (Minneapolis, MN, USA), Becton, Dickinson and Company (Franklin Lakes, NJ, USA), Carl Roth (Karlsruhe, Germany), Enzo Life Sciences, Inc. (Farmingdale, NY, USA), Fermentas GmbH (St. Leon-Rot, Germany), Merck Millipore (Darmstadt, Germany), Promega Corporation (Madison, WI, USA), Roche Diagnostics International AG (Rotkreuz, Switzerland), Santa Cruz (Dallas, TX, USA), Sigma-Aldrich (St. Louis, MO, USA), Thermo Fisher Scientific (Waltham, MA, USA), Th. Geyer GmbH & Co. KG (Renningen, Germany), and VWR International (Radnor, PA, USA).

Further chemicals and inhibitors, their purpose, and the used working concentrations are given in Table 3.3.

Table 3.3: Chemicals and inhibitors used in this study.

Chemical	Concentration	Effect	Company
Aphidicolin	100 nM	Inhibition of DNA polymerases α, δ, and ε	Santa Cruz, Dallas, TX, USA
2′-Deoxyadenosine monohydrate	30 µM	Nucleoside supplementation to reduce replication stress	Santa Cruz, Dallas, TX, USA
2′-Deoxycytidine hydrochloride	30 µM		
2′-Deoxyguanosine monohydrate	30 µM		
Thymidine	30 µM		
Dimethylenastron (DME)	2.0 µM	Inhibition of kinesin Eg5	Sigma-Aldrich, St Louis, MO, USA
ETP-46464	1.0 µM	Inhibition of ATR	Selleck Chemicals, Houston, TX, USA
Geneticin (G418) Sulfate	300 µg/ml - 500 µg/ml	Inhibition of translation; used as selection marker	Santa Cruz, Dallas, TX, USA
MK-1775	25 nM - 5.0 µM	Inhibition of Wee1	Selleck Chemicals, Houston, TX, USA
PHA-767491	0.5 µM	Inhibition of CDC7/CDK9	Selleck Chemicals, Houston, TX, USA
Ponasterone A	0.25 µM - 5.0 µM	Induction of *CDKN1A* expression in RKO-p21-Pon cells	Santa Cruz, Dallas, TX, USA
Puromycin dihydrochloride	1 µg/ml	Inhibition of translation; used as selection marker	Santa Cruz, Dallas, TX, USA
RO-3306	0.25 µM - 7.0 µM	Inhibition of CDK1	Santa Cruz, Dallas, TX, USA
Taxol	0.2 nM	Stabilisation of microtubules	Sigma-Aldrich, St Louis, MO, USA
Thymidine	2.0 mM	Cell cycle arrest at G1/S	Santa Cruz, Dallas, TX, USA
XL-413 hydrochloride	0.5 µM - 1.0 µM	Inhibition of CDC7	Tocris Bioscience, Bristol, UK

3.1.4 Oligonucleotides

Table 3.4 provides the siRNA sequences used in this study and the corresponding references.

Table 3.4: siRNAs used in this study.

Target gene	Sequence	Reference
CDC7	5'-AAGCUCAGCAGGAAAGGUG-3'	Im *et al*., 2009
CKAP5	5'-GAGCCCAGAGUGGUCCAAA-3'	De Luca *et al*., 2008
LUCIFERASE (LUC)	5'-CUUACGCUGAGUACUUCGAUU-3'	Elbashir *et al*., 2001
TP53	5'-GACUCCAGUGGUAAUCUAC-3'	Brummelkamp *et al*., 2002
TP73	5'-CAGGUGACCGACGUCGUGAAA-3'	Qiagen, Hilden, Germany
	5'-CUCGGGAGGGACUUCAACGAA-3'	
	5'-CCCGGGAUGCUCAACAACCAU-3'	
	5'-CCCGCUCUUGAAGAAACUCUA-3'	
MCM2	5'GGAGCUCAUUGGAGAUGGCAUGGAA-3'	Passerini *et al*., 2016
RIF1	5´-AAGAGCAUCUCAGGGUUUGCUdTdT-3'	Wang *et al*., 2009

3.1.5 Plasmids

The used plasmids, their purpose, and corresponding references are given in Table 3.5.

Table 3.5: Plasmids used in this study.

Vector	Purpose	Reference
pcDNA3.1-attB-FA-Myc-His	Human expression vector with CMV (cytomegalo-virus) promotor and attB sites for site-specific integration of genes in the human genome	Kindly provided by Prof. Olaf Stemmann (Bayreuth, Germany)
pcDNA3.1-Zeocin	Human expression vector with CMV promotor	Invitrogen, Carlsbad, CA, USA
pcDNA3.1-FLAG-*CDK1-AF* (T14A/Y15F)	CMV promotor driven expression of FLAG-tagged constitutively	Kindly provided by Makoto Iimori (Kyushu, Japan) and Prof. Lienhard Schmitz

Vector	Purpose	Reference
	active *CDK1* in human cells	(Gießen, Germany) (Seibert *et al*., 2019)
pcDNA3.1-FLAG-*CDK1-DN* (D145N)	CMV promotor driven expression of FLAG-tagged kinase-dead *CDK1* in human cells	Kindly provided by Makoto Iimori (Kyushu, Japan) and Prof. Lienhard Schmitz (Gießen, Germany) (Seibert *et al*., 2019)
pEGFP-*EB3*	CMV-promotor driven expression of GFP-tagged *EB3* in human cells	Kindly provided by Prof. Linda Wordeman (Seattle, WA, USA) (Stepanova *et al*., 2003)

3.1.6 Human cell lines

Human cell lines which were used for the experiments in this study, their origin, and references are given in Table 3.6.

Table 3.6: Human cell lines used in this study.

Cell line	Origin	Reference
DLD-1	Colon carcinoma	Sigma-Aldrich, St Louis, MO, USA
DLD-1-*CDKN1A*$^{-/-}$	Colon carcinoma	Horizon Discovery, Cambridge, UK
HCT116	Colon carcinoma	ATCC, Manassas, VA, USA
HCT116 + control shRNA	Colon carcinoma	Schmidt *et al.*, 2021
HCT116-*TP53*$^{-/-}$ + control shRNA	Colon carcinoma	Schmidt *et al.*, 2021
HCT116 + *TP73* shRNA	Colon carcinoma	Schmidt *et al.*, 2021
HCT116-*TP53*$^{-/-}$ + *TP73* shRNA	Colon carcinoma	Schmidt *et al.*, 2021
HT29	Colon carcinoma	ATCC, Manassas, VA, USA
RKO	Colon carcinoma	ATCC, Manassas, VA, USA
RKO-p21-Pon (ponasterone A inducible expression of *CDKN1A* in RKO)	Colon carcinoma	Kindly provided by Mathias Schmidt (Schmidt *et al*., 2000)
SW480	Colon carcinoma	ATCC, Manassas, VA, USA
SW620	Colon carcinoma	ATCC, Manassas, VA, USA

Details on cell lines generated during this study are indicated in

Table 3.7.

Table 3.7: Cell lines which were generated during this study.

Cell Line	Parental Cell Line	Plasmid	Selection Marker
HCT116 + vector	HCT116	pcDNA3.1-attB-FA-Myc-His	Geneticin
HCT116 + *CDK1-AF*	HCT116	pcDNA3.1-FLAG-*CDK1-AF*	Geneticin
HCT116 + *CDK1-DN*	HCT116	pcDNA3.1-FLAG-*CDK1-DN*	Geneticin

3.1.7 Antibodies

The primary antibodies, which were used in this study, are listed in Table 3.8. Details on their host species, clonality, and used dilutions are given.

Table 3.8: Primary antibodies used in this study.
IF: immunofluorescence, WB: Western blot, mAb: monoclonal antibody, pAb: polyclonal antibody.

Antigen	Species, Clonality	Clone Number	Use	Dilution	Catalogue Number, Company
α-tubulin	Mouse mAb	B-5-1-2	IF WB	1:700 1:1000	sc-23948, Santa Cruz, Dallas, TX, USA
β-actin	Mouse mAb	AC-15	WB	1:10000	A5441, Sigma-Aldrich, St Louis, MO, USA
CDC2 (CDK1)	Mouse mAb	17	WB	1:500	sc-54, Santa Cruz, Dallas, TX, USA
CDC7	Rabbit mAb	EPR 20337	WB	1:1000	ab229187, Abcam, Cambridge, UK
CENP-C	Guinea pig pAb	-	IF	1:1000	PD030, MBL International Corporation, Woburn, MA, USA
ch-TOG	Mouse mAb	H4	WB	1:300	sc-374394, Santa Cruz, Dallas, TX, USA
FLAG	Mouse mAb	M2	WB	1:500	F3165, Sigma-Aldrich, St Louis, MO, USA
MCM2	Rabbit mAb	D7G11	WB	1:5000	#3619, Cell Signaling Technology, Danvers, MA, USA
$p21^{CIP1}$	Mouse mAb	DCS60	WB	1:1000	#2946, Cell Signaling Technology, Danvers, MA, USA
p53	Mouse mAb	DO-1	WB	1:500	sc-126, Santa Cruz, Dallas, TX, USA

Antigen	Species, Clonality	Clone Number	Use	Dilution	Catalogue Number, Company
p73	Rabbit mAb	EP436Y	WB	1:1000	ab40658, Abcam, Cambridge, UK
Phospho-Tyr15-CDC2	Rabbit pAb	-	WB	1:1000	#9111, Cell Signaling Technology, Danvers, MA, USA
Phospho-Ser/Thr-Pro MPM-2	Mouse mAb	MPM-2	FACS	1:1600	05-368, Merck Millipore, Darmstadt, Germany
RIF1	Rabbit mAb	D2F2M	WB	1:1000	#95558, Cell Signaling Technology, Danvers, MA, USA

Table 3.9 lists the secondary antibodies used in this study including their host species, clonality, conjugated molecule, and dilution.

Table 3.9: Secondary antibodies used in this study**.**
IF: immunofluorescence, WB: Western blot, pAb: polyclonal antibody.

Antigen	Species, Clonality	Conjugate	Use	Dilution	Catalogue Number, Company
Anti-guinea pig	Goat pAb	Alexa-Fluor594	IF	1:1000	A-11076, Thermo Fisher Scientific, Waltham, MA, USA
Anti-mouse	Goat pAb	Alexa-Fluor488	FACS IF	1:2000 1:1000	A-11029, Thermo Fisher Scientific, Waltham, MA, USA
Anti-mouse	Goat pAb	Hoseradish peroxidase (HRP)	WB	1:10000	115-035-146, Jackson ImmunoResearch Laboratories, Inc., West Grove, PA, USA
Anti-rabbit	Goat pAb	Hoseradish peroxidase (HRP)	WB	1:10000	111-035-144, Jackson ImmunoResearch Laboratories, Inc., West Grove, PA, USA

3.2 Cell biological methods

3.2.1 Cultivation of human cell lines

DLD-1, DLD-1-*CDKN1A*$^{-/-}$, HCT116, HT29, RKO, SW480, and SW620 cells were cultured in RPMI1640 (PAN-Biotech GmbH, Aidenbach, Germany) supplemented with 10 % fetal bovine serum (FBS) (Corning Inc., Corning, NY, USA), and 1 % penicillin/streptomycin (100 units/ml penicillin, 100 µg/ml streptomycin) (Anprotec, Bruckberg, Germany). HCT116 + control shRNA, HCT116-*TP53*$^{-/-}$ + control shRNA,

HCT116 + *TP73* shRNA, and HCT116-*TP53*$^{-/-}$ + *TP73* shRNA cells were grown in RPMI1640 supplemented with 10 % FBS, 1 % penicillin/streptomycin, and 1 µg/ml Puromycin (Santa Cruz, Dallas, TX, USA). HCT116 + vector, HCT116 + *CDK1-AF*, and HCT116 + *CDK1-DN* cells were cultured in RPMI1640 supplemented with 10 % FBS, 1 % penicillin/streptomycin, and 300 µg/ml G418 (Santa Cruz, Dallas, TX, USA). RKO-p21-Pon cells were cultivated in DMEM (PAN-Biotech GmbH, Aidenbach, Germany) supplemented with 10 % FBS, 1 % penicillin/streptomycin, and 500 µg/ml G418. Cells were passaged three times a week. For this purpose, cells were washed with phosphate buffered saline (PBS), detached from cell culture dishes with Trypsin-EDTA (Anprotec, Bruckberg, Germany) and resuspended in growth medium. In dependence on the confluency and the growth rate of the used cell line, 7 % - 50 % of the cell suspension were transferred to new cell culture dishes filled with fresh growth medium. All cell lines were grown at 37 °C and 5 % CO_2.

For long-term preservation, cells were harvested at ~90 % confluency and resuspended in medium containing 20 % FBS and 10 % DMSO. Cells were slowly cooled down to -80 °C in an isopropanol-based NALGENE™ Cryo 1 °C Freezing Container (Thermo Fisher Scientific, Waltham, MA, USA) and transferred to liquid nitrogen after approximately 24 hours.

3.2.2 Transfection of human cells

Prior to lipid-based siRNA or plasmid transfections, cells were seeded into 6-well dishes and incubated in 1.5 ml antibiotic-free growth medium supplemented with 10 % FBS. Cells were 70 % - 80 % confluent at the time of transfection. Further experiments were performed 48 hours after transfection and transfection efficiency was analysed by Western blotting.

3.2.2.1 siRNA transfection using ScreenFect®siRNA

For the siRNA-mediated knockdown of target genes, ScreenFect®siRNA (ScreenFect GmbH, Eggenstein-Leopoldshafen, Germany) was used according to the manufacturer's instructions. Briefly, 4 µl ScreenFect®siRNA reagent were diluted in 30 µl ScreenFect® dilution buffer. Similarly, 35 pmol - 80 pmol siRNA were added to 30 µl ScreenFect® dilution buffer. Diluted siRNA and transfection reagent were gently mixed and incubated for 20 minutes at room temperature. Afterwards, the mixture was carefully dropped onto the cells which were seeded approximately 4 hours earlier. The growth medium was changed 24 hours after transfection.

3.2.2.2 Plasmid transfection using electroporation

Prior to electroporation, cells were harvested and centrifuged at 1500 rpm for 5 minutes. $2.5x10^6$ cells were resuspended in 400 µl growth medium, mixed with 10 µg plasmid DNA, and transferred to a 4 mm cuvette (Bio-Rad Laboratories, Inc., Hercules, CA, USA). Cells were transfected using the Gene Pulser Xcell© at 500 µF and 300 V (HCT116, HCT116-derived cell lines, SW620), 950 µF and 200 V (RKO), or 950 µF and 220 V (DLD1, DLD1-*CDKN1A*$^{-/-}$, SW480, HT29). 10 minutes after electroporation, cells were seeded into 6-well dishes and after 4 hours of incubation, fresh growth medium was added to the cells.

3.2.2.3 Plasmid transfection using Lipofectamine™ 3000

Cells were seeded into 6-well dishes one day before transfection. 6.25 µl Lipofectamine™ 3000 reagent (Thermo Fisher Scientific, Waltham, MA, USA) were mixed with 125 µl Opti-MEM™ medium (Thermo Fisher Scientific, Waltham, MA, USA). Additionally, 2.5 µg plasmid DNA and 5 µl P3000™ reagent (Thermo Fisher Scientific, Waltham, MA, USA) were diluted in 125 µl Opti-MEM™ medium. Diluted DNA and transfection reagents were gently mixed and incubated for 15 minutes at room temperature. The DNA-lipid complexes were carefully dropped onto the cells and after 24 hours, fresh growth medium was added to the cells.

3.2.2.4 Plasmid transfection using ScreenFect®A

ScreenFect®A (ScreenFect GmbH, Eggenstein-Leopoldshafen, Germany) was used for transient transfections of plasmid DNA. Approximately 4 hours prior to transfection, cells were seeded into 6-well dishes. Afterwards, 6 µl ScreenFect®A were added to 30 µl dilution buffer. In a second tube, 0.75 µg - 1.0 µg DNA were diluted in 30 µl dilution buffer. Subsequently, diluted DNA and transfection reagent were gently mixed and incubated for 20 minutes at room temperature. The transfection mix was carefully added to the cells and 24 hours after transfection, the growth medium was changed.

3.2.3 Generation of stable cell lines

To generate cell lines stably expressing *CDK1* mutants, HCT116 cells were transfected with Lipofectamine™ 3000 as described in chapter 3.2.2.3. Two days after transfection, cells were seeded in various dilutions (1:20 – 1:5000) in growth medium containing 300 µg/ml G418. After 10 - 14 days, single cell clones were isolated and further cultivated for 30 generations in total. To analyse the effects of long-term inhibitor treatments, single cells clones were generated and cultured for 30 generations in the presence or absence of 0.2 nM Taxol or 0.5 µM RO-3306.

3.2.4 Cell cycle synchronisation of human cells

To synchronise human cells at the G1/S transition, a double thymidine block was used. For this purpose, cells were treated with 2 mM thymidine for 16 hours followed by washing the cells 5-6 times with fresh growth medium for 30 minutes in total. After release into fresh growth medium for 7.5 hours, the cells were incubated with 2 mM thymidine for another 16 hours. Afterwards, the cells were washed as described previously and the cell population was released from the second thymidine block.

3.2.5 Flow cytometry

Cells were harvested using 0.5 mM EDTA in PBS, centrifuged at 1500 rpm for 5 minutes, and resuspended in PBS. To fix the cells, ice-cold 70 % ethanol was added dropwise while the cell suspension was continuously vortexed. The cells were stored in 70 % ethanol at 4 °C overnight. Afterwards, cells were washed with 0.05 % Triton-X-100 in PBS. To determine the mitotic index of a cell population, mitotic phospho-epitopes were stained with an anti-phospho-Ser/Thr-Pro MPM-2 antibody (Table 3.8). The primary antibody was diluted in PBS containing 0.2 % Triton X-100 and 2 % FBS. The cells were resuspended in 100 µl staining solution and incubated for 3 hours on ice. After washing twice with 0.05 % Triton X-100 in PBS, cells were incubated with 100 µl staining solution containing the secondary antibody conjugated to Alexa Fluor-488 (Table 3.9). After incubation for 2 hours on ice, cells were washed once with 0.05 % Triton X-100 in PBS and once with PBS. Subsequently, cells were treated with DNase-free RNase A (1 mg/ml in PBS) (AppliChem GmbH, Darmstadt, Germany) for 30 minutes at room temperature. To estimate the cellular DNA content and thus the cell cycle phase, cells were finally stained with the DNA intercalating agent propidium iodide (1 µg/ml in PBS). At least 10000 events per sample were recorded on a BD FACSCanto© II flow cytometer and data analysis was performed with the software BD FACSDiva.

3.2.6 Analysis of microtubule polymerisation rates

To determine microtubule polymerisation rates in living cells, cells were transfected with pEGFP-*EB3* which allows the visualisation of microtubule plus-tips. RKO-p21-Pon cells were transfected with 0.75 µg plasmid DNA using ScreenFect®A, all other cell lines were transfected with 10 µg plasmid DNA using electroporation. One day after transfection, cells were seeded in µ-Slide 8-Well dishes (ibidi GmbH, Gräfelfing, Germany). Approximately 48 hours after transfection, cells were treated with 2.0 µM DME, an inhibitor of the kinesin Eg5, for 45 minutes - 90 minutes to accumulate cells in prometaphase (Gartner *et al*., 2005). During image acquisition, cells were

incubated in phenol red-free growth medium supplemented with 10 % FBS and 2.0 µM DME at 37 °C and 5 % CO_2. Cells were recorded using a Delta Vision Elite© microscope in combination with a PCO Edge sCMOS camera and the softWoRx® 6.0 Software Suite. Images of 4 z-stacks with a z-optical spacing of 0.4 µm were taken every 2 seconds for 30 seconds in total. Images were deconvolved using the softWoRx® 6.0 Software Suite and analysed using the softWoRx® Explorer 1.3.0. The distance travelled by one plus-tip from one timeframe to the next was measured. 10 mitotic cells were analysed in one experiment and for each cell, average microtubule polymerisation rates were calculated from 20 microtubules.

3.2.7 Analysis of lagging chromosomes by immunofluorescence microscopy

In general, cells were accumulated in anaphase to facilitate the quantification of lagging chromosomes. For this purpose, cells were synchronised at the G1/S border by a double thymidine block and subsequently released for 8.5 hours - 9.5 hours. However, asynchronously growing cells were used for the analysis of lagging chromosomes if the growth medium of the cells was supplemented with nucleosides for 24 hours - 48 hours. Cells were fixed with 2 % paraformaldehyde for 5 minutes at room temperature and then with methanol for 5 minutes at -20 °C. Cells were washed once with PBS and blocked with 5 % FBS in PBS for 25 minutes at room temperature. Microtubules and kinetochores were stained with primary antibodies against α-tubulin and Centromere protein C (CENP-C) diluted in 2 % FBS in PBS as described in Table 3.8. After incubation for 1.5 hours at room temperature, samples were washed with PBS three times. Subsequently, samples were incubated with secondary antibodies conjugated to Alexa Fluor-488 and Alexa Fluor-594 (Table 3.9) which were diluted in 2 % FBS in PBS. After incubation for 1.5 hours at room temperature or overnight at 4 °C, the DNA was stained with Hoechst33342 (1:15000 in PBS; Thermo Fisher Scientific, Waltham, MA, USA) for 5 minutes at room temperature. Then, the washing procedure was repeated. Afterwards, samples were dried at room temperature, embedded in VECTASHIELD®, and imaged using a Leica DMI6000B fluorescence microscope equipped with a Leica DFC360 FX camera and the Leica LAS AF software. To determine the number of anaphase cells with lagging chromosomes, three independent experiments were performed and 100 anaphase cells were analysed in each experiment. Only chromosomes which were clearly separated from the two DNA masses in anaphase and were stained with both anti-CENP-C and Hoechst33342 were considered as lagging chromosomes.

3.2.8 Karyotype analysis by chromosome counting

After growing single cell clones for 30 generations, mitotic chromosome spreads were analysed to determine karyotype variability as a measure of W-CIN. Therefore, cells were grown in 6-well dishes and treated with 2 µM DME for 4 hours to accumulate cells in mitosis. Cells were harvested using 0.5 mM EDTA in PBS and resuspended in 750 µl hypotonic solution consisting of 40 % RPMI1640 and 60 % ddH_2O. After 15 minutes, 250 µl ice-cold fixative (75 % methanol + 25 % acetic acid) were added to the cell suspension. After incubation for 5 minutes, cells were centrifuged at 2000 rpm for 5 minutes. The cell pellet was carefully resuspended in 1 ml fixative and centrifuged one more time. The cells were gently mixed with 1 ml fixative again and stored at -20 °C until further use. Prior to staining, cells were centrifuged at 2000 rpm for 5 minutes and resuspended in 300 µl - 500 µl 100 % acetic acid. Cells were carefully dropped onto pre-cooled wet glass slides and incubated in a wet chamber at 42 °C for 5 minutes. Slides were dried at room temperature and subsequently stained with Giemsa solution (Sigma-Aldrich, St. Louis, MO, USA) for 15 minutes. After staining, slides were rinsed with water, dried at room temperature, and embedded in Euparal. Metaphase spreads were imaged using a Zeiss Axioscope FS microscope equipped with a Hamamatsu digital camera C4742-95 and the Hokawo Launcher 2.1 software. The chromosome numbers of 50 metaphase spreads were counted for three single cell clones for each condition.

3.3 Molecular biological methods

3.3.1 Transformation and cultivation of *Escherischia coli* (*E. coli*)

The *E. coli* strain DH5αF$^-$ϕ80*lac*ZΔM15 Δ(*lacZYA-argF*) U169 *deoR recA1 hsdR*17 (r_k^-, m_k^+) *phoA supE*44 *thi*-1 *gyr*A96 relA1λ$^-$ was used for amplification of plasmid DNA. Competence was induced by treatment with $CaCl_2$.

For transformation, 50 µl *E. coli* cells were thawed on ice and gently mixed with 1 µl plasmid DNA. After incubation on ice for 15 minutes, cells were subjected to a heat shock at 42 °C for 1 minute. Subsequently, 1 ml LB medium was added and the cells were incubated at 37 °C and 650 rpm for 1 hour. The cells were transferred into 200 ml LB medium supplemented with ampicillin (100 µg/ml, Carl Roth, Karlsruhe, Germany) or kanamycin (20 µg/ml, Carl Roth, Karlsruhe, Germany) and incubated at 37 °C with gentle agitation. After overnight incubation, cells were centrifuged at 3000 rpm for 20 minutes and cell pellets were stored at -20 °C.

3.3.2 Isolation of plasmid DNA

To isolate plasmid DNA from *E. coli*, the NucleoBond® Xtra Midi kit (Macherey-Nagel GmbH & Co.KG, Düren, Germany) was used according to the manufacturer's instructions. Plasmid DNA concentration and purity were determined with the spectrophotometer NanoDrop© 2000.

3.4 Protein biochemistry

3.4.1 Preparation of protein lysates

Cells were harvested using 0.5 mM EDTA in PBS and centrifuged at 2000 rpm for 5 minutes. Afterwards, cells were resuspended in 70 µl lysis buffer consisting of 50 mM Tris-HCl, pH 7.4, 150 mM NaCl, 5 mM EDTA, 5 mM EGTA, 1 % (v/v) NP-40, 0.1 % (w/v) SDS, 0.1 % (w/v) sodium deoxycholate, phosphatase inhibitor cocktail (25 mM β-glycerophosphate, 50 mM NaF, 5 mM Na_2MoO_4, 0.2 mM Na_3VO_4, 5 mM EDTA, 0.5 µM microcystin), and cOmplete™ EDTA-free protease inhibitor cocktail (Roche, Basel, Switzerland). After incubation on ice for 10 minutes, cells were centrifuged at 14800 rpm at 4 °C for 10 minutes. The supernatant was subsequently used for determination of protein concentration.

3.4.2 Determination of protein concentration

To determine the protein concentration in cell lysates, the Bio-Rad *DC* Protein Assay (Bio-Rad Laboratories, Inc., Hercules, CA, USA) was used according to the manufacturer's instructions. Six dilutions of bovine serum albumin (BSA) (Carl Roth, Karlsruhe, Germany) ranging from 0 mg/ml to 1.0 mg/ml were used as protein standard. Photometric measurements at a wavelength of 750 nm were performed on a Victor© X3 microplate reader. 50 µg or 100 µg of protein extract were mixed with 5x SDS sample buffer (15 % (w/v) SDS, 15 % (v/v) β-mercaptoethanol, 50 % glycerol, 0.25 % (w/v) bromophenol blue) and proteins were denatured at 95 °C for 5 minutes. Samples were stored at -20 °C until further use.

3.4.3 Sodium dodecylsulfate polyacrylamide gel electrophoresis (SDS-PAGE)

A discontinuous SDS-PAGE was used to separate proteins according to their molecular weight. A 5 % SDS stacking gel (157 mM Tris-HCl pH 6.8, 0.1 % (w/v) SDS, 5 % (v/v) acrylamide (Rotiphorese® Gel 30, Carl Roth, Karlsruhe, Germany)) was combined with a 7 % - 11 % SDS resolving gel (375 mM Tris-HCl pH 8.8, 0.1 % (w/v) SDS, 7 % - 11 % (v/v) acrylamide) depending on the size of the proteins of interest. To estimate the molecular weight of the separated proteins, 4 µl of prestained protein

markers (Protein Ladder Prestained 10-180 kDa, neoFroxx GmbH, Einhausen, Germany; ProSieve QuadColor Protein Marker 4.6-300 kDa, Lonza Group AG, Basel, Switzerland) were used. Gels were run at 28 mA for 1 hour and subsequently at 42 mA for approximately 3 hours in SDS gel running buffer (25 mM Tris-HCl pH 6.8, 192 mM glycine, 0.15 % (w/v) SDS).

3.4.4 Western blotting

A tank blot system was used to transfer proteins from SDS gels to nitrocellulose membranes. Transfer took place in a wet blotting chamber filled with blotting buffer (24.8 mM Tris-HCl pH 8.0, 170 mM glycine, 0.0025 % (w/v) SDS, 15 % (v/v) methanol) at 450 mA for 2 hours and 45 minutes. Afterwards, membranes were blocked in 5 % (w/v) nonfat dried milk powder (AppliChem GmbH, Darmstadt, Germany) in Tris-buffered saline (TBS) (50 mM Tris-HCl pH 7.2, 0.9 % (w/v) NaCl) for 30 minutes. After washing with TBS, membranes were incubated with primary antibodies at 4 °C overnight. Antibodies were diluted in 3 % (w/v) BSA in TBS as listed in Table 3.8. Afterwards, membranes were washed three times with TBS-T (TBS + 0.1 % Tween-20) and once with TBS. HRP-conjugated secondary antibodies were diluted in 3 % (w/v) non-fat dried milk powder in TBS as described in Table 3.9. Membranes were incubated in secondary antibodies for 1 hour at room temperature and afterwards, the washing procedure was repeated. To detect immobilised proteins, membranes were incubated with enhanced chemiluminescence solution (0.1 M Tris-HCl pH 8.5, 2.5 mM luminol, 0.4 mM p-coumaric acid, 0.06 % (v/v) H_2O_2) or WesternBright® Sirius® Chemiluminescent HRP Substrate (Advansta Inc., San José, CA, USA) for 1 minute and imaged using a Fusion-SL-3500.WL.

3.5 Statistical analysis

Statistical analysis was performed with the GraphPad Prism 5.0 software. Mean values and standard deviations (SD) were calculated for all data. Unpaired two-tailed *t*-tests (SD≠0) or two-tailed one-sample *t*-tests (SD=0) were performed to analyse statistical significance. p-values were indicated as:

ns (not significant): $p \geq 0.05$, *: $p < 0.05$, **: $p < 0.01$, ***: $p < 0.001$, ****: $p < 0.0001$

4 RESULTS

4.1 The p53/p73-p21^{CIP1} tumour suppressor pathway prevents chromosomal instability by limiting CDK1 activity

The majority of tumour cells is characterised by chromosomal instability which contributes to tumour heterogeneity, tumour progression, and therapy resistance (Sansregret *et al*., 2018). Our group has shown previously that W-CIN can be caused by abnormally high microtubule polymerisation rates, but the underlying mechanisms are only incompletely understood. Loss of the tumour suppressor BRCA1, loss of its positive regulator CHK2 or increased activity of its negative regulators Cep72 and Aurora A have been described as triggers for altered microtubule growth rates (Ertych *et al*., 2014, 2016; Lüddecke *et al*., 2016; Stolz *et al*., 2010). Additionally, mild replication stress in S phase results in abnormally high microtubule polymerisation rates and chromosome missegregation (Böhly *et al*., 2019). The identification of further pathways regulating microtubule growth rates is in the focus of this study.

4.1.1 The concomitant loss of p53 and p73 causes chromosome missegregation as a consequence of increased microtubule polymerisation rates

Although mutation of *TP53* is one of the most common defects in human cancers, it has been demonstrated earlier that loss of *TP53* alone does not induce increased microtubule polymerisation rates and chromosome missegregation in colorectal cancer cells (Bunz *et al*., 2002; Ertych *et al*., 2014). In contrast, overexpression of *ΔNp73*, a dominant negative regulator of both p53 and its homologue p73, is a cancer-relevant alteration which results in abnormally high microtubule growth rates and chromosomal instability (Schmidt *et al*., 2021).

For further analysis of the consequences of inactivation of both p53 and p73, cell lines with a stable shRNA-mediated knockdown of *TP73* were generated based on the chromosomally stable colorectal cancer cell line HCT116 and the established knockout cell line HCT116-*TP53*$^{-/-}$ (Bunz *et al*., 1998; Schmidt *et al*., 2021). Three different *TP53*/*TP73*-deficient single cell clones (HCT116-*TP53*$^{-/-}$ + *TP73* shRNA, clones 10.2, 17.2, 23.2) were characterised. Single cell clones with either no loss (HCT116 + control shRNA) or a single loss of one transcription factor (HCT116-*TP53*$^{-/-}$ + control shRNA, HCT116 + *TP73* shRNA) were used as controls. As expected, p53 was not detectable by Western blotting after *TP53* knockout and the

protein levels of p73 were also clearly reduced after shRNA-mediated knockdown of *TP73* (Figure 4.1a).

To analyse microtubule polymerisation rates, the microtubule end-binding protein 3 (EB3) was exploited. Transient expression of GFP-tagged *EB3* allows the detection of growing microtubules in living cells (Stepanova *et al*., 2003). Live-cell microscopy was performed in *EB3-GFP* expressing cells after cells were treated with the Eg5 inhibitor DME for 1 hour, which induces the formation of monopolar mitotic spindles and a cell cycle arrest in mitosis (Gartner *et al*., 2005). Cell cycle synchronisation ensures comparability of the results and does not alter microtubule polymerisation rates (Ertych *et al*., 2014). Mitotic cells were monitored for 30 seconds and images were acquired every two seconds. To calculate microtubule polymerisation rates, the growth of GFP-tagged microtubule plus-tips was measured between two timeframes, which is illustrated in Figure 4.1b.

HCT116 cells expressing control shRNA exhibited average microtubule polymerisation rates of 16.6 µm/min. The loss of either *TP53* or *TP73* slightly increased microtubule polymerisation rates to 16.8 µm/min, which is no significant difference in comparison to the *TP53*/*TP73*-proficient cell line. In contrast, the concomitant loss of both transcription factors significantly increased microtubule polymerisation rates to 19.3 µm/min - 19.6 µm/min (Figure 4.1c).

Previously, our group established a causal relationship between abnormally high microtubule polymerisation rates and the increased occurrence of lagging chromosomes in anaphase cells (Ertych *et al*., 2014). For the detection of lagging chromosomes, cells were accumulated in anaphase by a double thymidine block followed by release into the cell cycle for 8.5 hours. After fixation, the DNA, kinetochores, and microtubules were stained for fluorescence microscopy with Hoechst33342 and antibodies targeting CENP-C and α-tubulin, respectively. Only DNA structures, which showed a CENP-C signal and were clearly separated from the DNA located at the two spindle poles, were defined as lagging chromosomes. Representative images of a normal anaphase and an anaphase with a lagging chromosome are depicted in Figure 4.1e. 2.7 % of the analysed anaphase cells of HCT116 + control shRNA exhibited CENP-C-positive chromatids which were not correctly distributed to the two spindle poles. After loss of either *TP53* or *TP73,* the proportion of anaphase cells with lagging chromosomes increased to 4.0 % and 3.3 %, respectively, but this change was not statistically significant. The proportion of anaphase cells with lagging chromosomes significantly increased to 7.7 %, 7.0 %,

and 6.7 %, respectively, in three *TP53*/*TP73*-deficient HCT116-derived cell lines (Figure 4.1d).

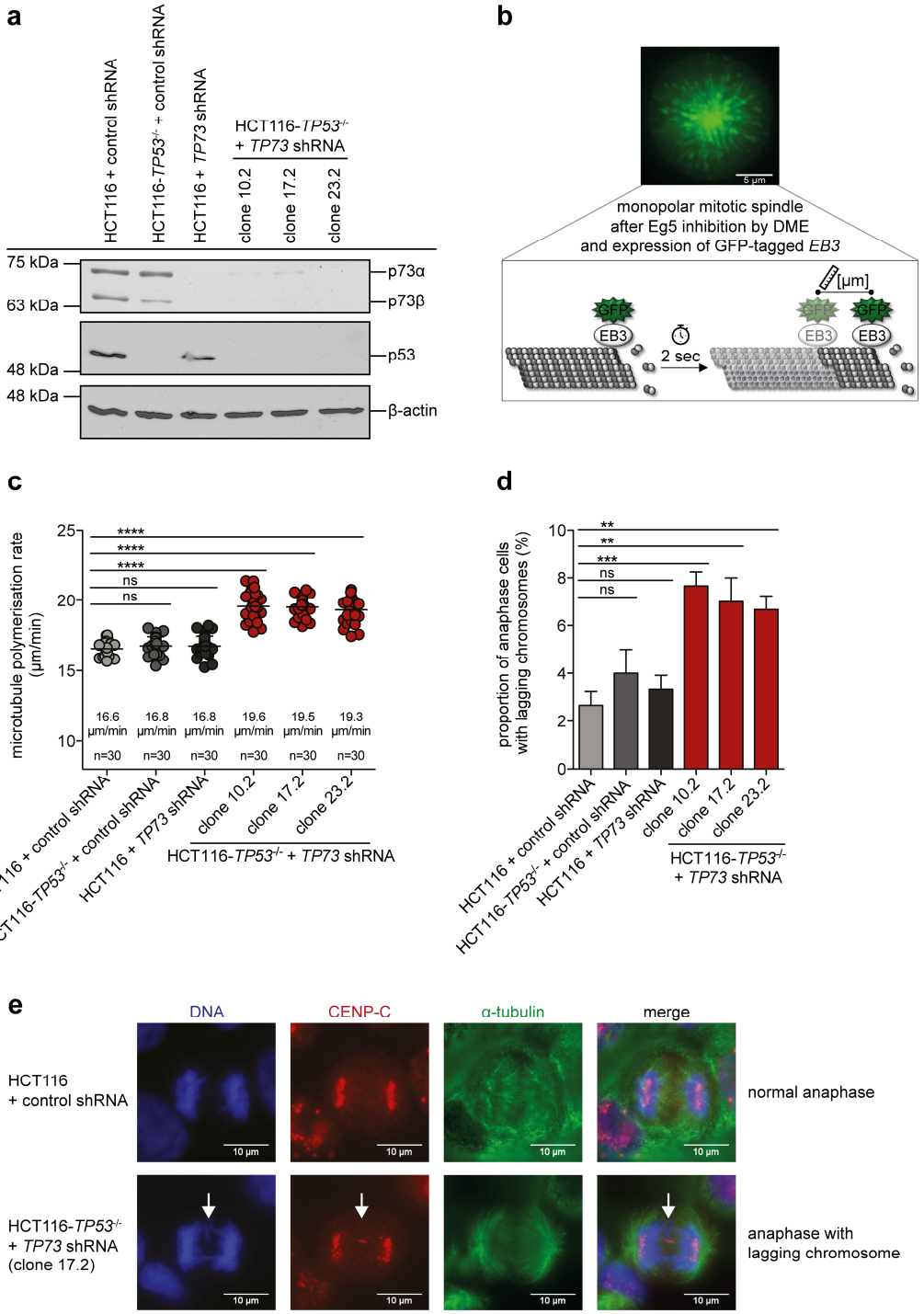

Figure 4.1: Concomitant loss of p53 and p73 leads to increased microtubule polymerisation rates and chromosome missegregation in HCT116 cells.
(a) A representative Western blot shows the p53 and p73 protein levels in the indicated cell lines. β-actin was used as loading control. **(b)** Scheme depicting EB3-GFP tracking experiments. Transient expression of GFP-tagged microtubule plus-end binding protein *EB3* allows the visualisation of growing microtubules in living cells. Additional treatment with the Eg5 inhibitor DME leads to the formation of monopolar mitotic spindles. A representative image of a monopolar spindle is shown (scale bar: 5 µm). The scheme illustrates that the growth of GFP-tagged microtubule plus-tips within two seconds is measured and used to

calculate microtubule polymerisation rates. **(c)** HCT116 cells with loss of p53, p73, or both, and the corresponding control cells were transfected with pEGFP-*EB3*. Live-cell microscopy was performed 48 hours after transfection to determine mitotic microtubule polymerisation rates. Cells were treated with 2.0 µM DME for 1 hour to accumulate them in prometaphase. Scatter dot plots show average microtubule polymerisation rates (20 microtubules/cell, three independent experiments with n=30 mitotic cells in total, mean ± SD, unpaired two-tailed *t*-test). **(d)** The indicated cell lines were synchronised at the G1/S transition with a double thymidine block and fixed after release for 8.5 hours. Microtubules, kinetochores, and DNA were stained for fluorescence microscopy. Bar graphs show the proportion of anaphase cells with lagging chromosomes (three independent experiments with n=300 anaphase cells in total, mean ± SD, unpaired two-tailed *t*-test). **(e)** Representative immunofluorescence images of a normal anaphase in HCT116 + control shRNA and an anaphase with lagging chromosome (white arrows) in HCT116-*TP53*$^{-/-}$ + *TP73* shRNA. Samples were prepared as described in (d). Scale bar: 10 µm.

Previous analyses of our lab showed that the correction of abnormally high microtubule polymerisation rates by treatment with Taxol, a microtubule-stabilising agent inhibiting microtubule polymerisation, suppressed chromosome mis-segregation and W-CIN in different chromosomally instable colorectal cancer cell lines (Ertych *et al*., 2014). To verify these findings in the context of *TP53/TP73* loss, the *TP53*/*TP73*-deficient HCT116-derived cell lines were treated with 0.2 nM Taxol before EB3-GFP tracking experiments were performed in mitotic cells. The microtubule polymerisation rates of HCT116-*TP53*$^{-/-}$ + *TP73* shRNA cells were significantly decreased from 19.3 µm/min - 19.6 µm/min to 16.4 µm/min - 16.7 µm/min (Figure 4.2a). The correction of microtubule polymerisation rates correlated with a reduced incidence of lagging chromosomes. The proportion of anaphase cells with lagging chromosomes in HCT116 cells with p53/p73 loss decreased from 6.7 % - 7.0 % to 2.7 % - 3.0 % after restoration of proper microtubule growth rates by treatment with low doses of Taxol (Figure 4.2b). In the p53/p73-proficient control cells, microtubule polymerisation rates were slightly increased from 16.4 µm/min to 16.7 µm/min (Figure 4.2a). This minor increase in microtubule polymerisation rates did not have any effect on the incidence of lagging chromosomes (Figure 4.2b). Additionally, a significant influence of Taxol treatment on the microtubule polymerisation rates of control shRNA expressing HCT116 cells could not be seen in further experiments (Figure 4.10a). Since the three *TP53*/*TP73*-deficient HCT116-derived cell lines behaved similarly regarding microtubule growth rates and chromosome segregation defects (Figure 4.1, Figure 4.2a, b), only the cell line HCT116-*TP53*$^{-/-}$ + *TP73* shRNA (clone 17.2) was used for further experiments.

The gene *CKAP5* encodes for the microtubule polymerase ch-TOG, which is responsible for the incorporation of tubulin dimers at the plus-tips of growing microtubules (Brouhard *et al*., 2008). Our group has demonstrated previously that reduced expression of *CKAP5* lowered microtubule polymerisation rates and

chromosome missegregation in chromosomally instable colorectal cancer cell lines (Ertych *et al*., 2014).

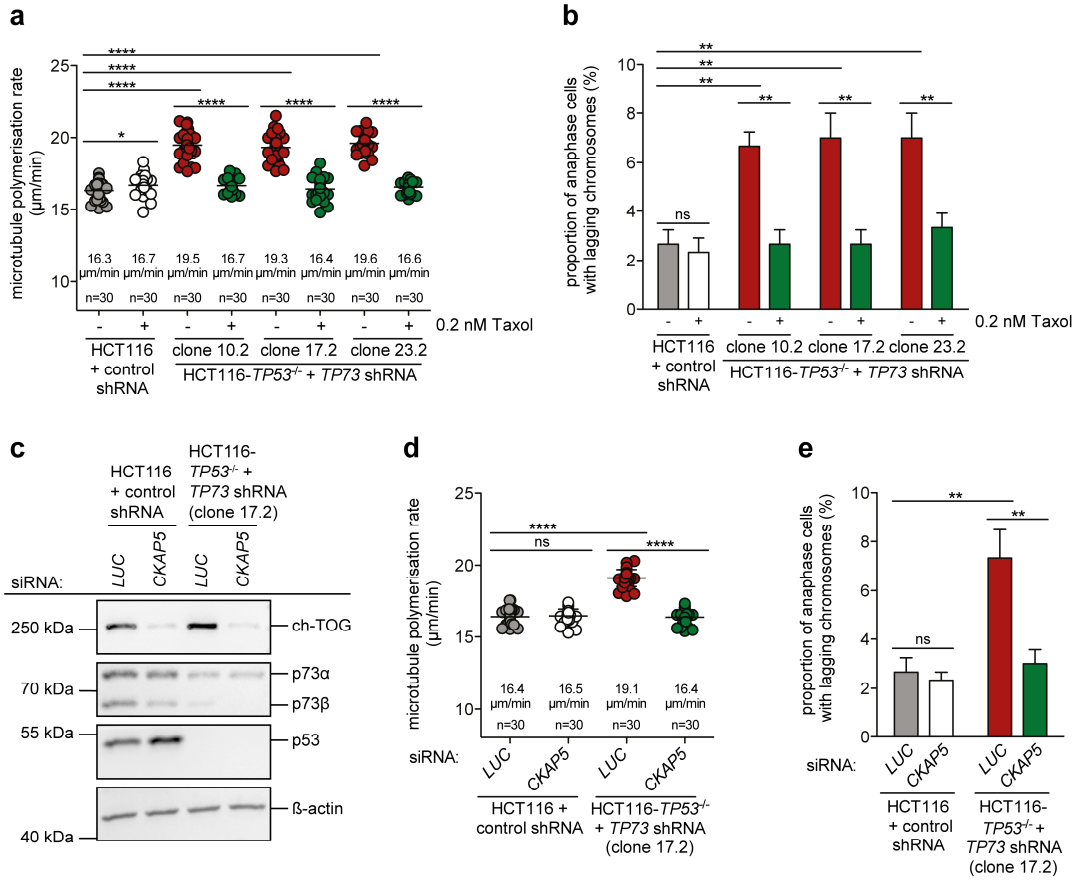

Figure 4.2: Restoration of normal microtubule polymerisation rates rescues chromosome segregation defects in HCT116 cells after loss of both p53 and p73.
(a) HCT116 + control shRNA and HCT116-*TP53*$^{-/-}$ + *TP73* shRNA cells were treated with 0.2 nM Taxol for 16 hours to restore normal microtubule polymerisation rates. Microtubule polymerisation rates were determined in mitotic cells expressing GFP-tagged *EB3.* Cells were accumulated in mitosis by treatment with 2.0 µM DME for 1 hour. Average microtubule polymerisation rates are depicted in the scatter dot plots (20 microtubules/cell, three independent experiments with n=30 mitotic cells in total, mean ± SD, unpaired two-tailed *t*-test). **(b)** HCT116 + control shRNA and HCT116-*TP53*$^{-/-}$ + *TP73* shRNA cells were synchronised with a double thymidine block and released for 8.5 hours to accumulate cells in anaphase. Additionally, cells were treated with 0.2 nM Taxol for 24 hours prior to fixation. The proportion of anaphase cells with lagging chromosomes is shown (three independent experiments with n=300 anaphase cells in total, mean ± SD, unpaired two-tailed *t*-test). **(c)** HCT116-*TP53*$^{-/-}$ + *TP73* shRNA and the corresponding control cells were transfected with 60 pmol *CKAP5* siRNA or *LUCIFERASE* (*LUC*) siRNA. A representative Western blot shows the protein levels of ch-TOG, p73, and p53 48 hours after transfection. β-actin served as loading control. **(d)** EB3-GFP tracking experiments were performed in HCT116 cells after loss of p53 and p73 and after restoration of proper microtubule polymerisation by siRNA-mediated knockdown of *CKAP5*. Scatter dot plots show average microtubule polymerisation rates (20 microtubules/cell, three independent experiments with n=30 mitotic cells in total, mean ± SD, unpaired two-tailed *t*-test). **(e)** After transfection with 60 pmol *LUCIFERASE* (*LUC*) or *CKAP5* siRNA, the indicated cell lines were synchronised with a double thymidine block and released for 8.5 hours. The DNA, CENP-C, and α-tubulin were stained for fluorescence microscopy. The proportion of anaphase cells exhibiting lagging chromosomes is depicted (three independent experiments with n=300 anaphase cells in total, mean ± SD, unpaired two-tailed *t*-test).

Accordingly, the siRNA-mediated knockdown of *CKAP5* was used as a second approach to restore proper microtubule polymerisation rates in HCT116 cells after loss of p53 and p73. Transfection of HCT116 + control shRNA and HCT116-*TP53*$^{-/-}$ + *TP73* shRNA cells with *CKAP5* siRNA strongly reduced ch-TOG protein levels in both cell lines. Interestingly, the protein levels of ch-TOG were slightly higher in *TP53*/*TP73*-deficient HCT116 cells than in *TP53*/*TP73*-proficient HCT116 cells after transfection with *LUCIFERASE* siRNA, which was used as control (Figure 4.2c). The knockdown of *CKAP5* resulted in a significant reduction of microtubule polymerisation rates in *TP53*/*TP73*-deficient HCT116 cells from 19.1 µm/min to 16.4 µm/min which corresponds to the value of the control cells. Reduced *CKAP5* expression did not influence microtubule growth rates of control cells (Figure 4.2d). Analysis of anaphase cells revealed that the restoration of proper microtubule polymerisation rates by *CKAP5* knockdown resulted in a significantly reduced incidence of lagging chromosomes in *TP53*/*TP73*-deficient HCT116 cells. The proportion of anaphase cells with lagging chromosomes decreased from 7.3 % in cells transfected with *LUCIFERASE* siRNA to 3.0 % in cells after *CKAP5* knockdown. *CKAP5* expression did not significantly influence chromosome segregation in p53/p73-proficient control cells (Figure 4.2e).

High microtubule polymerisation rates cause a higher incidence of lagging chromosomes, which have been described as a prestage of chromosome missegregation, aneuploidy, and chromosomal instability (Ertych *et al*., 2014; Gregan *et al*., 2011). W-CIN, the perpetual loss or gain of whole chromosomes, causes the development of a heterogenous cell population showing karyotypes with variable chromosome numbers. To prove that increased microtubule polymerisation rates in response to *TP53/TP73* loss are responsible for chromosomal instability, karyotype variability was analysed with or without restoration of normal microtubule growth rates by Taxol treatment. For this purpose, single cell clones were generated based on HCT116 + control shRNA and HCT116-*TP53*$^{-/-}$ + *TP73* shRNA cells, which is illustrated in Figure 4.3. Single cells were seeded, and single cell clones were isolated after 10 to 14 days. Cells were cultivated under the continuous presence or absence of 0.2 nM Taxol for 30 days which correlates with ~30 cell divisions. Subsequently, the chromosome numbers in metaphase chromosome spreads were counted to estimate karyotype variability and, thus, whole chromosome instability. Three single cell clones were analysed per condition and representative images of chromosome spreads are shown (Figure 4.3).

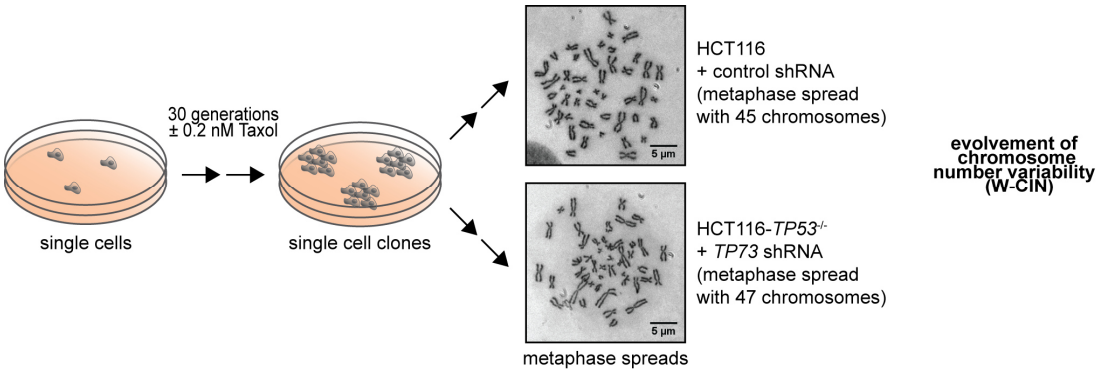

Figure 4.3: Generation of single cell clones for the analysis of karyotype variability as a measure of W-CIN.
To demonstrate the causal relationship between increased microtubule polymerisation rates and W-CIN, single cell clones of different cell lines were generated in the absence or presence of 0.2 nM Taxol. Single cells were seeded and cultivated for 30 generations with or without continuous Taxol treatment. To determine karyotype variability as a measure of W-CIN, metaphase spreads were prepared and the chromosome numbers of 50 mitotic cells were counted for three single cell clones per condition. Images of mitotic chromosome spreads of single cell clones derived from HCT116 + control shRNA and HCT116-*TP53*$^{-/-}$ + *TP73* shRNA cells are shown. Scale bar: 5 µm.

Figure 4.4a illustrates the individual chromosome numbers which could be detected in single cell clones derived from *TP53*/*TP73*-deficient HCT116 cells or the corresponding control cells with either no loss or with loss of only one transcription factor. Figure 4.4b summarises these results and depicts the percentage of cells with a karyotype deviating from the modal number. 82 % - 84 % of HCT116 cells stably transfected with control shRNA exhibited a near-diploid karyotype with 45 chromosomes (44, X), which represents the modal number of HCT116. This level was not changed by treatment with low doses of Taxol. The loss of either p53 or p73 hardly affected this stable karyotype (Figure 4.4a). After loss of either p53 or p73, 18 % - 20 % or 16 % - 24 % of the analysed cells showed a deviation from the modal chromosome number, respectively. In contrast, the loss of both transcription factors significantly induced chromosomal instability. In subclones derived from HCT116-*TP53*$^{-/-}$ + *TP73* shRNA cells, up to 40 % - 48 % of the cells exhibited a deviant karyotype (Figure 4.4b). It is of note that chromosomal instability was not only reflected by the reduced number of cells with a karyotype corresponding to the modal number of 45 chromosomes, but also by the higher diversity of the observed individual karyotypes. Restoration of normal microtubule polymerisation rates by continuous Taxol treatment suppressed the development of chromosomal instability (Figure 4.4a). In subclones which were continuously incubated with low-dose Taxol, only 20 % - 22 % of the analysed mitotic cells revealed a deviant karyotype, which was comparable with the level in control cells (Figure 4.4b).

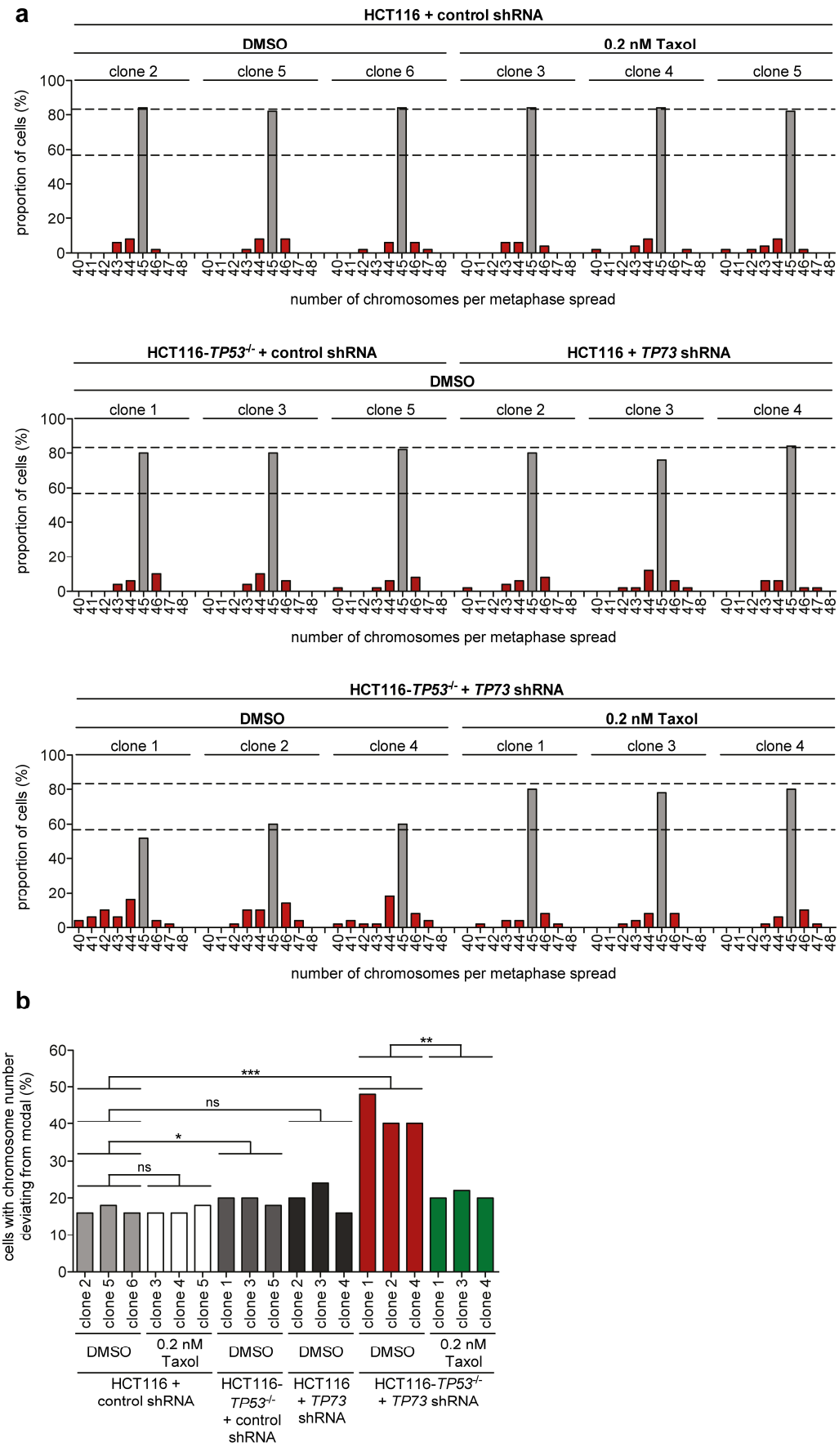

Figure 4.4: Increased microtubule polymerisation rates induce chromosomal instability upon loss of both p53 and p73.

(a) Quantification of karyotype variability in HCT116 cells after loss of p53, p73, or both, and after continuous treatment with low-dose Taxol or DMSO as a control. Single cell clones were generated from the indicated cell lines in the presence or absence of 0.2 nM Taxol as depicted in Figure 4.3. Cells were arrested in mitosis by treatment with 2.0 µM DME for 4 hours before chromosome spreads were prepared. Three single cell clones were analysed for each condition. The proportion of cells exhibiting the indicated chromosome numbers is depicted (n=50 metaphase spreads per clone). Dashed lines represent the average proportion of cells with 45 chromosomes in DMSO-treated clones derived from HCT116 + control shRNA and HCT116-*TP53*$^{-/-}$ + *TP73* shRNA cells, respectively. **(b)** The graph illustrates the proportion of cells with a chromosome number deviating from the modal number (45 chromosomes in HCT116). The calculation is based on the results shown in (a) (n=50 metaphase spreads per clone, unpaired two-tailed *t*-test).

To sum up, the simultaneous loss of the transcription factors p53 and p73 resulted in increased microtubule polymerisation rates which trigger chromosome missegregation and W-CIN. The restoration of normal microtubule growth rates was sufficient to prevent chromosome segregation defects and W-CIN. These results confirm previous findings by our group (Berger, 2016).

4.1.2 Decreased *CDKN1A* expression in response to p53/p73 loss increases microtubule growth rates and induces chromosome missegregation

The gene *CDKN1A*, which encodes for the cell cycle regulator p21^{CIP1}, can be induced upon DNA damage by both p53 and p73 (Jost *et al*., 1997; Kaghad *et al*., 1997). Previous work from our lab revealed reduced *CDKN1A* expression after loss of either p53 or p73 in HCT116 cells. In comparison to cells with a single loss of one transcription factor, the depletion of both p53 and p73 decreased *CDKN1A* expression even further. Knockdown of *CDKN1A* by siRNA resulted in increased microtubule polymerisation rates and a higher incidence of lagging chromosomes in HCT116 cells. Altogether, these results suggested that the mitotic defects observed upon loss of *TP53* and *TP73* might be a consequence of the reduced transcription of *CDKN1A* (Berger, 2016).

To further investigate the relevance of p21^{CIP1} for the maintenance of normal microtubule growth rates and chromosomal stability, the chromosomally stable colorectal cancer cell line DLD-1 and its derivative DLD-1-*CDKN1A*$^{-/-}$ were used. The protein levels of p73, p53, and p21^{CIP1} were analysed by Western blotting. Both DLD-1 and DLD-1-*CDKN1A*$^{-/-}$ cells showed comparable protein levels of p53 and p73. As expected, p21^{CIP1} was not detectable after *CDKN1A*$^{-/-}$ knockout (Figure 4.5a). EB3-GFP tracking experiments were performed to determine microtubule polymerisation rates in the presence or absence of the microtubule-stabilising drug Taxol. Knockout of *CDKN1A* significantly increased microtubule polymerisation rates from 16.4 µm/min to 19.2 µm/min. Treatment with 0.2 nM Taxol rescued the abnormally

high microtubule growth rates in DLD-1-*CDKN1A*$^{-/-}$ cells to 16.7 µm/min. Incubation with Taxol did not significantly influence microtubule growth rates in wildtype DLD-1 cells (DMSO: 16.4 µm/min, Taxol: 16.6 µm/min) (Figure 4.5b). Corresponding results were obtained for the quantification of lagging chromosomes. Loss of *CDKN1A* raised the incidence of lagging chromosomes from 1.7 % to 6.0 %. After restoration of normal microtubule polymerisation rates by Taxol treatment, only 2.7 % of anaphase cells of DLD-1-*CDKN1A*$^{-/-}$ exhibited lagging chromosomes. The analysis of anaphase cells after DMSO and Taxol treatment revealed the occurrence of lagging chromosomes in 1.7 % and 2.0 % of wildtype DLD-1 cells, respectively (Figure 4.5c).

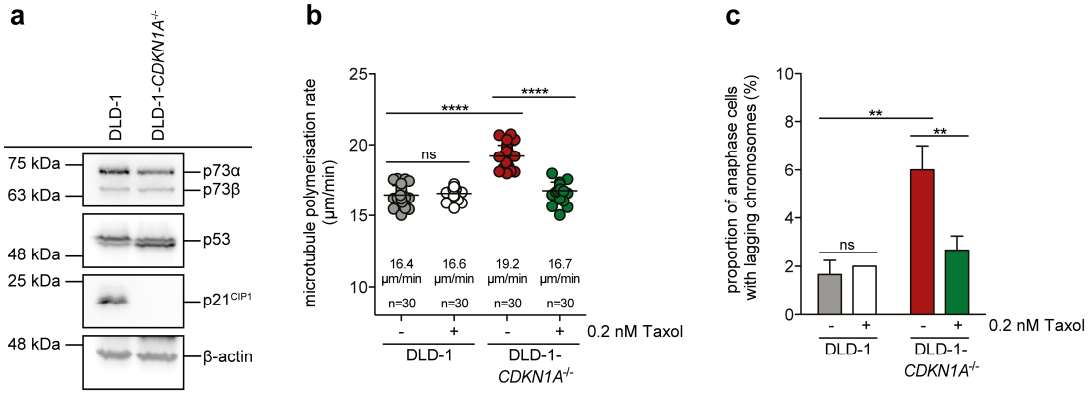

Figure 4.5: Loss of p21^{CIP1} results in increased microtubule polymerisation rates and lagging chromosomes in DLD-1 cells.
(a) A representative Western blot shows the protein levels of p73, p53, and p21^{CIP1} in DLD-1 and DLD-1-*CDKN1A*$^{-/-}$ cells. β-actin was used as loading control. **(b)** 48 hours after transfection with pEGFP-*EB3*, microtubule polymerisation rates were measured in DLD-1 and DLD-1-*CDKN1A*$^{-/-}$ cells in the absence or presence of 0.2 nM Taxol. Cells were accumulated in mitosis by treatment with 2.0 µM DME for 1 hour. Average microtubule polymerisation rates are depicted in the scatter dot plots (20 microtubules/cell, three independent experiments with n=30 mitotic cells in total, mean ± SD, unpaired two-tailed *t*-test). **(c)** The occurrence of lagging chromosomes was quantified in DLD-1 and DLD-1-*CDKN1A*$^{-/-}$ cells. Accumulation of cells in anaphase was achieved by a double thymidine block and subsequent release for 9 hours. Cells were treated with low-dose Taxol for 24 hours prior to fixation. The DNA, kinetochores, and microtubules were stained for fluorescence microscopy. The bar diagram shows the proportion of anaphase cells exhibiting lagging chromosomes (three independent experiments with n=300 anaphase cells in total, mean ± SD, SD≠0: unpaired two-tailed *t*-test, SD=0: two-tailed one-sample *t*-test).

To assess the level of chromosomal instability after loss of the cell cycle regulator p21^{CIP1}, single cell clones were generated from DLD-1 and DLD-1-*CDKN1A*$^{-/-}$ cells. The cells were cultured in the presence or absence of 0.2 nM Taxol for 30 generations. EB3-GFP tracking experiments revealed microtubule polymerisation rates ranging from 16.6 µm/min to 16.9 µm/min for three DMSO treated DLD-1-derived single cell clones (Figure 4.6a). These results were comparable with the results obtained for the parental cells (Figure 4.5b). Long-term Taxol treatment slightly decreased microtubule polymerisation rates, the results ranged from 15.8 µm/min to

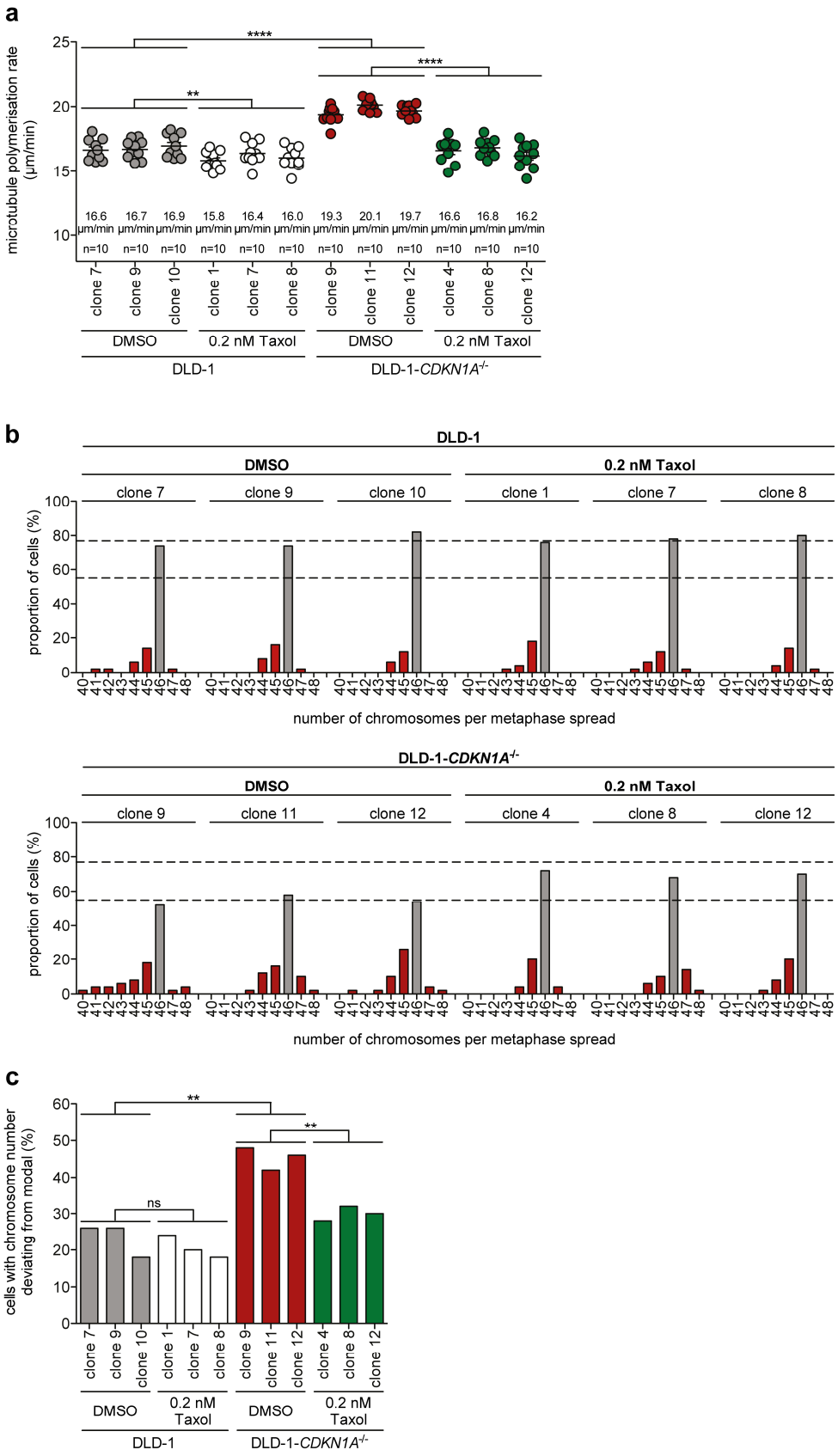

Figure 4.6: Restoration of normal microtubule polymerisation rates after loss of p21^{CIP1} suppresses W-CIN in DLD-1 cells.
(a) Single cell clones were generated from DLD-1 cells with or without knockdown of *CDKN1A*. Cells were incubated with 0.2 nM Taxol or DMSO for 30 days. To perform EB3-GFP tracking

experiments, cells were transfected with pEGFP-*EB3* and cells were accumulated in mitosis by treatment with 2.0 µM DME for 1 hour. The scatter dot plots show the average microtubule polymerisation rates of the indicated single cell clones (20 microtubules/cell, n=10 mitotic cells, mean ± SD, unpaired two-tailed *t*-test). **(b)** The indicated single cell clones were treated with 2.0 µM DME for 5 hours to accumulate cells in mitosis. Chromosome spreads of three clones per condition were analysed to determine chromosome numbers per cell. The percentage of cells with the indicated chromosome numbers is depicted (n=50 metaphase spreads per clone). Dashed lines represent the average proportion of cells with 46 chromosomes in DMSO-treated clones derived from DLD-1 and DLD-1-*CDKN1A*$^{-/-}$ cells, respectively. **(c)** The proportion of cells with a chromosome number differing from the modal number (46 chromosomes in DLD-1) is depicted. The calculation summarises the results in (b) (n=50 metaphase spreads per clone, unpaired two-tailed *t*-test).

16.4 µm/min. However, this difference between DMSO and Taxol treated cells seemed to be negligible as it did not affect chromosome segregation (Figure 4.6b, c). The DMSO treated single cell clones derived from DLD-1-*CDKN1A*$^{-/-}$ cells showed average microtubule polymerisation rates ranging from 19.3 µm/min to 20.1 µm/min. Upon long-term Taxol treatment, microtubule polymerisation rates could be significantly reduced to 16.2 µm/min, 16.6 µm/min, and 16.8 µm/min, respectively (Figure 4.6a). The following karyotype analyses in three different single cell clones per condition showed a correlation between microtubule growth rates and karyotype variability. Counting of chromosomes in metaphase spreads revealed that 74 % - 82 % of the DLD-1 cells treated with DMSO and 76 % - 82 % of cells treated with Taxol contained 46 chromosomes, which corresponds to the modal number of DLD-1 cells. After *CDKN1A* loss, the number of cells with a karyotype corresponding to the modal number was considerably reduced to 52 % - 58 %. Accordingly, the number of different karyotypes, which could be observed, increased upon *CDKN1A* loss. Restoration of normal microtubule growth rates by Taxol treatment reduced karyotype variability. The proportion of DLD-1-*CDKN1A*$^{-/-}$ cells with 46 chromosomes increased significantly from 52 % - 58 % to 68 % - 74 % upon Taxol treatment (Figure 4.6b, c).

To find out if reduced *CDKN1A* expression as a consequence of loss of *TP53* and *TP73* is responsible for the occurrence of mitotic defects, *CDKN1A* expression was induced after knockdown of *TP53* and *TP73*. For this purpose, RKO-p21-Pon cells were used. This cell line derived from the chromosomally stable colorectal cancer cell line RKO and allows the Ponasterone A inducible expression of *CDKN1A* (Schmidt *et al*., 2000).

The gene product of *CDKN1A,* p21^{CIP1}, is a cell cycle regulator inhibiting CDK1 and CDK2 and, thus, inducing cell cycle arrest at G1 and G2 (Medema *et al*., 1998). Therefore, it was necessary to find a suitable concentration of Ponasterone A which

allows low to moderate expression of *CDKN1A* without affecting cell cycle progression. RKO-p21-Pon cells were treated with increasing concentrations of Ponasterone A for 24 hours. Subsequently, induced $p21^{CIP1}$ protein levels were assessed by Western blotting and the cell cycle profiles were examined by flow cytometry after DNA staining with propidium iodide. To distinguish between mitotic cells and cells in G2, mitotic phospho-epitopes were stained with MPM-2 antibodies targeting phosphorylated Ser/Thr-Pro motives. 0.5 µM Ponasterone A were sufficient to detect increased $p21^{CIP1}$ protein levels in comparison to DMSO treated control cells. Higher Ponasterone A concentrations resulted in further increase of *CDKN1A* expression (Figure 4.7a). Cells with high $p21^{CIP1}$ protein levels, which were induced by treatment with 5.0 µM Ponasterone A, were neither able to enter S phase nor mitosis, which represents cell cycle arrest in G1 (2N DNA content) and G2 phase (4N DNA content). Ponasterone A concentrations up to 1.5 µM induced a moderate *CDKN1A* expression which hardly affected cell cycle progression (Figure 4.7b).

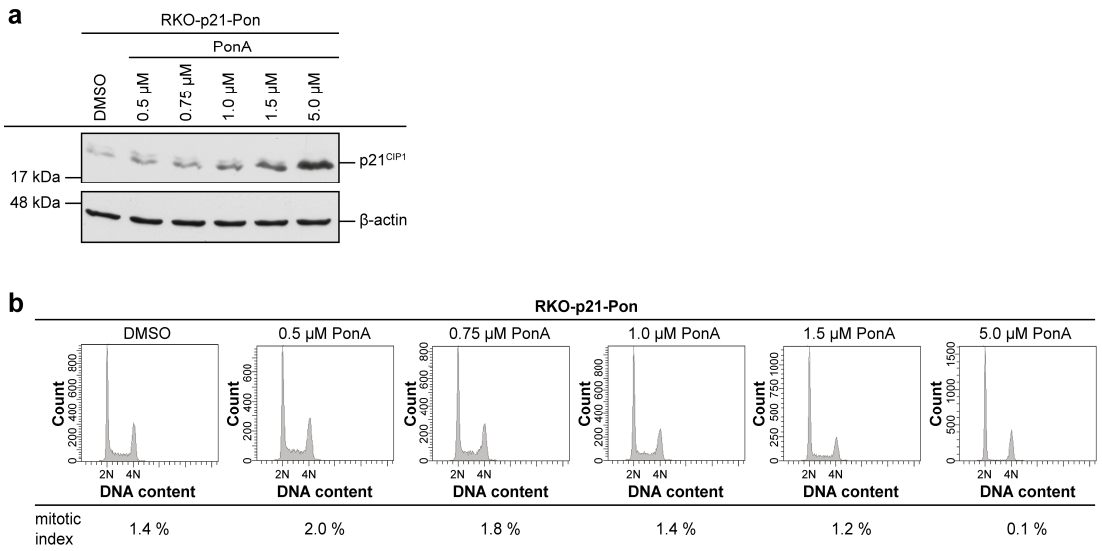

Figure 4.7: Ponasterone A inducible expression of *CDKN1A* in RKO-p21-Pon cells.
(a) RKO-p21-Pon cells were cultivated in the presence of increasing concentrations of PonA for 24 hours, DMSO was used as control. The protein levels of $p21^{CIP1}$ were assessed by Western blotting, β-actin was detected as loading control. **(b)** After treatment with the indicated PonA concentrations for 24 hours, cells were fixed and stained with propidium iodide to determine the DNA content and thus the cell cycle phase by flow cytometry. Additional staining of mitotic phospho-epitopes with anti-phospho-Ser/Thr-Pro MPM-2 antibodies was used to distinguish between cells in G2 and mitotic cells. Flow cytometry profiles are shown. High PonA-induced *CDKN1A* expression results in cell cycle arrest at G1 and G2.

RKO-p21-Pon cells were transfected with *TP53* and *TP73* siRNA or *LUCIFERASE* siRNA as a control. To induce *CDKN1A* expression, cells were incubated with 0.25 µM - 0.75 µM Ponasterone A for 24 hours. In addition, treatment with 0.2 nM Taxol was used to restore normal microtubule polymerisation rates after *TP53*/*TP73*

depletion independent of *CDKN1A* expression. The knockdown of *TP53* and *TP73* as well as the moderately induced expression of *CDKN1A* upon Ponasterone A treatment were confirmed by Western blotting. Treatment with 0.2 nM Taxol after knockdown of *TP53* and *TP73* did not impact protein levels of p73, p53, and $p21^{CIP1}$ (Figure 4.8a). Analysis of microtubule polymerisation rates revealed an increase from 16.4 µm/min in cells transfected with *LUCIFERASE* siRNA to 19.5 µm/min upon knockdown of both *TP53* and *TP73*. This could be gradually reduced to 18.4 µm/min, 17.0 µm/min, and 16.7 µm/min after treatment with 0.25 µM, 0.5 µM, and 0.75 µM Ponasterone A, respectively. Additionally, normal microtubule polymerisation rates could be restored in *TP53*/*TP73* depleted cells by treatment with low-dose Taxol (16.9 µm/min) (Figure 4.8b).

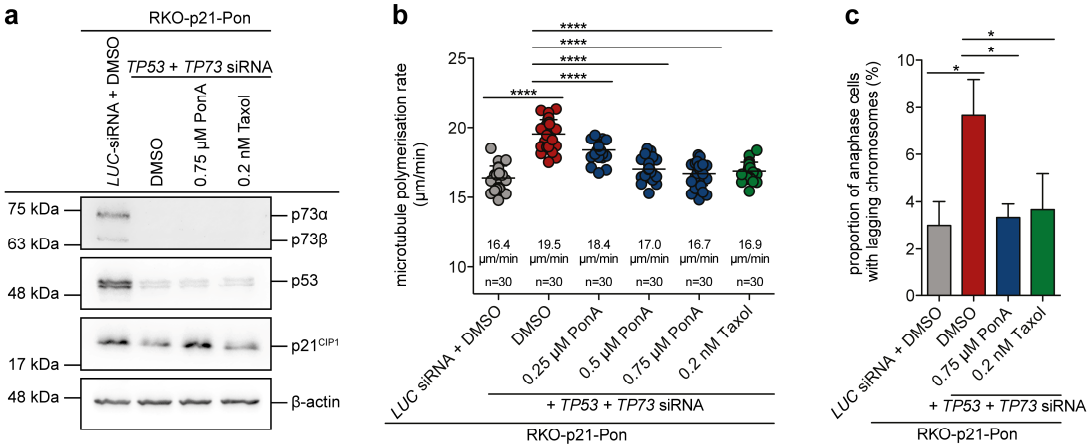

Figure 4.8: Ponasterone A inducible *CDKN1A* expression in RKO-p21-Pon cells rescues mitotic defects after loss of p53 and p73.
(a) RKO-p21-Pon cells were transfected with 80 pmol *LUCIFERASE* (*LUC*) siRNA or a combination of 45 pmol *TP53* siRNA and 35 pmol *TP73* siRNA. Cells were treated with Ponasterone A (PonA) or low-dose Taxol for 24 hours. Protein levels of p73, p53, and $p21^{CIP1}$ were detected by Western blotting. β-actin levels were detected to confirm equal protein loading. **(b)** Mitotic microtubule polymerisation rates were determined in RKO-p21-Pon cells after transfection with pEGFP-*EB3*, siRNA-mediated knockdown of *TP53* and *TP73,* and PonA induced expression of *CDKN1A.* Low-dose Taxol treatment after knockdown of *TP53* and *TP73* was used to correct microtubule polymerisation rates independent of *CDKN1A* expression. Cells were accumulated in mitosis by treatment with 2.0 µM DME for 1 hour. Scatter dot plots show average microtubule polymerisation rates (20 microtubules/cell, three independent experiments with n=30 mitotic cells in total, mean ± SD, unpaired two-tailed *t*-test). **(c)** After siRNA transfection, RKO-p21-Pon cells were synchronised at the G1/S transition with a double thymidine block and subsequently released for 9.0 hours. Additionally, cells were treated with 0.75 µM PonA or 0.2 nM Taxol for 24 hours prior to fixation. Fluorescence microscopy was performed to quantify the occurrence of lagging chromosomes in anaphase. The bar graphs show the percentage of anaphase cells with at least one lagging CENP-C positive chromatid (three independent experiments with n=300 anaphase cells in total, mean ± SD, unpaired two-tailed *t*-test).

In accordance with the increased microtubule growth rates, lagging chromosomes occurred more frequently after knockdown of *TP53* and *TP73.* The incidence of

lagging chromosomes increased from 3.0 % (*LUCIFERASE* siRNA) to 7.6 % (*TP53* + *TP73* siRNA). After Ponasterone A induced expression of *CDKN1A* and restoration of normal microtubule growth rates by Taxol treatment, the proportion of anaphase cells displaying lagging chromosomes was reduced to 3.3 % and 3.7 %, respectively (Figure 4.8c).

These results indicate that loss of the transcription factors p53 and p73 diminishes *CDKN1A* expression which, in turn, elevates microtubule polymerisation rates and impairs chromosome segregation and, consequently, chromosomal stability.

4.1.3 Mild inhibition of CDK1 rescues mitotic defects and chromosomal instability upon loss of p53/p73 or p21^{CIP1}

P21^{CIP1} modulates the cell cycle by inhibiting CDK1 and CDK2 (Medema *et al*., 1998). Thus, we assumed that increased activity of CDK1, one of the major regulators of mitosis, might be responsible for the mitotic defects and chromosomal instability observed upon loss of *TP53*/*TP73* or *CDKN1A*. To test this hypothesis, *TP53*/*TP73*- or *CDKN1A*-deficient colorectal cancer cells were analysed after CDK1 inhibition by RO-3306, which is a selective ATP-competitive small-molecule inhibitor of CDK1 (Vassilev *et al*., 2006).

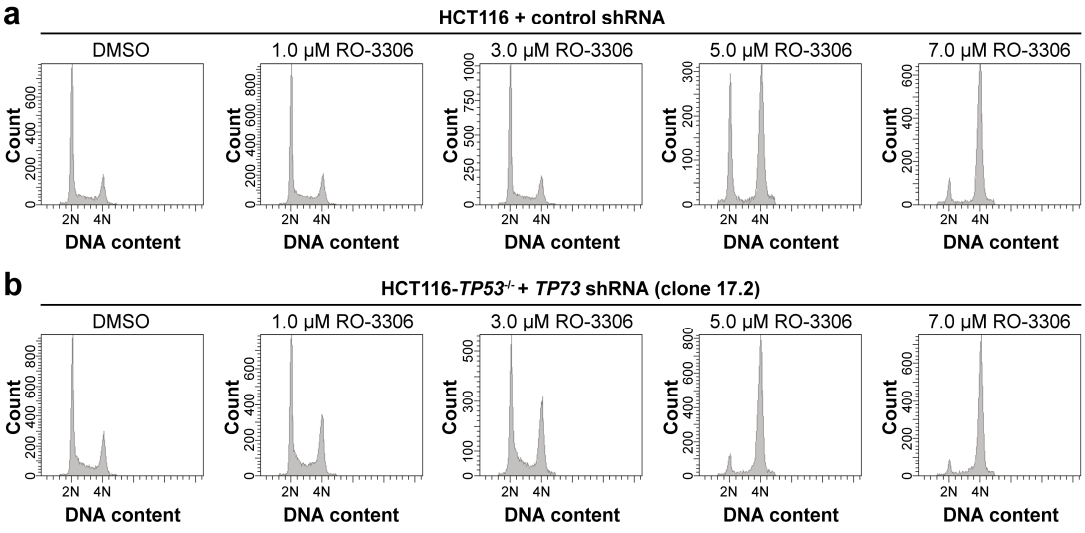

Figure 4.9: High concentrations of the CDK1 inhibitor RO-3306 induce cell cycle arrest in G2 phase.
(a) HCT116 cells stably expressing control shRNA were treated with increasing concentrations of the CDK1 inhibitor RO-3306 for 16 hours. After fixation and staining with propidium iodide, cell cycle profiles were determined by flow cytometry. High inhibitor concentrations led to accumulation of cells in G2. **(b)** *TP53*/*TP73*-deficient HCT116 cells were treated as described in (a). Cell cycle analysis shows a cell cycle arrest in G2 after inhibition of CDK1 with high concentrations of RO-3306.

Since CDK1 is essential for mitotic entry, it was necessary to determine a suitable inhibitor concentration that prevents cell cycle arrest. HCT116 + control shRNA and HCT116-TP53-/- + TP73 shRNA cells were treated with increasing concentrations of RO-3306 for 16 hours. Subsequently, cell cycle analysis was performed by flow cytometry. HCT116 + control shRNA cells tolerated the treatment with up to 3.0 µM RO-3306 without any detectable impairment of cell cycle progression. After treatment with 5.0 µM or 7.0 µM RO-3306, cells accumulated in G2 phase (4N DNA content) (Figure 4.9a). TP53/TP73-deficient HCT116 cells seemed to be more sensitive to CDK1 inhibition. Considerable cell cycle arrest at G2 could already be detected after incubation with 5.0 µM RO-3306 (Figure 4.9b). To prevent any effects of the inhibitor on cell cycle progression, up to 1.0 µM RO-3306 were used for the following experiments.

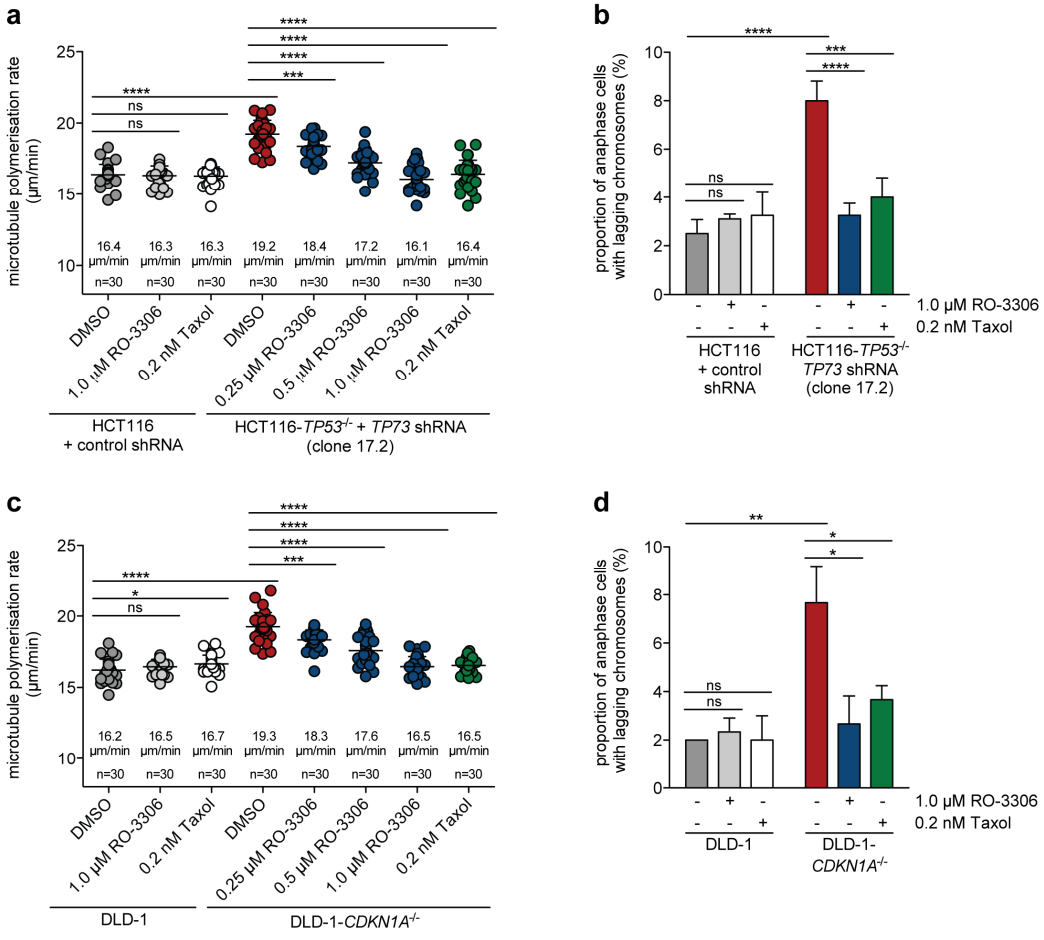

Figure 4.10: Low concentrations of the CDK1 inhibitor RO-3306 rescue mitotic defects in *TP53/TP73*-deficient HCT116 and *CDKN1A*-deficient DLD-1 cells.
(a) *TP53/TP73*-deficient HCT116 cells and the corresponding control cells were treated with the CDK1 inhibitor RO-3306 and the microtubule stabilising agent Taxol in the indicated concentrations for 16 hours. To determine microtubule polymerisation rates, live-cell microscopy was performed in cells expressing GFP-tagged *EB3*. Cells were treated with 2.0 µM DME for 1 hour prior to EB3-GFP tracking experiments. Scatter dot plots show average microtubule polymerisation rates of mitotic cells (20 microtubules/cell, three independent experiments with n=30 mitotic cells in total, mean ± SD, unpaired two-tailed *t*-test). **(b)** HCT116

+ control shRNA and HCT116-*TP53*$^{-/-}$ + *TP73*-shRNA cells were released for 8.5 hours after synchronisation at G1/S with a double thymidine block. Cells were treated with 1.0 µM RO-3306 or 0.2 nM Taxol for 24 hours. After fixation, cells were stained for fluorescence microscopy with Hoechst33342 and with antibodies targeting CENP-C and α-tubulin. The proportion of anaphase cells exhibiting lagging chromosomes was calculated and illustrated in the bar graphs (four independent experiments with n=400 anaphase cells in total, mean ± SD, unpaired two-tailed *t*-test). **(c)** DLD-1 and DLD-1-*CDKN1A*$^{-/-}$ cells were treated as in (a) and mitotic microtubule polymerisation rates were determined. Average microtubule polymerisation rates are depicted in the scatter dot plots (20 microtubules/cell, three independent experiments with n=30 mitotic cells in total, mean ± SD, unpaired two-tailed *t*-test) **(d)** DLD-1 cells with or without knockout of *CDKN1A* were synchronised at the G1/S border by a double thymidine block and released for 9 hours. Further treatments as described in (b). The occurrence of lagging chromosomes in anaphase was quantified (three independent experiments with n=300 anaphase cells in total, mean ± SD, SD≠0: unpaired two-tailed *t*-test, SD=0: two-tailed one-sample *t*-test).

The abnormally high microtubule polymerisation rates in *TP53*/*TP73*-deficient HCT116 cells (19.2 µm/min) could be gradually reduced to 18.4 µm/min, 17.2 µm/min, and 16.1 µm/min after treatment with 0.25 µM, 0.5 µM, and 1.0 µM RO-3306, respectively. Additionally, proper microtubule polymerisation rates could be restored by Taxol treatment (16.4 µm/min) (Figure 4.10a). Similar results were obtained after analysing microtubule polymerisation rates in DLD-1-*CDKN1A*$^{-/-}$ cells (Figure 4.10c). In control shRNA expressing HCT116 cells, microtubule polymerisation rates were neither significantly influenced by RO-3306 nor by Taxol treatment (DMSO: 16.4 µm/min; RO-3306, Taxol: 16.3 µm/min) (Figure 4.10a). Treatment of DLD-1 cells with RO-3306 did not significantly affect microtubule growth rates whereas Taxol treatment slightly increased microtubule polymerisation rates from 16.2 µm/min to 16.7 µm/min (Figure 4.10c). However, a significant influence of short-term Taxol treatment on microtubule growth rates or chromosome segregation in wildtype DLD-1 cells could neither be observed in previous EB3-GFP tracking experiments (Figure 4.5b) nor during the analysis of lagging chromosomes (Figure 4.5c, Figure 4.10d). In accordance with the rescue of aberrant microtubule polymerisation rates, the incidence of lagging chromosomes in *TP53*/*TP73*-deficient HCT116 cells was significantly reduced from 8.0 % to 3.3 % after CDK1 inhibition and to 4.0 % after Taxol treatment (Figure 4.10c). The CDK1 inhibitor RO-3306 as well as Taxol had similar effects on the number of anaphase cells with lagging chromosomes in DLD-1-*CDKN1A*$^{-/-}$ cells (Figure 4.10d). Neither RO-3306 nor Taxol treatment had a significant influence on the proportion of lagging chromosomes in anaphase cells of HCT116 + control shRNA and DLD-1 cells (Figure 4.10b, d).

To test for a role of increased CDK1 activity in the induction of W-CIN, single cell clones were generated based on HCT116 + control shRNA and HCT116-*TP53*$^{-/-}$ + *TP73* shRNA cells in the continuous presence or absence of RO-3306.

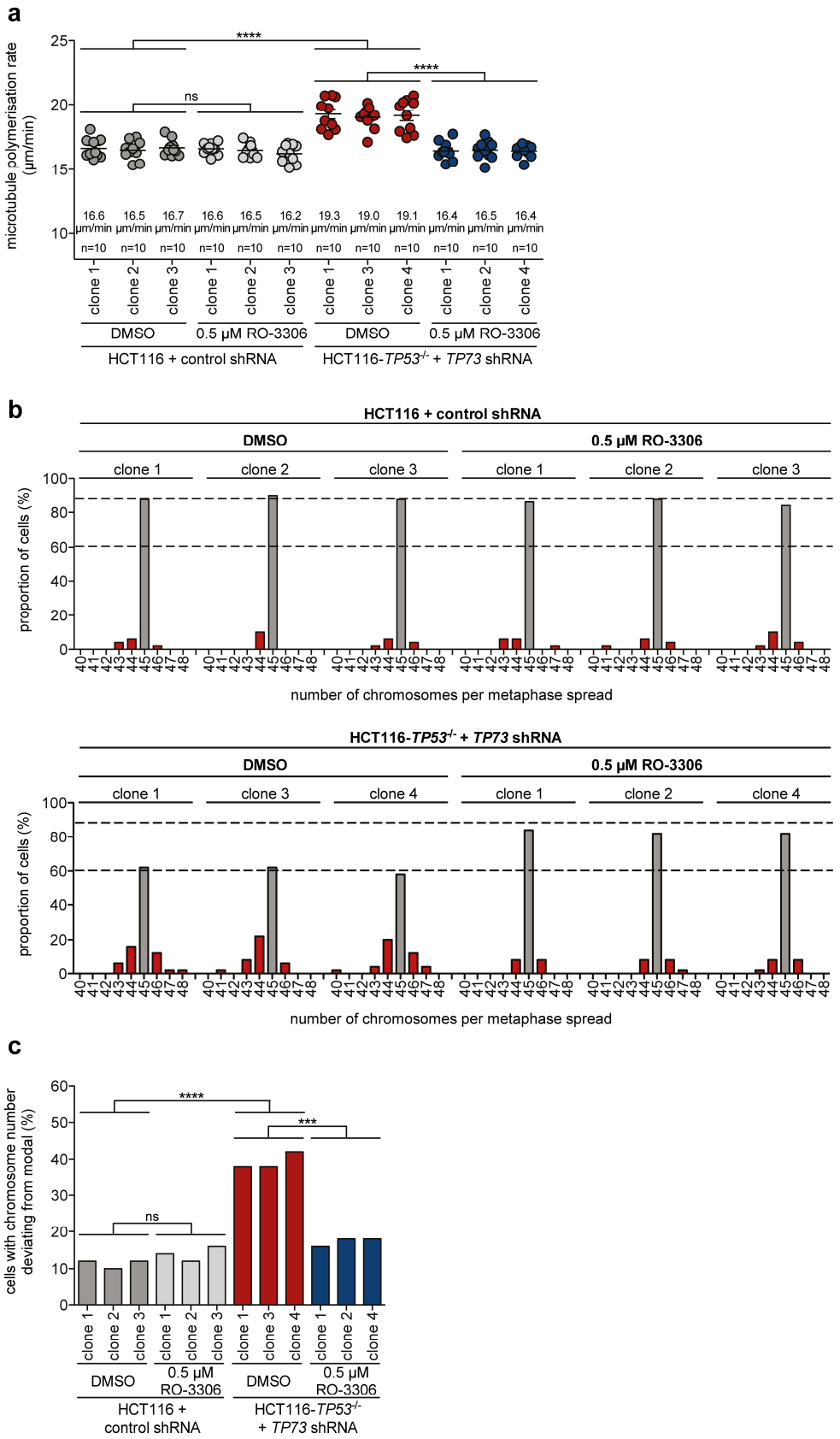

Figure 4.11: Long-term treatment with the CDK1 inhibitor RO-3306 reduces microtubule growth rates and karyotype variability in HCT116 after loss of p53 and p73.
(a) Single cell clones were generated from *TP53*/*TP73*-deficient or control HCT116 cells. Cells were treated with 0.5 µM RO-3306 or DMSO for 30 generations. Microtubule polymerisation rates were measured in cells expressing GFP-tagged *EB3*, which were arrested in mitosis by

treatment with 2.0 µM DME for 1 hour. Average microtubule polymerisation rates are illustrated in scatter dot plots (20 microtubules/cell, n=10 mitotic cells, mean ± SD, unpaired two-tailed *t*-test). **(b)** To prepare mitotic chromosome spreads, cells were accumulated in mitosis by treatment with 2.0 µM DME for 4 hours. Chromosome numbers were counted to determine karyotype variability as a measure of W-CIN. The percentage of cells with the indicated numbers of chromosomes is shown (n=50 metaphase spreads per clone). Dashed lines represent the average proportion of cells with 45 chromosomes in DMSO-treated clones derived from HCT116 + control shRNA and HCT116-*TP53*$^{-/-}$ + *TP73* shRNA cells, respectively. **(c)** The bar graphs show the proportion of cells exhibiting a chromosome number deviating from the modal number (45 chromosomes in HCT116) based on the results shown in (b) (n=50 metaphase spreads per clone, unpaired two-tailed *t*-test).

However, the concentration of 1.0 µM RO-3306, which was used for short-term treatments (Figure 4.10), was not suitable for long-term experiments because it impaired cell proliferation. A possible explanation might be the intracellular accumulation of the inhibitor upon continuous exposure. In consequence, single cell clones were treated with only 0.5 µM RO-3306 for 30 generations.

EB3-GFP tracking experiments showed that this concentration was sufficient to rescue aberrant microtubule growth rates in single cell clones derived from HCT116-*TP53*$^{-/-}$ + *TP73*-shRNA. Microtubule polymerisation rates of TP53/*TP73*-deficient HCT116 cells were reduced from 19.0 µm/min - 19.3 µm/min to 16.4 µm/min - 16.5 µm/min by treatment with RO-3306, which was comparable to the values of control cells. Microtubule polymerisation rates in control shRNA expressing single cell clones ranged from 16.5 µm/min to 16.7 µm/min and were not affected by continuous treatment with RO-3306 (Figure 4.11a). Chromosomes were counted in mitotic chromosome spreads of three single cell clones per condition to evaluate the influence of CDK1 activity on karyotype variability and, thus, W-CIN. The analysis of mitotic chromosome spreads revealed that the proportion of cells with an aberrant karyotype increased from 10 % - 12 % in control cells to 38 % - 42 % in *TP53*/*TP73*-deficient HCT116 cells (Figure 4.11b, c), which is in line with the previous results (Figure 4.4). Prolonged exposure to 0.5 µM RO-3306 was not only sufficient to restore normal microtubule growth rates upon loss of *TP53* and *TP73* (Figure 4.11a), but also to suppress chromosomal instability (Figure 4.11b, c). Only 16 % - 18 % of the *TP53*/*TP73*-deficient HCT116 cells exhibited a karyotype deviating from the modal number after continuous treatment with the CDK1 inhibitor. In control cells, mild CDK1 inhibition did not significantly change karyotype variability (Figure 4.11b, c).

Additionally, EB3-GFP tracking experiments and karyotype analyses were performed in DLD-1 and DLD-1-*CDKN1A*$^{-/-}$ derived single cell clones which were continuously treated with 0.5 µM RO-3306 or its solvent.

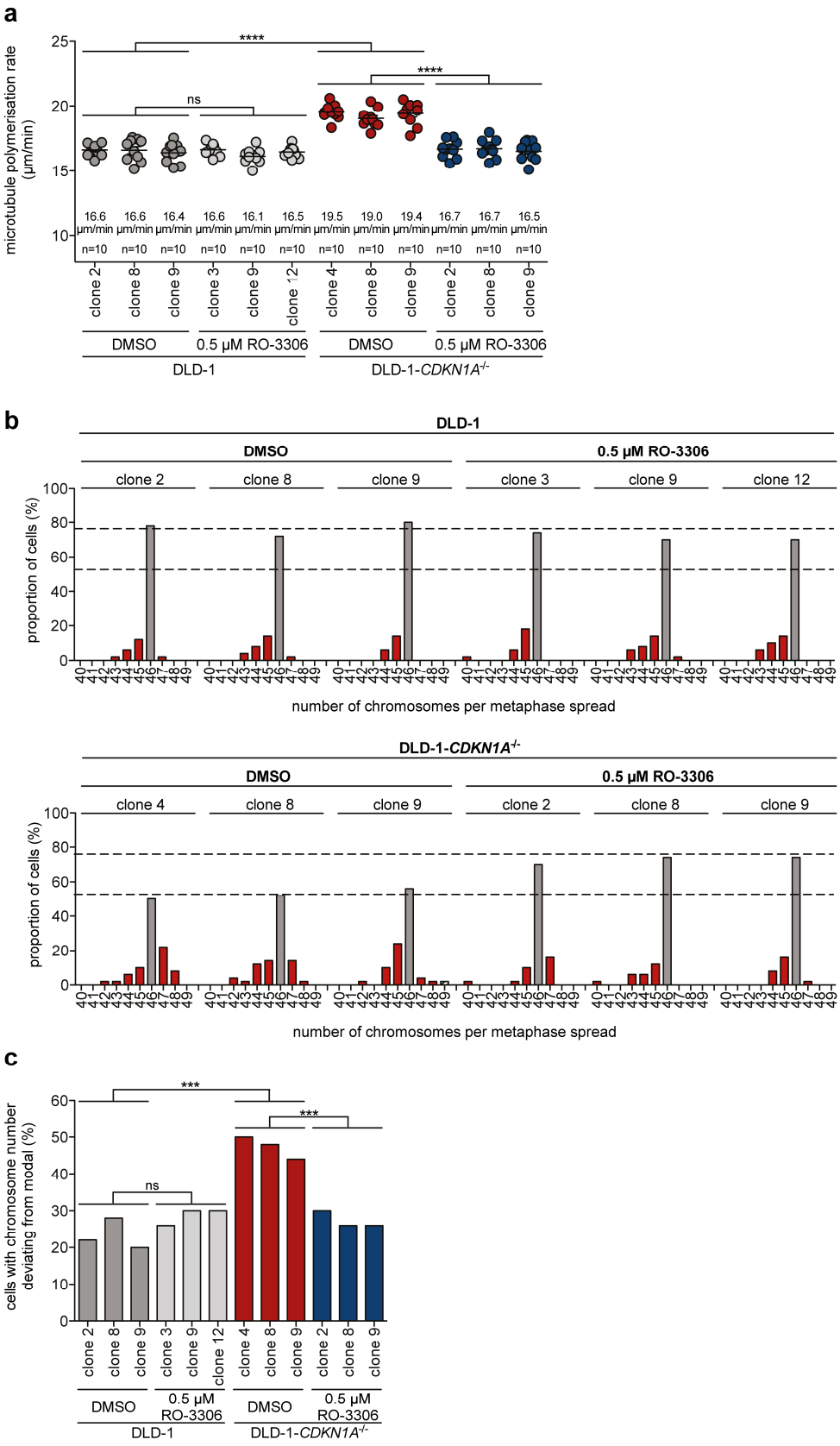

Figure 4.12: Mild CDK1 inhibition rescues microtubule polymerisation rates and high karyotype variability in DLD-1 cells upon *CDKN1A* loss.
(a) Single cell clones were generated from DLD-1 or DLD-1-*CDKN1A*$^{-/-}$ cells. Cells were cultured in the presence or absence of 0.5 µM RO-3306 for 30 generations. EB3-GFP tracking experiments were performed in mitotic cells after treatment with 2.0 µM DME for 1 hour.

Scatter dot plots display average microtubule polymerisation rates (20 microtubules/cell, n=10 mitotic cells, mean ± SD, unpaired two-tailed *t*-test). **(b)** Cells were accumulated in mitosis by treatment with 2.0 µM DME for 5 hours and mitotic chromosome spreads were used to perform karyotype analysis. Bar graphs show the percentage of cells with the indicated chromosome numbers (n=50 metaphase spreads per clone). Dashed lines represent the average proportion of cells with 46 chromosomes in DMSO-treated clones derived from DLD-1 and DLD-1-*CDKN1A*$^{-/-}$ cells, respectively. **(c)** The proportion of cells with a chromosome number differing from the modal number (46 chromosomes in DLD-1) is depicted. Calculations are based on the results shown in (b) (n=50 metaphase spreads per clone, unpaired two-tailed *t*-test).

Prolonged exposure to 0.5 µM RO-3306 was sufficient to reduce microtubule polymerisation rates in DLD-1-*CDKN1A* derived single cell clones from 19.0 µm/min - 19.5 µm/min to 16.5 µm/min - 16.7 µm/min, a level comparable to the corresponding wildtype cells (16.4 µm/min - 16.6 µm/min). Mild CDK1 inhibition did not influence microtubule polymerisation rates of DLD-1 derived single cell clones (Figure 4.12a). Analysis of mitotic chromosome spreads showed that most DLD-1 cells (72 % - 80 %) had a karyotype with 46 chromosomes which represents the modal number of this cell line. The proportion of cells with a karyotype differing from the modal number was not significantly influenced by RO-3306. In single cell clones derived from DLD-1-*CDKN1A*$^{-/-}$, the proportion of cells with an aberrant karyotype was reduced from 44 % - 50 % to 26 % - 30 % by continuous treatment with 0.5 µM RO-3306 (Figure 4.12b, c).

To sum up, it was possible to rescue increased microtubule polymerisation rates and chromosome missegregation, which occur upon loss of *TP53/TP73* or *CDKN1A,* by mild inhibition of CDK1. This suggests that loss of the p53/p73-p21^{CIP1} pathway results in unleashed CDK1 activity which acts as the actual trigger for the mitotic defects and chromosomal instability.

4.1.4 Increased CDK1 activity induces abnormal microtubule polymerisation rates and chromosomal instability

CDK1 is tightly regulated throughout the cell cycle, both by association or dissociation of its cyclin subunits and regulatory phosphorylations. The kinase Wee1 phosphorylates CDK1 at Tyr15 which contributes to its inhibition. Therefore, Wee1 inhibition by the established ATP-competitive inhibitor MK-1775 was used to induce CDK1 activity in the following experiments (Hirai *et al*., 2009).

At first, a suitable inhibitor concentration, which does not induce premature mitotic entry, was determined. HCT116 cells were synchronised at the G1/S transition with a double thymidine block. After thymidine removal, cells were released into medium containing 10 nM - 5.0 µM MK-1775 for either four hours or eight hours.

Phosphorylated as well as total CDK1 protein levels were detected by Western blotting and the mitotic indices of the cell populations were determined by flow cytometry. For this purpose, cells were stained with propidium iodide to assess the DNA content and with MPM-2 antibodies targeting phospho-Ser/Thr-Pro motives to determine the proportion of mitotic cells. Reduction of the inhibitory phosphorylation of CDK1 by increasing MK-1775 concentrations was accompanied by premature mitotic entry. Upon treatment with 5.0 µM MK-1775, 28.7 % of the cells entered mitosis 4 hours after release of a double thymidine block (Figure 4.13a). After 8 hours of release, 7.4 % of the untreated cells entered mitosis whereas this proportion was increased to 36.7 % - 59.4 % by treatment with 0.25 µM - 5.0 µM MK-1775 (Figure 4.13b). Premature mitotic entry, centromere fragmentation, and mitotic arrest upon Wee1 inhibition with high concentrations (1.0 µM) of MK-1775 have been observed previously (Lewis *et al.*, 2017). After use of up to 0.1 µM MK-1775, only moderate effects on the phosphorylation level of CDK1 were detected, which was associated with timely entry into mitosis (Figure 4.13). Accordingly, MK-1775 concentrations below 0.1 µM were used for the following experiments.

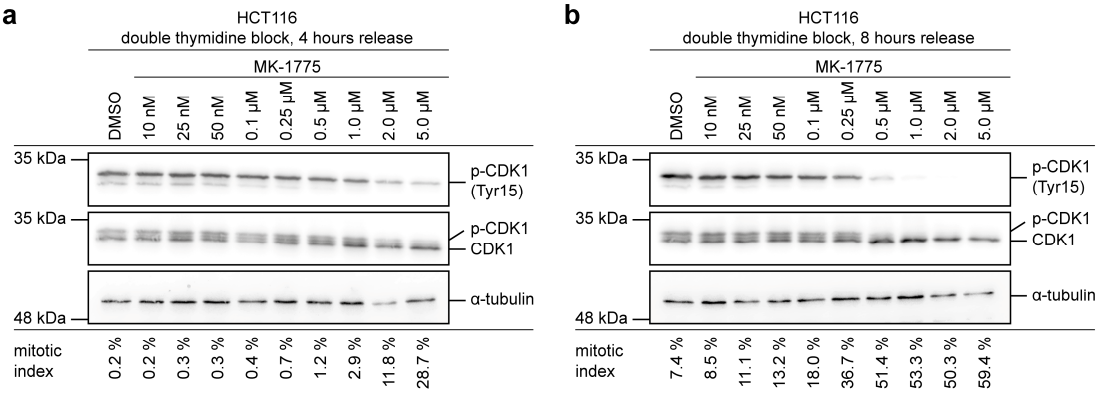

Figure 4.13: Treatment with high concentrations of the Wee1 inhibitor MK-1775 leads to premature entry into mitosis.
HCT116 cells were synchronised at the G1/S transition by a double thymidine block. After washout, cells were released into fresh growth medium containing the indicated concentrations of the Wee1 inhibitor MK-1775 for 4 hours **(a)** or 8 hours **(b)**. Western blotting revealed that the Wee1-mediated inhibitory phosphorylation of CDK1 (Tyr15) was reduced upon treatment with increasing inhibitor concentrations. Total CDK1 and α-tubulin were used as controls. The mitotic indices of the cell populations were analysed by flow cytometry. For this purpose, cells were fixed, and the DNA and mitotic phospho-epitopes were stained with propidium iodide and anti-phospho-Ser/Thr-Pro MPM-2 antibodies, respectively.

To assess the impact of elevated CDK1 activity as a consequence of Wee1 inhibition on microtubule growth rates, EB3-GFP tracking experiments were performed in HCT116 cells upon treatment with MK-1775 for 16 hours. The activation of CDK1 led to a significant increase of microtubule polymerisation rates from 16.4 µm/min in control cells to 17.6 µm/min, 18.3 µm/min, and 18.8 µm/min after treatment with

25 nM, 50 nM, and 75 nM MK-1775, respectively. The effect of Wee1 inhibition by MK-1775 on microtubule growth rates of HCT116 cells could be reversed by simultaneous inhibition of CDK1 by RO-3306 (16.6 µm/min) (Figure 4.14a). This indicates that increased microtubule polymerisation rates observed upon Wee1 inhibition are indeed caused by elevated CDK1 activity. As a consequence of abnormally high microtubule polymerisation rates, the percentage of anaphase cells with lagging chromosomes was also increased upon Wee1 inhibition. Treatment of HCT116 cells with 75 nM MK-1775 led to the occurrence of lagging chromosomes in 8.3 % of the analysed anaphase cells. In comparison, the incidence of lagging chromosomes in solvent-treated control cells was only 2.7 %. The combination of Wee1 inhibition with CDK1 inhibition prevented chromosome segregation defects (3.0 %) (Figure 4.14b).

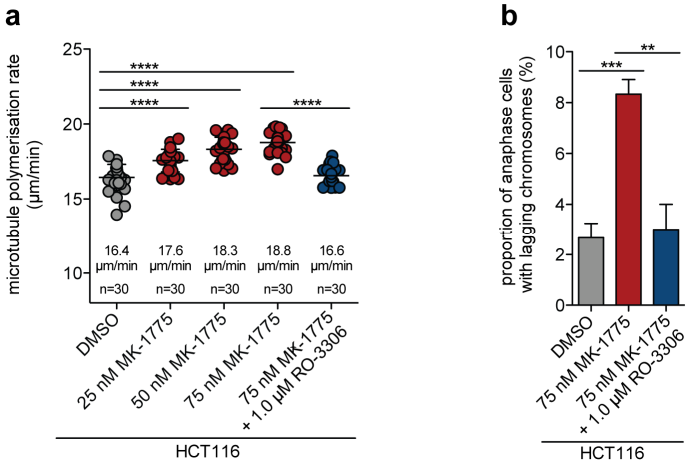

Figure 4.14: Increased CDK1 activity upon Wee1 inhibition causes increased microtubule polymerisation rates and chromosome missegregation in HCT116 cells.
(a) HCT116 cells expressing GFP-tagged *EB3* were treated with increasing concentrations of the Wee1 inhibitor MK-1775 in the presence or absence of the CDK1 inhibitor RO-3306 for 16 hours. Cells were arrested in mitosis by treatment with 2.0 µM DME for 1 hour. Average microtubule polymerisation rates were determined in mitotic cells and are illustrated in the scatter dot plots (20 microtubules/cell, three independent experiments with n=30 mitotic cells in total, mean ± SD, unpaired two-tailed *t*-test). **(b)** HCT116 cells were synchronised at the G1/S transition by a double thymidine block and subsequently released for 8.5 hours to accumulate cells in anaphase. Cells were additionally treated with 75 nM MK-1775 alone or in combination with 1.0 µM RO-3306 for 24 hours prior to fixation. Cells were stained and fluorescence microscopy was used to determine the amount of anaphase cells with lagging chromosomes (three independent experiments with n=300 anaphase cells in total, mean ± SD, unpaired two-tailed *t*-test).

Together, these results suggest that increased CDK1 activity is sufficient to induce mitotic errors independent of the p53/p73-p21^{CIP1} axis. To verify that increased CDK1 activity is the cause of the observed defects and to exclude unspecific effects of the used Wee1 inhibitor, a constitutively active mutant of *CDK1* (*CDK1-AF*) was expressed in HCT116 cells. As a control, a kinase-dead mutant (*CDK1-DN*) was used.

The expression of the *CDK1* mutants was confirmed by Western blotting. It is of note that the expression level of the exogenous *CDK1* mutants was considerably lower than the expression level of endogenous *CDK1* (Figure 4.15a). Nonetheless, the moderate expression of the constitutively active mutant *CDK1-AF* increased microtubule polymerisation rates from 16.4 µm/min to 19.0 µm/min. In contrast, the expression of the kinase-dead mutant *CDK1-DN* had no significant influence on microtubule growth rates in comparison to cells transfected with the control vector.

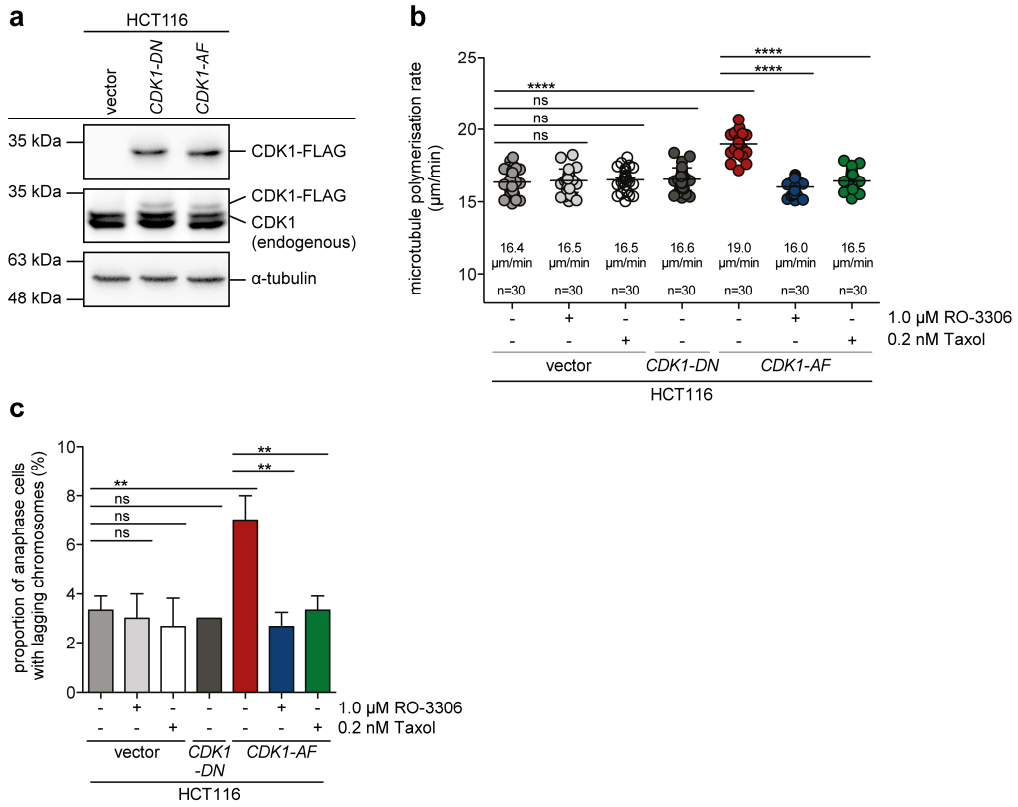

Figure 4.15: Transient expression of a constitutively active *CDK1* mutant results in elevated microtubule growth rates and chromosome missegregation in HCT116 cells. **(a)** FLAG-tagged kinase-dead (*CDK1-DN*) or constitutively active (*CDK1-AF*) *CDK1* mutants were transiently expressed in HCT116 cells. Protein levels of endogenous and FLAG-tagged CDK1 were assessed by Western blotting using anti-CDK1 and anti-FLAG antibodies. α-tubulin was used to confirm equal protein loading. **(b)** HCT116 cells were transfected with FLAG-tagged *CDK1* mutants and GFP-tagged *EB3* 48 hours prior to live-cell microscopy and treated with 1.0 µM RO-3306 or 0.2 nM Taxol for 16 hours prior to EB3-GFP tracking experiments. Cells were accumulated in mitosis by treatment with 2.0 µM DME for 1 hour. Average microtubule polymerisation rates are illustrated in the scatter dot plots (20 microtubules/cell, three independent experiments with n=30 mitotic cells in total, mean ± SD, unpaired two-tailed *t*-test). **(c)** HCT116 cells were transiently transfected with pcDNA3.1-FLAG-*CDK1-AF/-DN*, subjected to a double thymidine block, and subsequently released for 8.5 hours to accumulate cells in anaphase. Cells were treated with RO-3306 or Taxol for the last 24 hours before fixation. Cells were fixed and stained for fluorescence microscopy. Bar graphs show the proportion of anaphase cells exhibiting delayed CENP-C positive chromatids (three independent experiments with n=300 anaphase cells in total, mean ± SD, SD≠0: unpaired two-tailed *t*-test, SD=0: two-tailed one-sample *t*-test).

Both the CDK1 inhibitor RO-3306 and the microtubule stabilising agent Taxol could reduce microtubule polymerisation rates after *CDK1-AF* expression to levels observed in control cells (RO-3306: 16.0 µm/min, Taxol: 16.5 µm/min). Treatment of control cells with Taxol or RO-3306 did not influence microtubule polymerisation rates. (Figure 4.15b). Increased microtubule polymerisation rates induced by elevated CDK1 activity also triggered the occurrence of lagging chromosomes in anaphase. 7.3 % of anaphase cells exhibited lagging chromosomes after expression of *CDK1-AF*. This could be diminished to 2.7 % and 3.3 % by CDK1 inhibition with RO-3306 or by restoration of normal microtubule growth rates by Taxol treatment, respectively. The incidence of lagging chromosomes did not change after expression of the kinase-dead *CDK1* mutant (3.0 %). Furthermore, neither RO-3306 nor Taxol treatments influenced chromosome segregation in HCT116 cells transfected with a control vector (Figure 4.15c).

To elucidate the effect of increased CDK1 activity on chromosomal stability, stable cell lines were generated. Single cell clones were isolated and cultured for 30 generations after transfection of HCT116 cells with either a control vector or plasmids encoding for *CDK1-AF* or *CDK1*-DN. Three single cell clones were characterised for each condition. Western blotting revealed different expression levels of the *CDK1* mutants in the various single cell clones (Figure 4.16a). The analysis of microtubule growth rates and chromosome segregation showed that low expression levels of *CDK1-AF* resulted in mitotic defects whereas *CDK1-DN* expression had no significant effects in comparison to control clones. In *CDK1-AF* expressing single cell clones, microtubule growth rates ranged from 18.6 µm/min to 19.6 µm/min and, consequently, lagging chromosomes occurred in 6.7 % - 7.7 % of the analysed anaphase cells (Figure 4.16b, c). After stable expression of *CDK1-DN*, microtubule polymerisation rates ranged from 16.3 µm/min to 17.0 µm/min which is comparable with the results from control clones (Figure 4.16b). Accordingly, the incidence of lagging chromosomes ranged between 2.3 % and 4.0 % in control and *CDK1-DN* expressing single cell clones (Figure 4.16c).

To find out if increased CDK1 activity induces chromosomal instability, karyotype analyses were performed using mitotic chromosome spreads. An aberrant karyotype could be detected in 14 % - 16 % of the analysed mitotic control cells. Similar results (18 % - 20 %) were obtained for single cell clones with permanent *CDK1-DN* expression. A significant increase of the proportion of cells with a karyotype deviating from the modal number to 32 % - 34 % was observed upon expression of *CDK1-AF*

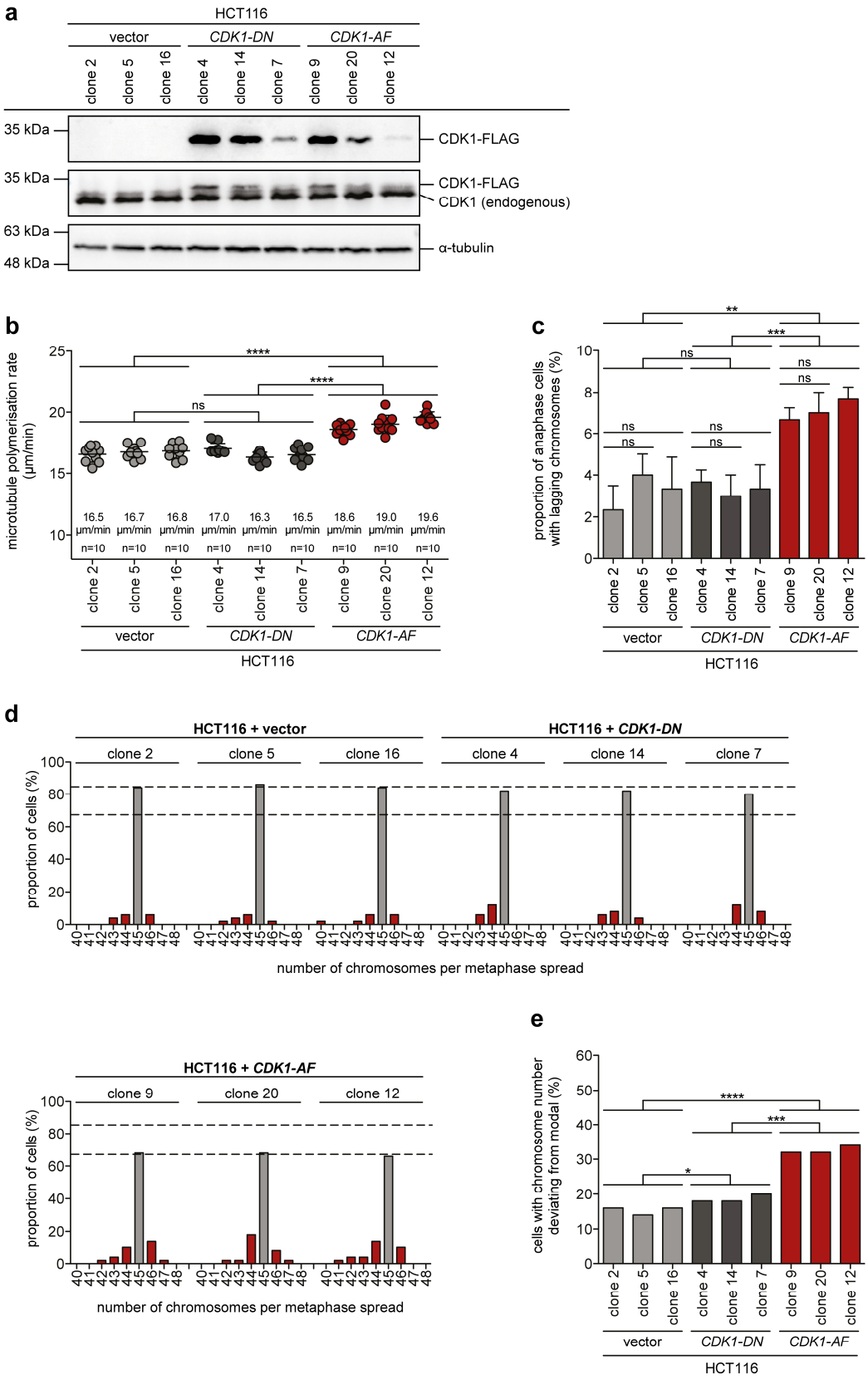

Figure 4.16: Stable expression of a constitutively active *CDK1* mutant causes mitotic errors and chromosomal instability in HCT116 cells.
(a) Stable expression of *CDK1* mutants. Single cell clones were generated after transfection of HCT116 cells with pcDNA3.1-FLAG-*CDK1-AF/-DN*. Western blots show the protein levels of endogenous and FLAG-tagged CDK1 in three single cell clones per condition. α-tubulin was

used as loading control. **(b)** *CDK1-AF/-DN* expressing single cell clones were transfected with pEGFP-*EB3*. 48 hours after transfection, cells were accumulated in mitosis by treatment with 2.0 µM DME for 1 hour and live-cell microscopy was performed. Scatter dot plots depict average microtubule polymerisation rates (20 microtubules/cell, n=10 mitotic cells, mean ± SD, unpaired two-tailed *t*-test). **(c)** Lagging chromosomes were analysed in HCT116 derived single cell clones expressing *CDK1* mutants. For this purpose, cells were fixed 8.5 hours after release from a double thymidine block, and the DNA, CENP-C, and α-tubulin were stained for fluorescence microscopy. The bar graphs show the proportion of anaphase cells with lagging chromosomes (three independent experiments with n=300 anaphase cells in total, mean ± SD, unpaired two-tailed *t*-test). **(d)** Mitotic chromosome spreads were used for karyotype analysis. The indicated single cell clones were arrested in mitosis by treatment with 2.0 µM DME for 4 hours before fixation. The proportion of cells with the indicated chromosome numbers is shown in the bar graphs (n= 50 metaphase spreads per clone). Dashed lines represent the average proportion of HCT116 cells with 45 chromosomes in clones transfected with either a control vector or a plasmid encoding *CDK1-AF*. **(e)** The percentage of cells with a chromosome number which differs from the modal number (45 chromosomes in HCT1116) is illustrated. Calculations are based on the results shown in (d) (n=50 metaphase spreads per clone, unpaired two-tailed *t*-test).

(Figure 4.16d, e). However, this level was not as high as in HCT116 cells after loss of *TP53* and *TP73* (Figure 4.4, Figure 4.11b, c).

The results obtained after Wee1 inhibition and *CDK1-AF/-DN* expression indicate that increased CDK1 activity is a trigger for elevated microtubule polymerisation rates, chromosome missegregation, and W-CIN.

4.1.5 Inhibition of CDK1 reduces increased microtubule polymerisation rates and chromosome missegregation in chromosomally instable colorectal cancer cell lines

Previous work demonstrated that colorectal cancer cell lines exhibiting W-CIN show elevated microtubule polymerisation rates and a higher incidence of lagging chromosomes in comparison to colorectal cancer cell lines characterised by a MIN/MSI phenotype (Ertych *et al*., 2014). These results could be confirmed in this study. The chromosomally stable cancer cell lines HCT116, DLD-1, and RKO showed microtubule polymerisation rates ranging from 16.6 µm/min to 16.7 µm/min whereas the chromosomally instable cell lines SW480, SW620, and HT29 exhibited microtubule polymerisation rates of 19.0 µm/min, 19.1 µm/min, and 19.9 µm/min, respectively (Figure 4.17a). Accordingly, the proportion of anaphase cells with lagging chromosomes was significantly higher in W-CIN cell lines (7.7 % - 8.7 %) than in MIN/MSI cell lines (2.0 % - 3.3 %) (Figure 4.17b). Importantly, mild inhibition of CDK1 using 1.0 µM RO-3306 restored normal microtubule growth rates (16.7 µm/min - 17.0 µm/min) and reduced the occurrence of lagging chromosomes (3.7 % - 4.3 %) in W-CIN cell lines. In MIN/MSI cell lines, RO-3306 did neither affect microtubule growth rates nor chromosome segregation (Figure 4.17a, b).

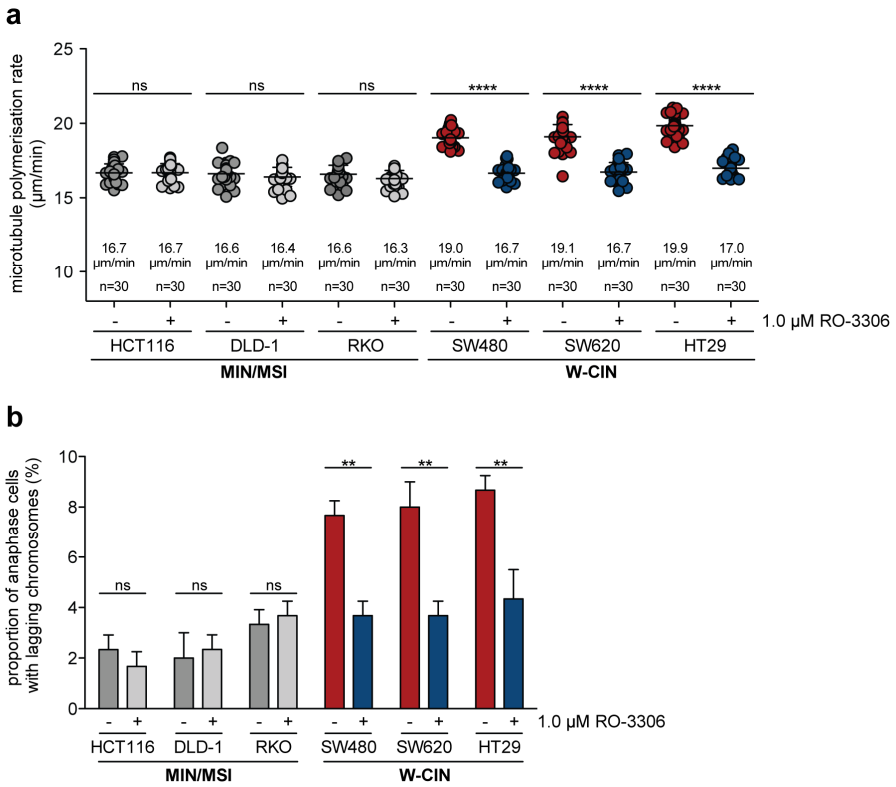

Figure 4.17: CDK1 inhibition rescues increased microtubule polymerisation rates and the occurrence of lagging chromosomes in chromosomally instable cell lines.
(a) Different colorectal cancer cell lines either characterised by MIN/MSI or W-CIN were transfected with pEGFP-*EB3.* Cells were treated with the CDK1 inhibitor RO-3306 for 16 hours. To accumulate cells in mitosis, cells were incubated with 2.0 µM DME for 1-2 hours. Scatter dot plots depict average microtubule-plus end assembly rates (20 microtubules/cell, three independent experiments with n=30 mitotic cells in total, mean ± SD, unpaired two-tailed *t*-test). **(b)** Chromosomally stable or instable colorectal cancer cell lines were synchronised at the G1/S transition with a double thymidine block and released for 8.5-9.0 hours. Cells were cultured in the presence or absence of 1.0 µM RO-3306 for the last 24 hours prior to fixation. After fixation, the DNA, α-tubulin, and CENP-C were stained for fluorescence microscopy. The proportion of cells with lagging chromosomes is shown in the bar graphs (three independent experiments with n=300 anaphase cells in total, mean ± SD, unpaired two-tailed *t*-test).

Thus, mild CDK1 inhibition reduced abnormally high microtubule growth rates and the increased incidence of lagging chromosomes in the analysed cell lines characterised by W-CIN.

Western blotting was performed to elucidate if MIN/MSI and W-CIN cell lines differ in the protein levels of p73, p53, $p21^{CIP1}$, inactive phospho-CDK1 (Tyr15), and total CDK1. A clear correlation between W-CIN and reduced protein levels of p73, p53, or $p21^{CIP}$, or an increase in CDK1 levels or activity could not be detected. Interestingly, p53 protein levels were higher in the W-CIN cell lines than in MIN/MSI cell lines which seemed to contradict the hypothesis that p53 loss together with p73 loss might trigger W-CIN. However, the cell lines SW480, SW620, and HT29 carry mutations in the gene

TP53 which abrogate normal p53 function and are associated with hyperstabilisation of mutant p53 (Li *et al*., 2011; Muller and Vousden, 2014).

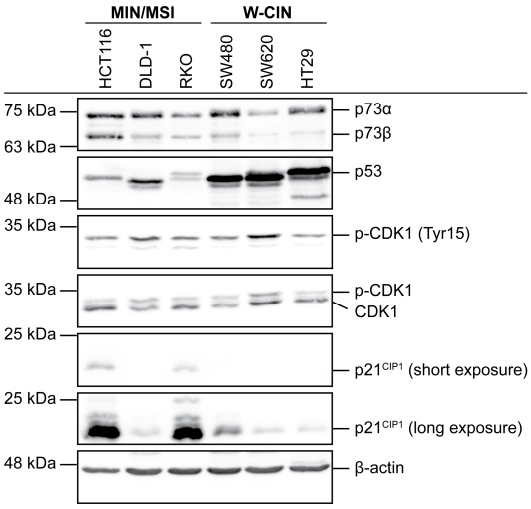

Figure 4.18: Protein levels of p73, p53, p21^{CIP1}, phospho-CDK1 (Tyr15), and CDK1 in different chromosomally stable (MIN/MSI) and instable (W-CIN) cell lines.
A representative Western blot detecting p73, p53, phospho-CDK1 (Tyr15), CDK1, and p21^{CIP1} in the indicated colorectal cancer cell lines. β-actin was used as loading control. Whole cell lysates were generated from asynchronously growing cells.

4.2 A possible link between increased CDK1 activity in S phase, deregulated DNA replication, and W-CIN

The experiments described in chapter 4.1 suggest that elevated activity of CDK1, a kinase known to regulate mitosis, can cause an increase in mitotic microtubule polymerisation rates, chromosome missegregation, and W-CIN. The aim of the next part of this study was to clarify if the observed mitotic defects were the result of increased CDK1 activity during mitosis or possibly during another cell cycle phase.

4.2.1 Elevated CDK1 activity in S phase increases microtubule polymerisation rates in mitosis and contributes to chromosome missegregation

At first, cell cycle progression of HCT116 cells was monitored by flow cytometry. After synchronisation by a double thymidine block, cells were washed with fresh growth medium for 30 minutes to remove thymidine and, thus, to allow cell cycle progression. Samples were fixed for analysis by flow cytometry 2.0, 4.0, 6.0, or 8.0 hours after thymidine washout to monitor cell cycle progression over time. Asynchronously growing cells and cells arrested at the G1/S border were used as controls. Cells were stained with propidium iodide to assess the DNA content and with MPM-2 antibodies targeting mitotic phospho-epitopes to distinguish G2 cells from mitotic cells. Analysis

of an asynchronously growing population of HCT116 cells revealed that 59.4 % of the cells were in G1 (2N DNA content), 16.2 % in S (2N - 4N DNA content), and 23.9 % in G2/M (4N DNA content), the mitotic index was 4.7 %. As expected, more than 90 % of the cells accumulated in G1/S after a double thymidine block. Cells progressed through S phase during the next hours which was reflected by an S phase population of 75.6 % 2.0 hours after washout and 56.4 % 4.0 hours after washout, respectively. 6.0 hours after thymidine removal, more than 80 % of the cells reached G2 phase. After 8.0 hours, most cells were still in G2 and cells started to enter mitosis which was reflected by the higher mitotic index (6.8 %). A small proportion of cells remained arrested in G1 after thymidine removal (Figure 4.19a).

Based on these results, a schedule for inhibitor treatments during specific intervals throughout the cell cycle was established (Figure 4.19b). The beginning of S phase was defined as timepoint t=0.0 h. If a double thymidine block was used for cell cycle synchronisation, washout started at t=-0.5 h. The period from t=0.0 h - 2.0 h was considered as early S phase, during t=2.0 h - 4.0 h cells progressed to late S phase,

a

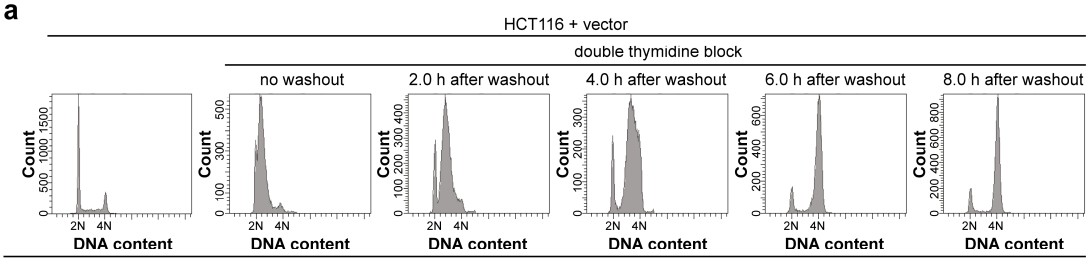

G1	59.4 %	50.7 %	16.3 %	12.1 %	10.2 %	12.0 %
S	16.2 %	44.2 %	75.6 %	56.4 %	8.3 %	4.0 %
G2/M	23.9 %	4.4 %	7.3 %	30.9 %	80.6 %	83.0 %
mitotic index	4.7 %	0.5 %	0.2 %	0.3 %	0.5 %	6.9 %

b

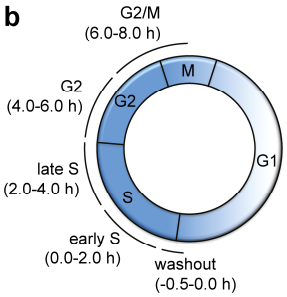

Figure 4.19: HCT116 cells progress from the G1/S border to mitosis within 8.5 hours.
(a) HCT116 cells were either grown asynchronously or subjected to a double thymidine block. Cells were washed with fresh growth medium for 30 minutes to remove thymidine. After release for additional 2.0 hours, 4.0 hours, 6.0 hours, or 8.0 hours, cells were fixed, stained with propidium iodide and anti-phospho-Ser/Thr-Pro MPM-2 antibodies, and analysed by flow cytometry. Cell cycle profiles and mitotic indices of the analysed cell populations are shown. **(b)** Scheme depicting a possible schedule for inhibitor treatments during defined intervals throughout the cell cycle based on the results shown in (a).

during t=4.0 h - 6.0 h cells reached G2 phase, t=6.0 h - 8.0 h included late G2 phase and entry to mitosis. The following EB3-GFP tracking experiments and quantifications of lagging chromosomes were performed in mitosis at t=8.0 h.

To find out if mitotic defects occurred because of elevated CDK1 activity in mitosis or during another cell cycle phase, *TP53*/*TP73*-deficient HCT116 cells and *CDKN1A*-deficient DLD-1 cells were treated with 1.0 µM RO-3306 for 2 hours during different cell cycle phases (Figure 4.19b).

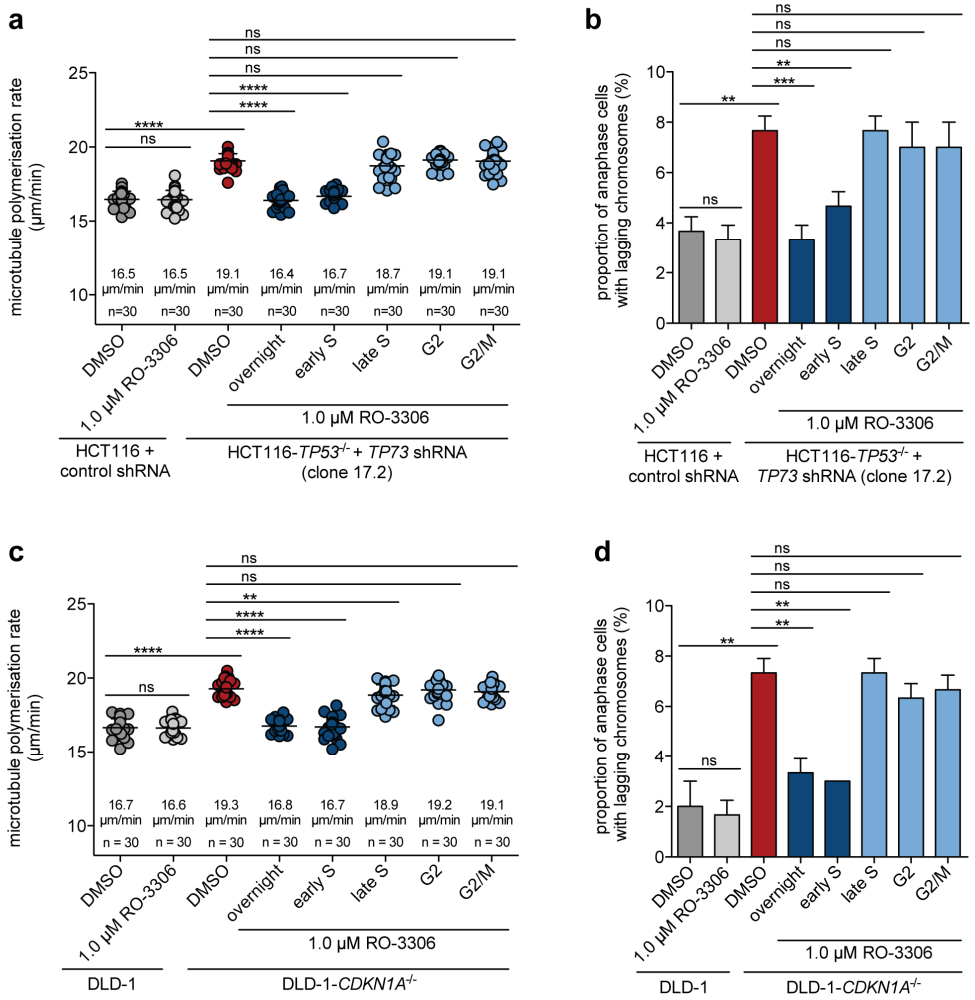

Figure 4.20: Mild inhibition of CDK1 in early S-phase restores normal microtubule polymerisation rates and chromosome segregation after loss of *TP53*/*TP73* or *CDKN1A*. **(a)** After transfection with pEGFP-*EB3*, HCT116 + control shRNA and HCT116-*TP53*$^{-/-}$ + *TP73* shRNA were treated with 1.0 µM RO-3306 either overnight or for 2 hours during early S phase, late S phase, G2 phase, or late G2/M. Overnight treatment with DMSO was used as control. 45 minutes before measurement, cells were additionally treated with 2.0 µM DME to arrest cells in mitosis. Average microtubule polymerisation rates are depicted in the scatter dot plots (20 microtubules/cell, three independent experiments with n=30 mitotic cells in total, mean ± SD, unpaired two-tailed *t*-test). **(b)** *TP53*/*TP73*-deficient HCT116 cells were subjected to a double thymidine block and then released for 8.5 hours. Cells were treated with 1.0 µM RO-3306 either for 24 hours or after thymidine washout for 2 hours during early S phase, late S phase, G2 phase, or G2/M. DMSO treatment for 24 hours was used as control. After fixation, cells were stained for fluorescence microscopy and anaphase cells were analysed. Bar graphs show the proportion of anaphase cells with lagging chromosomes (three independent

experiments with n=300 anaphase cells in total, mean ± SD, unpaired two-tailed *t*-test). **(c)** DLD-1 and DLD-1-*CDKN1A*$^{-/-}$ cells were treated as in (a). Scatter dot plots display average microtubule polymerisation rates (20 microtubules/cell, three independent experiments with n=30 mitotic cells in total, mean ± SD, unpaired two-tailed *t*-test). **(d)** DLD-1 and DLD-1-*CDKN1A*$^{-/-}$ cells were synchronised at the G1/S border by a double thymidine block and released for 9 hours. Further treatment as in (b). The percentage of cells exhibiting lagging chromosomes is depicted in the bar graphs (three independent experiments with n=300 anaphase cells in total, mean ± SD, SD≠0: unpaired two-tailed *t*-test, SD=0: two-tailed one-sample *t*-test).

As shown before (Figure 4.1c), EB3-GFP tracking experiments showed the increase of microtubule polymerisation rates from 16.5 µm/min to 19.1 µm/min after loss of *TP53*/*TP73*. A reduction to 16.4 µm/min could be observed after overnight treatment (16 hours) with 1.0 µM RO-3306 which is in accordance with previous results Figure 4.10a). Interestingly, mild inhibition of CDK1 for 2 hours during early S phase was as efficient as overnight treatment and reduced microtubule polymerisation rates to 16.7 µm/min. In contrast, microtubule polymerisation rates were not significantly influenced by treatment during late S phase (18.7 µm/min), G2 phase (19.1 µm/min) or late G2/M (19.1 µm/min) (Figure 4.20a). Similar results were obtained for DLD-1-*CDKN1A*$^{-/-}$ cells (Figure 4.20c). Corresponding to the increase in microtubule polymerisation rates, the proportion of cells with lagging chromosomes increased from 3.7 % to 7.7 % after loss of *TP53* and *TP73*. The incidence of lagging chromosomes could be reduced to 3.3 % after CDK1 inhibition overnight or to 4.7 % after CDK1 inhibition during early S phase, whereas the exposure to RO-3306 at later timepoints did not have a significant effect (late S: 7.7 %, G2: 7.0 %, G2/M: 7.0 %) (Figure 4.20b). The analyses of anaphase cells revealed similar results for DLD-1-*CDKN1A*$^{-/-}$ cells (Figure 4.20d). These first result surprisingly indicate that increased microtubule polymerisation rates and chromosome missegregation in mitosis are caused by unleashed CDK1 activity during S phase.

To further support these results, the Wee1 inhibitor MK-1775 was used to increase CDK1 activity in HCT116 cells in different time periods throughout the cell cycle (Figure 4.19b). DMSO treatment and overnight exposure to MK-1775 were used as controls. The presence of 75 nM MK-1775 either overnight or during early S phase increased microtubule polymerisation rates in HCT116 cells from 16.7 µm/min to 19.2 µm/min and 19.0 µm/min, respectively. In contrast, Wee1 inhibition during late S, G2, and G2/M phase resulted in microtubule polymerisation rates of 16.9 µm/min, 16.6 µm/min, and 16.4 µm/min, which were comparable with the growth rates determined in DMSO treated control cells (16.7 µm/min) (Figure 4.21a). The elevated microtubule polymerisation rates, which were induced by Wee1 inhibition overnight or during early S phase, caused a higher incidence of lagging chromosomes.

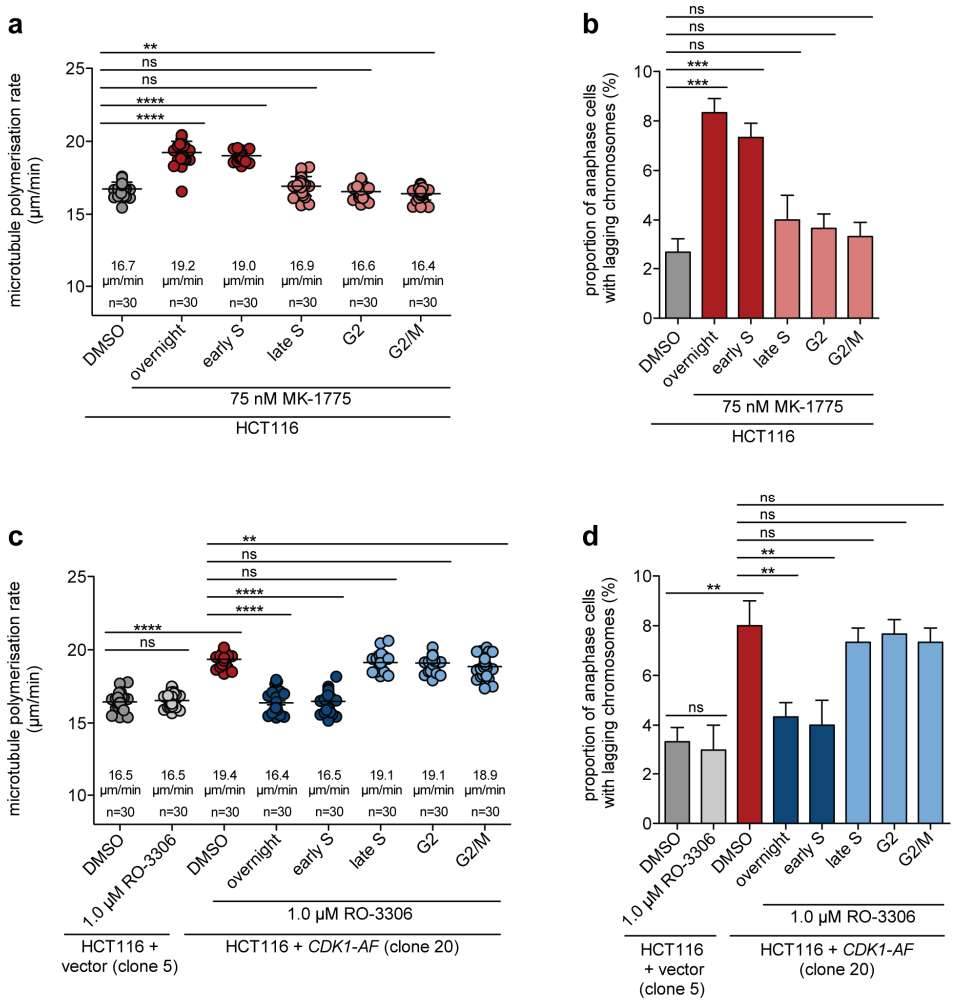

Figure 4.21: Increased CDK1 activity in early S phase elevates microtubule growth rates in mitosis and triggers chromosome missegregation in HCT116 cells.
(a) HCT116 cells transfected with pEGFP-*EB3* were exposed to 75 nM MK-1775 either overnight or for 2 hours during different cell cycle phases. Live-cell microscopy was performed after accumulation of cells in mitosis by treatment with 2.0 µM DME for 45 minutes. Average microtubule polymerisation rates are depicted in the scatter dot plots (20 microtubules/cell, three independent experiments with n=30 mitotic cells in total, mean ± SD, unpaired two-tailed *t*-test). **(b)** HCT116 cells were fixed 8.5 hours after release from a double thymidine block. Cells were treated with 75 nM MK-1775 either for 24 hours prior to fixation or for 2 hours during early S, late S, G2, or late G2/M. Microtubules, kinetochores and the DNA were stained for fluorescence microscopy to quantify lagging chromosomes. The incidence of lagging chromosomes in anaphase cells is shown in the bar graphs (three independent experiments with n=300 anaphase cells in total, mean ± SD, unpaired two-tailed *t*-test). **(c)** HCT116 +*CDK1-AF* and the corresponding control cells were transfected with pEGFP-*EB3*. Prior to live-cell microscopy, cells were treated with 1.0 µM RO-3306 for 16 hours or for 2 hours during early S, late S, G2, or G2/M. To accumulate cells in mitosis, cells were treated with 2.0 µM DME for 45 minutes. Scatter dot plots show average microtubule polymerisation rates of mitotic cells (20 microtubules/cell, three independent experiments with n=30 mitotic cells in total, mean ± SD, unpaired two-tailed *t*-test). **(d)** HCT116 + vector and HCT116 + *CDK1-AF* were synchronised at the G1/S border by a double thymidine block and released for 8.5 hours. Cells were treated with the CDK1 inhibitor RO-3306 either for 24 hours prior to fixation or for 2 hours during the indicated cell cycle phases. Fluorescence microscopy was performed in cells stained with Hoechst33342, anti-CENP-C and anti-α-tubulin antibodies. Bar graphs display the percentage of anaphase cells exhibiting lagging chromosomes (three independent experiments with n=300 anaphase cells in total, mean ± SD, unpaired two-tailed *t*-test).

The proportion of anaphase cells with chromosome segregation defects increased from 2.7 % in control cells to 8.3 % and 7.3 % after Wee1 inhibition overnight or during early S phase, respectively. In comparison to DMSO treated control cells, the incidence of lagging chromosomes did not change significantly after Wee1 inhibition during late S phase (4.0 %), G2 phase (3.7 %), or late G2/M (3.3 %) (Figure 4.21b).

To further confirm elevated CDK1 activity in early S phase as a cause for the observed mitotic defects, HCT116 cells stably expressing *CDK1-AF* were exposed to the CDK1 inhibitor RO-3306 for 2 hours in different cell cycle phases (Figure 4.19b). Only overnight treatment or treatment during early S phase significantly reduced microtubule polymerisation rates from 19.4 µm/min to 16.4 µm/min and 16.5 µm/min, respectively. Microtubule polymerisation rates ranged from 18.9 µm/min to 19.1 µm/min after CDK1 inhibition during late S, G2, or G2/M phase (Figure 4.21c). Corresponding to the effects on microtubule growth rates, mild CDK1 inhibition overnight or during early S phase prevented the occurrence of lagging chromosomes in HCT116 + *CDK1-AF* cells, whereas the incidence of lagging chromosomes remained unchanged after treatment at later time points (Figure 4.21d).

These results indicate that unleashed CDK1 activity specifically during early S phase causes increased microtubule polymerisation rates and chromosome segregation defects in the following mitosis.

4.2.2 Mild replication stress triggers increased microtubule polymerisation rates and chromosome segregation defects in mitosis

A first link between replication stress, which describes the impairment of replication fork progression during S phase, and W-CIN has been suggested previously (Burrell *et al*., 2013a). Moreover, our group has recently shown that mild replication stress induces an increase in microtubule polymerisation rates and chromosome missegregation (Böhly *et al*., 2019). In the light of these findings we hypothesised that deregulated CDK1 activity during early S phase might interfere with DNA replication which leads to defects in the following mitosis.

Aphidicolin, an inhibitor of the DNA polymerases α, δ, and ε (Baranovskiy *et al*., 2014; Cheng and Kuchta, 1993; Ikegami *et al*., 1978; Pletts Goscin and Byrnes, 1982), was used to induce mild replication stress in HCT116 cells. EB3-GFP tracking experiments after exposure to 100 nM Aphidicolin for 24 hours increased microtubule polymerisation rates from 16.7 µm/min to 19.2 µm/min (Figure 4.22a). Accordingly, the incidence of lagging chromosomes rose from 3.3 % in control cells to 7.0 % in

Aphidicolin treated cells (Figure 4.22b). It is of note that cell cycle progression was delayed upon Aphidicolin treatment. Therefore, the cells, which were fixed for the analysis of lagging chromosomes, had to be released for 9.5 hours after synchronisation with a double thymidine block. These results confirm previous findings from our lab (Böhly *et al*., 2019) and are in line with the hypothesis that increased CDK1 activity might influence DNA replication.

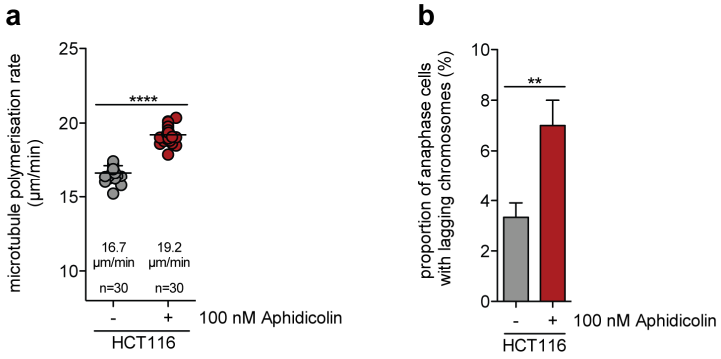

Figure 4.22: Mild replication stress induced by Aphidicolin treatment increases microtubule polymerisation rates and the incidence of lagging chromosomes in HCT116 cells.
(a) HCT116 cells were transfected with pEGFP-*EB3*. 24 hours prior to live-cell microscopy, cells were incubated with 100 nM Aphidicolin. Live-cell microscopy was performed in mitotic cells after treatment with 2.0 µM DME for 1 hour. Scatter dot plots show average microtubule polymerisation rates (20 microtubules/cell, three independent experiments with n=30 mitotic cells in total, mean ± SD, unpaired two-tailed *t*-test). **(b)** HCT116 cells were synchronised with a double thymidine block and then released for 9.5 hours. 24 hours prior to fixation, Aphidicolin was added. Cells were stained for fluorescence microscopy and chromosome segregation was evaluated in anaphase cells. Bar graphs display the percentage of anaphase cells with lagging chromosomes (three independent experiments with n=300 anaphase cells in total, mean ± SD, unpaired two-tailed *t*-test).

4.2.3 Elevated origin firing during DNA replication increases microtubule growth rates and the incidence of lagging chromosomes

Moiseeva *et al.* (2019) described a role of CDK1 activity, which can be increased by inhibition of ATR-CHK1 signalling, in the regulation of CDC7-dependent origin firing during S-phase (Figure 1.5). To test if inhibition of ATR signalling mimics the mitotic defects observed upon increased CDK1 activity, EB3-GFP tracking experiments were performed in HCT116 cells after ATR inhibition using the small molecule inhibitor ETP-46464 (Toledo *et al*., 2011). In fact, exposure to the ATR inhibitor for 16 hours increased microtubule polymerisation rates from 16.5 µm/min to 19.5 µm/min (Figure 4.24a). In accordance with the pathway described by Moiseeva *et al.* (2019), mild inhibition of CDK1 and CDC7 by RO-3306 and XL-413 (Koltun *et al*., 2012), respectively, rescued the elevated microtubule growth rates upon ATR inhibition (1.0 µM RO-3306: 16.4 µm/min, 1.0 µM XL-413: 16.3 µm/min) (Figure 4.24a).

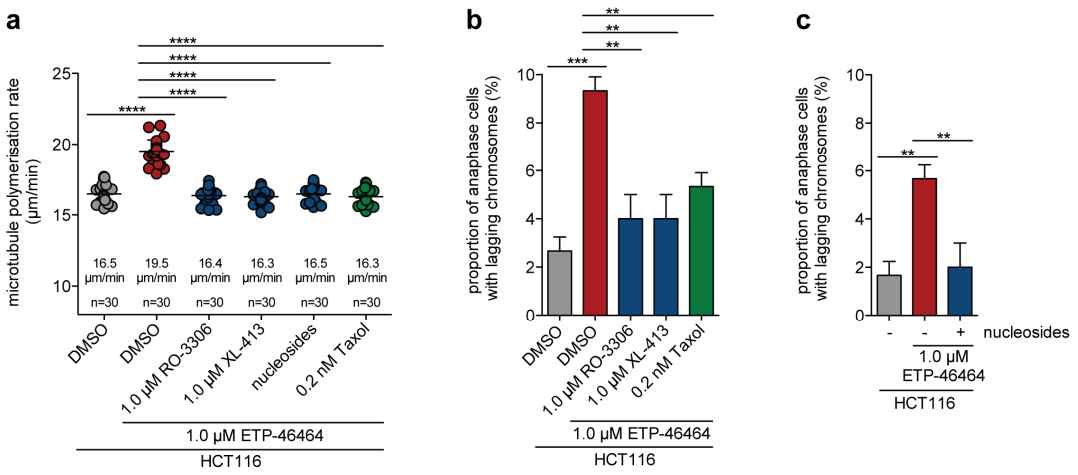

Figure 4.23: ATR inhibition induces increased microtubule polymerisation rates and lagging chromosomes in HCT116 cells.
(a) The kinase ATR was inhibited in *EB3-GFP* expressing HCT116 cells by treatment with 1.0 µM ETP-46464 for 16 hours. ATR inhibition was combined with treatment with 1.0 µM RO-3306, 1.0 µM XL-413, nucleosides (30 µM 2′-deoxyadenosine monohydrate, 30 µM 2′-deoxycytidine hydrochloride, 30 µM 2′-deoxyguanosine monohydrate, 30 µM thymidine), or 0.2 nM Taxol. Live-cell microscopy was performed after cells were accumulated in mitosis by treatment with 2.0 µM DME for 1 hour. Average microtubule polymerisation rates are shown in scatter dot plots (20 microtubules/cell, three independent experiments with n=30 mitotic cells in total, mean ± SD, unpaired two-tailed *t*-test). **(b)** HCT116 cells were arrested at the G1/S border by a double thymidine block and then released into the cell cycle for 8.5 hours. Cells were treated with 1.0 µM ETP-46464 for 24 hours prior to fixation. Cells were additionally treated with 1.0 µM RO-3306, 1.0 µM XL-413, or 0.2 nM Taxol. After fixation, cells were stained for fluorescence microscopy and the occurrence of lagging chromosomes during anaphase was quantified. Bar graphs illustrate the percentage of anaphase cells with lagging chromosomes (three independent experiments with n=300 anaphase cells in total, mean ± SD, unpaired two-tailed *t*-test). **(c)** Asynchronously growing cells were treated with the ATR inhibitor ETP-46464 for 24 hours. Additionally, growth medium was supplemented with nucleosides (30 µM 2′-deoxyadenosine monohydrate, 30 µM 2′-deoxycytidine hydrochloride, 30 µM 2′-deoxyguanosine monohydrate, 30 µM thymidine). Cells were fixed and stained for fluorescence microscopy. Bar graphs show the incidence of lagging chromosomes in anaphase cells (three independent experiments with n=300 anaphase cells in total, mean ± SD, unpaired two-tailed *t*-test).

It has been described before that supplementation with nucleosides can rescue replication stress (Bester *et al*., 2011), which can be a consequence of increased origin firing (Zhong *et al*., 2013). Therefore, EB3-GFP tracking experiments were performed in HCT116 cells after treatment with 1.0 µM ETP-46464 in combination with 30 µM 2′-deoxyadenosine monohydrate, 30 µM 2′-deoxycytidine hydrochloride, 30 µM 2′-deoxyguanosine monohydrate, and 30 µM thymidine. Nucleoside supplementation reduced microtubule growth rates upon ATR inhibition from 19.5 µm/min to 16.5 µm/min indicating an interplay of origin firing and replication stress. However, it is of note that neither origin firing nor replication stress were directly detected by DNA combing assays. As a control, the microtubule-stabilising agent Taxol was used to restore normal microtubule polymerisation rates after ATR inhibition (16.3 µm/min) (Figure 4.23a). The proportion of cells with chromosome

segregation defects rose significantly from 2.7 % to 9.3 % upon ATR inhibition. The incidence of lagging chromosomes could be significantly reduced to 4.0 % after additional treatment with 1.0 µM RO-3306 or 1.0 µM XL-413, and to 5.3 % after treatment with 0.2 nM Taxol (Figure 4.23b). The influence of nucleoside supplementation on the incidence of lagging chromosomes after ATR inhibition was evaluated in asynchronously growing cells. HCT116 cells were treated with 1.0 µM ETP-46464 ± nucleosides for 24 hours prior to fixation. The inhibition of ATR increased the incidence of lagging chromosomes from 1.7 % to 5.7 % in asynchronously growing cells. The additional supplementation with nucleosides reduced the proportion of cells with lagging chromosomes to 2.0 % (Figure 4.23c). It is of note that lagging chromosomes occurred more frequently when the ATR inhibitor was applied overnight in cells subjected to a double thymidine block (synchronised cells: 9.3 %, asynchronous cells: 5.7 %) (Figure 4.23b, c). These results might indicate additive effects of ATR inhibition and a double thymidine block, which is based on the interference with DNA replication.

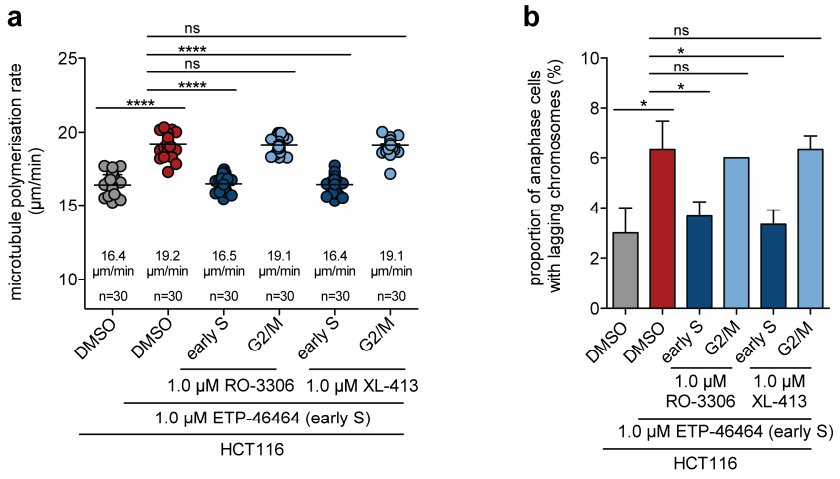

Figure 4.24: ATR inhibition in early S phase is sufficient to induce mitotic defects which can be rescued by simultaneous partial inhibition of CDK1 or CDC7.
(a) HCT116 cells expressing *EB3-GFP* were exposed to 1.0 µM ETP-46464 for 2 hours during early S phase. ATR inhibition was combined with partial CDK1 or CDC7 inhibition either at the same time (early S phase) or during G2/M. Microtubule polymerisation rates were determined in mitotic cells which were arrested in mitosis by treatment with 2.0 µM DME for 45 minutes. Scatter dot plots show average microtubule polymerisation rates which were determined in mitotic cells (20 microtubules/cell, three independent experiments with n=30 mitotic cells in total, mean ± SD, unpaired two-tailed t-test). **(b)** After synchronisation by a double thymidine block, HCT116 cells were released for 8.5 hours. Cells were treated with 1.0 µM ETP-46464 for 2 hours after thymidine washout (early S phase). Additionally, 1.0 µM RO-3306 or 1.0 µM XL-413 were added for 2 hours during early S phase or G2/M. To evaluate chromosome segregation, anaphase cells were analysed after staining for fluorescence microscopy. Bar graphs show the percentage of anaphase cells with lagging chromosomes (three independent experiments with n=300 anaphase cells in total, mean ± SD, SD≠0: unpaired two-tailed *t*-test, SD=0: two-tailed one-sample *t*-test).

To verify that alterations during S phase were responsible for the observed defects in the following mitosis, ATR was inhibited for only 2 hours during early S phase either alone or together with CDK1 or CDC7. As controls, the CDK1 and CDC7 inhibitors were also applied during G2/M. EB3-GFP tracking experiments showed an increase of mitotic microtubule growth rates from 16.4 µm/min to 19.2 µm/min after ATR inhibition during early S phase. The additional inhibition of CDK1 during early S phase was sufficient to restore normal microtubule polymerisation rates (16.5 µm/min) whereas inhibitor treatment during G2/M did not result in a rescue (19.1 µm/min). Similar results were obtained for CDC7 inhibition during early S phase (16.4 µm/min) and G2/M (19.1 µm/min) (Figure 4.24a). The incidence of lagging chromosomes rose from 3.0 % to 6.3 % after exposure of HCT116 cells to 1.0 µM ETP-46464 for 2 hours during early S phase. This effect could be prevented by combining ATR inhibition with partial CDK1 or CDC7 inhibition during early S phase (1.0 µM RO-3306: 3.7 %, 1.0 µM XL-413: 3.3 %). Treatment with CDK1 or CDC7 inhibitors during G2/M did not reduce the percentage of cells with lagging chromosomes upon ATR inhibition (1.0 µM RO-3306: 6.0 %, 1.0 µM XL-413: 6.3 %) (Figure 4.24b).

To test if RIF1, as a target of CDK1 (Figure 1.5), might be relevant for the maintenance of normal microtubule growth rates and chromosome segregation fidelity, HCT116 cells were analysed after transfection with siRNAs targeting either *RIF1* or *LUCIFERASE* as a control. The knockdown efficiency was confirmed by Western blotting (Figure 4.25a). EB3-GFP tracking experiments revealed an increase of microtubule polymerisation rates from 16.5 µm/min to 19.2 µm/min after knockdown of *RIF1*. The inhibition of CDK1, which acts upstream of RIF1 according to the model proposed by Moiseeva *et al.* (2019) (Figure 1.5), had only a minor effect on microtubule growth rates after knockdown of *RIF1* (18.9 µm/min). In contrast, the treatment with 0.5 µM and 1.0 µM XL-413 gradually reduced microtubule polymerisation rates to 17.0 µm/min and 16.5 µm/min, respectively. Additionally, Taxol treatment after *RIF1* knockdown resulted in microtubule growth rates of 16.6 µm/min, which were comparable with those in control cells transfected with *LUCIFERASE* siRNA. The different inhibitor treatments did not have a significant effect on microtubule growth rates in control cells (Figure 4.25b). Lagging chromosomes occurred more frequently after knockdown of *RIF1.* The number of cells with CENP-C positive lagging chromatids in anaphase increased from 3.0 % to 6.7 % after *RIF1* knockdown. In accordance with the results from EB3-GFP tracking experiments, the proportion of cells exhibiting lagging chromosomes was significantly reduced after treatment with XL-413 (0.5 µM: 3.7 %, 1.0 µM: 2.7 %) and 0.2 nM Taxol

(3.3 %), but not after treatment with 1.0 µM RO-3306 (6.3 %). An influence of the different inhibitors on chromosome segregation in cells transfected with *LUCIFERASE* siRNA could not be detected (Figure 4.25c).

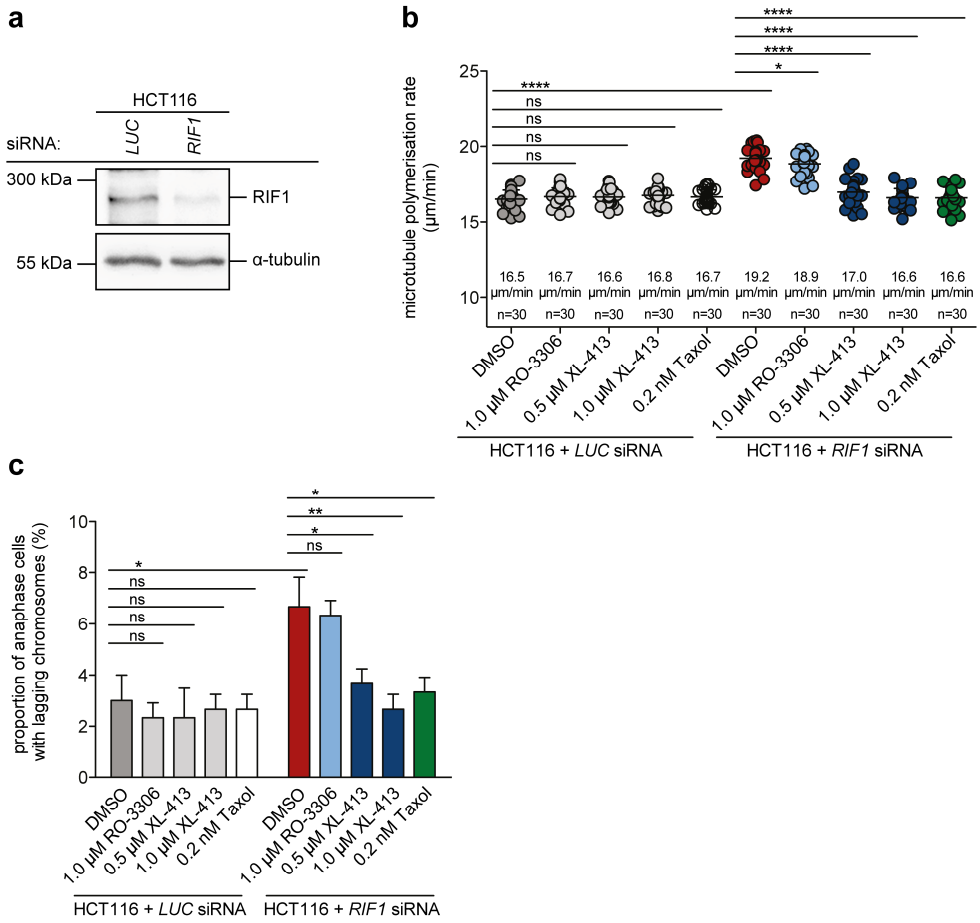

Figure 4.25: Knockdown of *RIF1* results in increased microtubule polymerisation rates and a higher incidence of lagging chromosomes in HCT116 cells.
(a) HCT116 cells were transfected with 60 pmol *LUCIFERASE* (*LUC*) or 60 pmol *RIF1* siRNA. Protein levels of RIF1 were assessed by Western blotting to confirm knockdown efficiency. α-tubulin was detected to verify equal protein loading. **(b)** HCT116 cells were transfected with pEGFP-*EB3* and siRNAs targeting *RIF1* or *LUCIFERASE* (*LUC*) as a control. Cells were exposed to the indicated inhibitors for 16 hours prior to live-cell microscopy. Additionally, cells were accumulated in mitosis by treatment with 2.0 µM DME for 1 hour. Average microtubule polymerisation rates are depicted in scatter dot plots (20 microtubules/cell, three independent experiments with n=30 mitotic cells in total, mean ± SD, unpaired two-tailed *t*-test). **(c)** HCT116 cells were transfected with 60 pmol *LUCIFERASE* (*LUC*) or *RIF1* siRNA and subsequently subjected to a double thymidine block. After thymidine removal, cells were released into the cell cycle for 8.5 hours, fixed, and stained for fluorescence microscopy. Bar graphs show the proportion of anaphase cells with lagging chromosomes (three independent experiments with n=300 anaphase cells in total, mean ± SD, unpaired two-tailed *t*-test).

ATR inhibition has been described to promote CDC7-dependent origin firing via increased CDK1 activity and the consequently reduced activity of the phosphatase complex RIF1-PP1 (Moiseeva *et al*., 2019). The results presented here support the relevance of this pathway for the induction of chromosome missegregation in mitosis.

In fact, both ATR inhibition and depletion of *RIF1* mimic the mitotic defects that are caused by increased CDK1 activity.

4.2.4 Nucleoside supplementation restores normal microtubule polymerisation rates and chromosome segregation in cells with increased CDK1 activity

Nucleoside supplementation has been described as a possible approach to reduce replication stress (Bester *et al*., 2011). To test if replication stress might be a trigger for elevated microtubule growth rates and the increased incidence of lagging chromosomes upon loss of the transcription factors p53 and p73, *TP53*/*TP73*-deficient HCT116 cells were incubated with 30 µM 2′-deoxyadenosine monohydrate, 30 µM 2′-deoxycytidine hydrochloride, 30 µM 2′-deoxyguanosine monohydrate, and 30 µM thymidine for 48 hours.

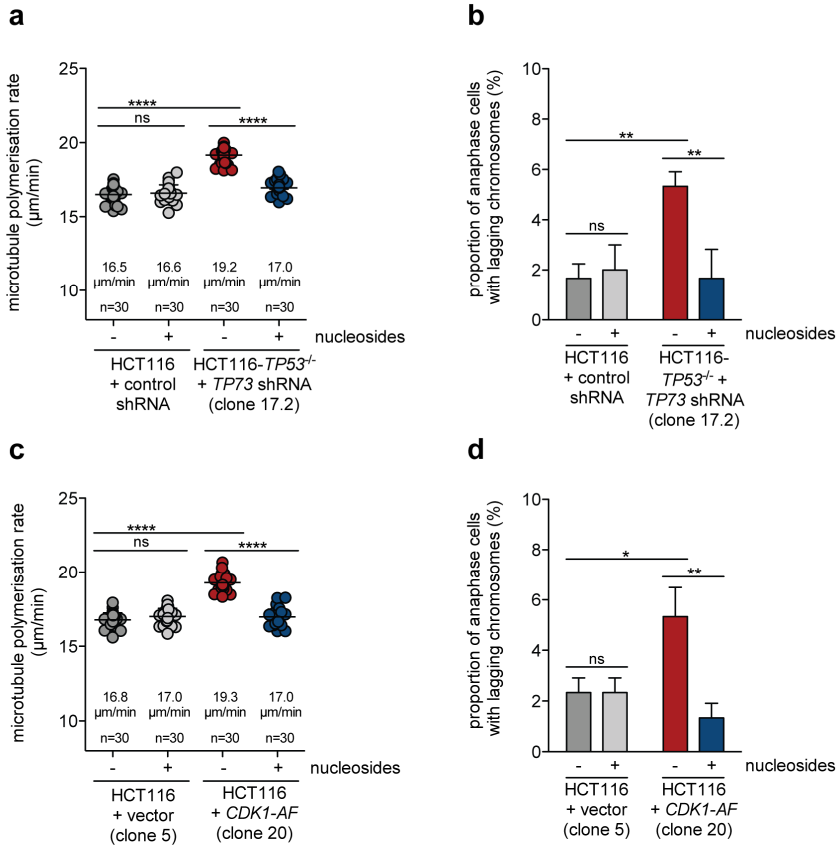

Figure 4.26: Nucleoside supplementation was sufficient to restore normal microtubule polymerisation rates and chromosome segregation after loss of *TP53*/*TP73* or expression of *CDK1-AF* in HCT116 cells.
(a) EB3-GFP tracking experiments were performed in *TP53*/*TP73*-deficient HCT116 and the corresponding control cells after incubation with 30 µM 2′-deoxyadenosine monohydrate, 30 µM 2′-deoxycytidine hydrochloride, 30 µM 2′-deoxyguanosine monohydrate, and 30 µM thymidine for 48 hours. To arrest cells in mitosis, they were treated with 2.0 µM DME for 1 hour prior to live-cell microscopy. Scatter dot plots show average microtubule polymerisation rates (20 microtubules/cell, three independent experiments with n=30 mitotic cells in total, mean ± SD, unpaired two-tailed *t*-test). **(b)** Asynchronously growing *TP53*/*TP73*-deficient HCT116 and the corresponding control cells were treated with 30 µM 2′-deoxyadenosine monohydrate, 30 µM 2′-deoxycytidine hydrochloride, 30 µM 2′-deoxyguanosine monohydrate, and 30 µM

thymidine for 48 hours. After fixation, DNA, kinetochores, and microtubules were stained for fluorescence microscopy. Anaphase cells were analysed to quantify the occurrence of lagging chromosomes, which is shown in the bar graphs (three independent experiments with n=300 anaphase cells in total, mean ± SD, unpaired two-tailed *t*-test). **(c)** HCT116 + vector and HCT116 + *CDK1-AF* cells were treated as in (a). Average microtubule polymerisation rates are illustrated in the scatter dot plots (20 microtubules/cell, three independent experiments with n=30 mitotic cells in total, mean ± SD, unpaired two-tailed *t*-test). **(d)** HCT116 cells stably expressing *CDK1-AF* and the corresponding control cells were treated as described in (b). Bar graphs show the percentage of anaphase cells exhibiting lagging chromosomes (three independent experiments with n=300 anaphase cells in total, mean ± SD, unpaired two-tailed *t*-test).

Nucleoside supplementation rescued microtubule polymerisation rates in *TP53*/*TP73*-deficient HCT116 cells from 19.2 µm/min to 17.0 µm/min. In contrast, microtubule growth rates of control cells (16.5 µm/min) were not influenced by nucleoside supplementation (Figure 4.26a). Similar results were obtained in EB3-GFP tracking experiments performed with HCT116 + *CDK1-AF* and the corresponding control cells (Figure 4.26c). The influence of nucleoside supplementation on the occurrence of lagging chromosomes was analysed in asynchronously growing cells. After loss of p53 and p73, 5.0 % of the analysed anaphase cells exhibited lagging chromosomes (Figure 4.26b), which was a lower incidence than observed in previous experiments (e. g. Figure 4.1b, Figure 4.2b, e). This indicates that a double thymidine block, which interferes with DNA replication, might influence chromosome segregation to some extent. Nonetheless, significant differences between the indicated cell lines and treatment conditions could be observed. After nucleoside supplementation, lagging chromosomes could be observed in only 1.7 % of the analysed anaphase cells. In control cells, the proportion of anaphase cells with lagging chromosomes was 1.7 % and 2.0 % without and after nucleoside supplementation, respectively (Figure 4.26b). Nucleoside supplementation had similar effects on the incidence of lagging chromosomes in HCT116 + *CDK1-AF* (Figure 4.26d).

These results suggest that mitotic defects occur because of impaired DNA replication as a consequence of increased CDK1 activity, either due to *TP53*/*TP73* depletion or *CDK1-AF* expression.

4.2.5 Inhibition of origin firing rescues mitotic defects in cells with increased CDK1 activity

To test if the mitotic defects observed upon *TP53*/*TP73* depletion or *CDK1-AF* expression might depend on CDC7-dependent origin firing, cells were treated with two structurally different CDC7 inhibitors, namely XL-413 and PHA-767491 (Koltun *et al*., 2012; Montagnoli *et al*., 2008), and mitotic phenotypes were evaluated.

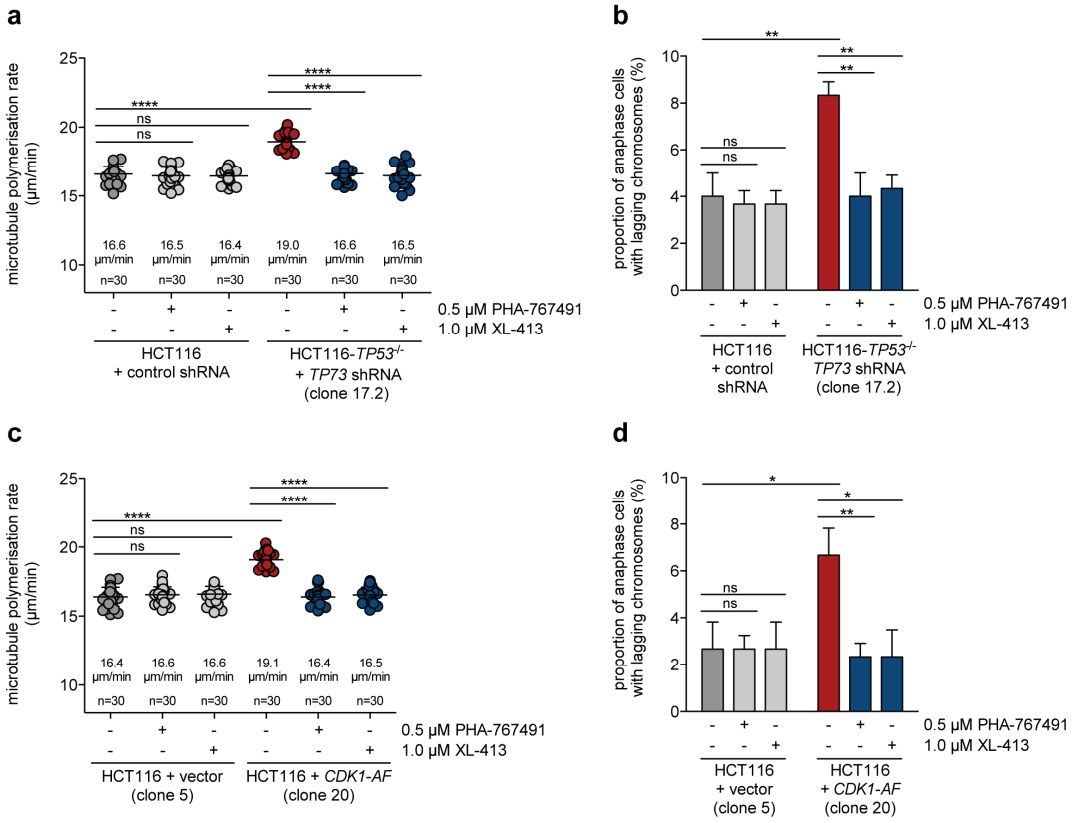

Figure 4.27: Inhibition of CDC7 rescues mitotic defects induced by loss of *TP53*/*TP73* or expression of *CDK1-AF* in HCT116 cells.
(a) HCT116 + control shRNA and HCT116-*TP53*$^{-/-}$ + *TP73* shRNA cells were transfected with pEGFP-*EB3*. 16 hours prior to live-cell microscopy, cells were treated with the CDC7 inhibitors PHA-767491 and XL-413. Cells were accumulated in mitosis by treatment with 2.0 µM DME for 1 hour. Average microtubule polymerisation rates were determined in mitotic cells and are illustrated in the scatter dot plots (20 microtubules/cell, three independent experiments with n=30 mitotic cells in total, mean ± SD, unpaired two-tailed *t*-test). **(b)** *TP53*/*TP73*-deficient HCT116 and the corresponding control cells were accumulated in anaphase by a double thymidine block followed by release for 8.5 hours. 24 hours prior to fixation, cells were treated with 0.5 µM PHA-767491 and 1.0 µM XL-413. Cells were stained for fluorescence microscopy and the incidence of lagging chromosomes was quantified, which is depicted in the bar graphs (three independent experiments with n=300 anaphase cells in total, mean ± SD, unpaired two-tailed *t*-test). **(c)** HCT116 + *CDK1-AF* and the corresponding control cells were treated as described in (a). Scatter dot plots display average microtubule polymerisation rates (20 microtubules/cell, three independent experiments with n=30 mitotic cells in total, mean ± SD, unpaired two-tailed *t*-test). **(d)** HCT116 cells stably transfected with an empty vector or a plasmid encoding for *CDK1-AF* were treated as in (b). Bar graphs show the percentage of anaphase cells with at least one delayed CENP-C positive chromatid (three independent experiments with n=300 anaphase cells in total, mean ± SD, unpaired two-tailed *t*-test).

Interestingly, increased microtubule polymerisation rates in *TP53*/*TP73*-deficient HCT116 cells could be rescued from 19.0 µm/min to 16.6 µm/min and 16.5 µm/min by treatment with PHA-767491 and XL-413, respectively. The CDC7 inhibitors did not have a significant influence on microtubule polymerisation rates of control cells (Figure 4.27a). The restoration of normal microtubule growth rates by CDC7 inhibition also led to a reduction of the incidence of lagging chromosomes after *TP53*/*TP73* depletion. The proportion of anaphase cells with lagging chromosomes in *TP53*/*TP73*-

deficient HCT116 cells was reduced from 8.3 % to 4.0 % and 4.3 % by treatment with 0.5 µM PHA-767491 and 1.0 µM XL-413, respectively. In control cells, 4.0 % of anaphase cells exhibited lagging chromosomes, which was not significantly changed by CDC7 inhibition (Figure 4.27b). CDC7 inhibition by PHA-767491 and XL-413 had similar effects on microtubule polymerisation rates and the occurrence of lagging chromosomes in HCT116 cells expressing *CDK1-AF* (Figure 4.27c, d).

To confirm that CDC7 activity is important during S phase, microtubule polymerisation rates and lagging chromosomes were analysed after specific CDC7 inhibition in S phase.

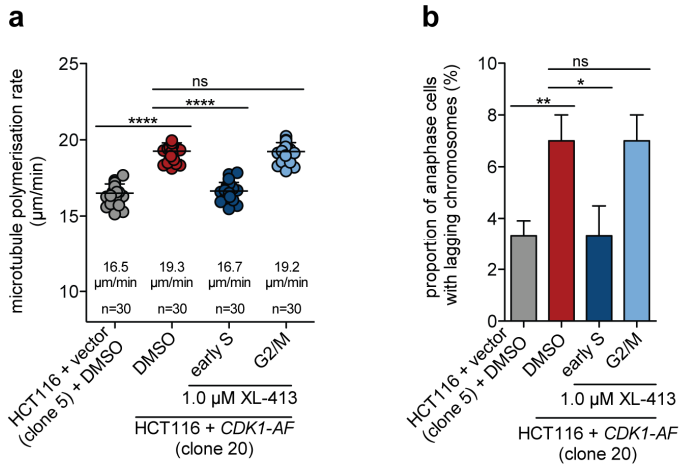

Figure 4.28: CDC7 inhibition in S phase restores normal microtubule polymerisation rates and chromosome segregation in HCT116 cells after expression of *CDK1-AF*.
(a) EB3-GFP tracking experiments were performed in HCT116 + vector and HCT116 + *CDK1-AF*. Cells were exposed to the CDC7 inhibitor XL-413 for 2 hours during early S or G2/M. To accumulate cells in mitosis, cells were treated with 2.0 µM DME for 45 minutes prior to live-cell microscopy. Scatter dot plots show average microtubule polymerisation rates (20 microtubules/cell, three independent experiments with n=30 mitotic cells in total, mean ± SD, unpaired two-tailed *t*-test). **(b)** *CDK1-AF* expressing HCT116 and the corresponding control cells were subjected to a double thymidine block and subsequently released for 8.5 hours. After thymidine removal, cells were treated with 1.0 µM XL-413 for 2 hours during early S phase or during G2/M. After fixation, DNA, kinetochores, and microtubules were stained for fluorescence microscopy. Bar graphs display the proportion of anaphase cells exhibiting lagging chromosomes (three independent experiments with n=300 anaphase cells in total, mean ± SD, unpaired two-tailed *t*-test).

EB3-GFP tracking experiments in *CDK1-AF* expressing HCT116 cells revealed that microtubule polymerisation rates were reduced from 19.3 µm/min to 16.7 µm/min after inhibition of CDC7 using XL-413 for 2 hours specifically during early S phase (Figure 4.28a). Correspondingly, treatment with XL-413 during early S phase decreased the incidence of lagging chromosomes from 7.0 % to 3.3 % (Figure 4.28b). The exposure to XL-413 during G2/M did neither change microtubule growth rates nor the occurrence of lagging chromosomes in comparison with solvent treated *CDK1-AF*

expressing HCT116 cells (Figure 4.28a, b). These results suggest that CDC7 specifically acts during S phase to mediate the mitotic defects observed upon *TP53*/*TP73* loss or *CDK1-AF* expression.

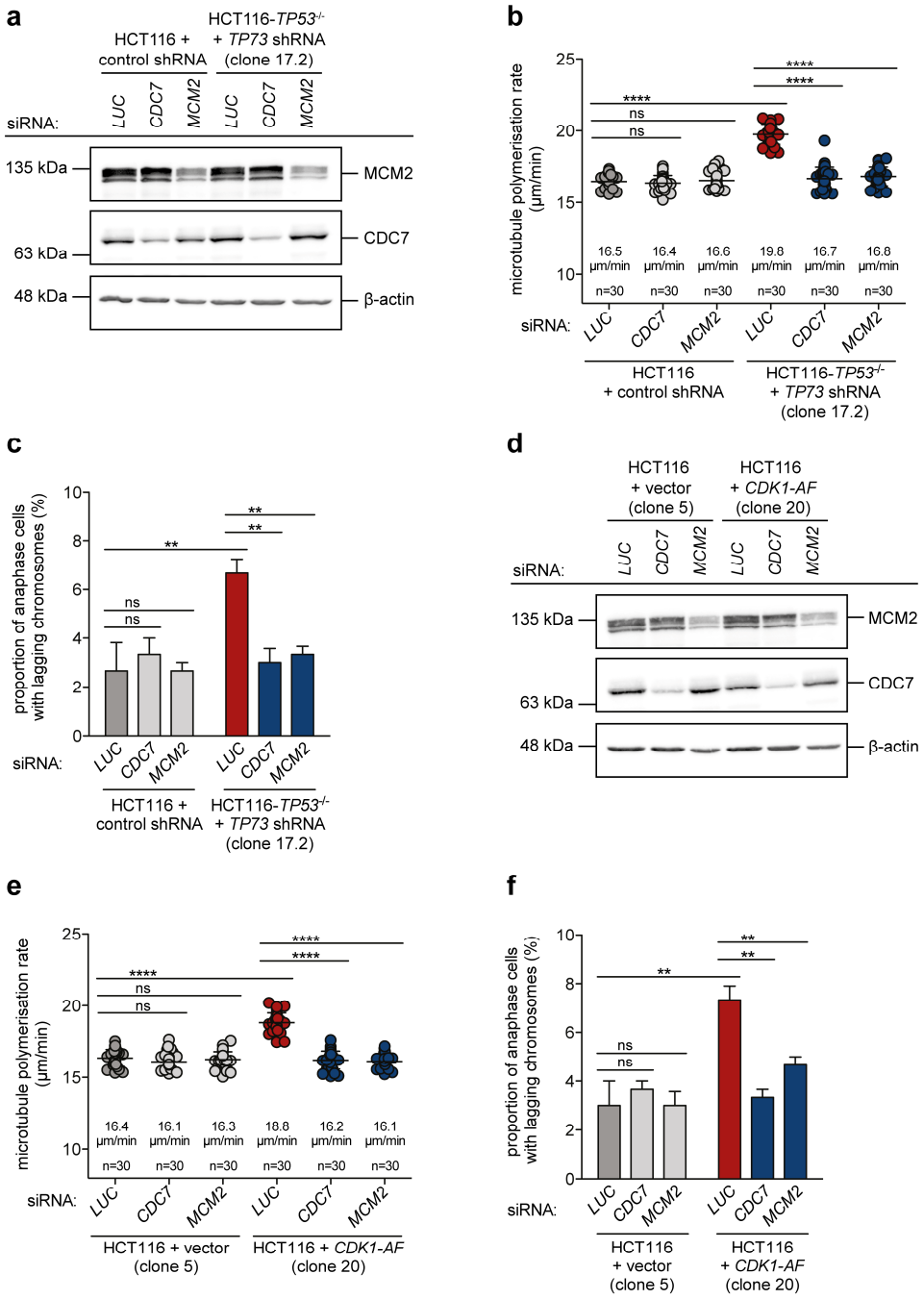

Figure 4.29: Knockdown of *CDC7* or *MCM2* restores normal microtubule polymerisation rates and chromosome segregation in HCT116 cells after loss of *TP53*/*TP73* or upon expression of *CDK1-AF*.
(a) *TP53*/*TP73*-deficient HCT116 cells and the corresponding control cells were transfected with 60 pmol siRNA targeting *LUCIFERASE* (*LUC*), *CDC7*, or *MCM2*. The protein levels of CDC7 and MCM2 48 hours after transfection were detected by Western blotting. β-actin was used as loading control. **(b)** EB3-GFP tracking experiments were performed after knockdown of *CDC7* or *MCM2* in the indicated cell lines. 48 hours after transfection, cells were accumulated in mitosis by treatment with 2.0 µM DME for 1 hour. Average microtubule growth

rates are shown in the scatter dot plots (20 microtubules/cell, three independent experiments with n=30 mitotic cells in total, mean ± SD, unpaired two-tailed *t*-test). **(c)** HCT116 + control shRNA and HCT116-*TP53*$^{-/-}$ + *TP73* shRNA were transfected with 60 pmol *LUCIFERASE* (*LUC*) siRNA, *CDC7* siRNA, or *MCM2* siRNA. Afterwards, a double thymidine block with subsequent release into the cell cycle for 8.5 hours was used to accumulate cells in anaphase. After fixation, cells were stained for fluorescence microscopy and anaphase cells were analysed to quantify the incidence of lagging chromosomes. Bar graphs show the proportion of anaphase cells with lagging chromosomes (three independent experiments with n=300 anaphase cells in total, mean ± SD, unpaired two-tailed *t*-test). **(d)** The indicated cell lines were transfected with 60 pmol *LUCIFERASE* (*LUC*) siRNA, *CDC7* siRNA, or *MCM2* siRNA. The knockdown efficiency was examined by Western blotting. β-actin was detected to confirm equal protein loading. **(e)** HCT116 + vector and HCT116 + *CDK1-AF* were treated as described in (b). EB3-GFP tracking experiments allowed the determination of average microtubule polymerization rates, which are illustrated in the scatter dot plots (20 microtubules/cell, three independent experiments with n=30 mitotic cells in total, mean ± SD, unpaired two-tailed *t*-test). **(f)** HCT116 cells expressing *CDK1-AF* and the corresponding control cells were treated as described in (c). Bar graphs depict the percentage of anaphase cells showing CENP-C-positive chromatids which were not correctly distributed to the two spindle poles (three independent experiments with n=300 anaphase cells in total, mean ± SD, unpaired two-tailed *t*-test).

To exclude unspecific effects of the used CDC7 inhibitors, siRNA targeting *CDC7* was used to modulate CDC7 activity in *TP53*/*TP73*-deficient HCT116 cells and in HCT116 cells expressing *CDK1-AF*. Additionally, siRNA-mediated knockdown of *MCM2* was used as a second approach to reduce origin firing and, thus, influence DNA replication. MCM2 is a component of the replicative helicase and its CDC7-mediated phosphorylation is required for the activation of origins of replication (Tsuji *et al*., 2006). The reduced expression of *CDC7* and *MCM2* after siRNA transfection of HCT116-*TP53*$^{-/-}$ + *TP73* shRNA cells, HCT116 + *CDK1-AF* cells, and the corresponding control cells was confirmed by Western blotting (Figure 4.29a, d). In HCT116-*TP53*$^{-/-}$ + *TP73* shRNA cells, microtubule polymerisation rates were reduced from 19.8 µm/min to 16.7 µm/min and 16.8 µm/min after transfection with *CDC7* siRNA and *MCM2* siRNA, respectively. In accordance with the results obtained from EB3-GFP tracking experiments, the proportion of lagging chromosomes in *TP53*/*TP73*-deficient HCT116 cells decreased from 6.7 % to 3.0 % and 3.3 % after knockdown of *CDC7* or *MCM2,* respectively (Figure 4.29c). Similarly, the knockdown of *CDC7* or *MCM2* rescued the elevated microtubule growth rates and the increased incidence of lagging chromosomes in HCT116 cells expressing *CDK1-AF* (Figure 4.29e, f). *CDC7* or *MCM2* expression levels did neither impact microtubule polymerisation rates nor chromosome segregation in the control cells stably transfected with either control shRNA (Figure 4.29b, c) or an empty vector (Figure 4.29e, f).

4.2.6 CDC7 inhibition restores normal microtubule growth rates and reduces chromosome missegregation in colorectal cancer cell lines exhibiting W-CIN

It has been shown before that replication fork progression is impaired in cancer cell lines characterised by W-CIN (Burrell *et al*., 2013a). In addition, our lab has shown previously that elevated microtubule growth rates and the incidence of lagging chromosomes in W-CIN cell lines were reduced by nucleoside supplementation (Böhly *et al*., 2019). This indicates that replication stress during S phase can induce abnormally high microtubule growth rates and chromosome missegregation.

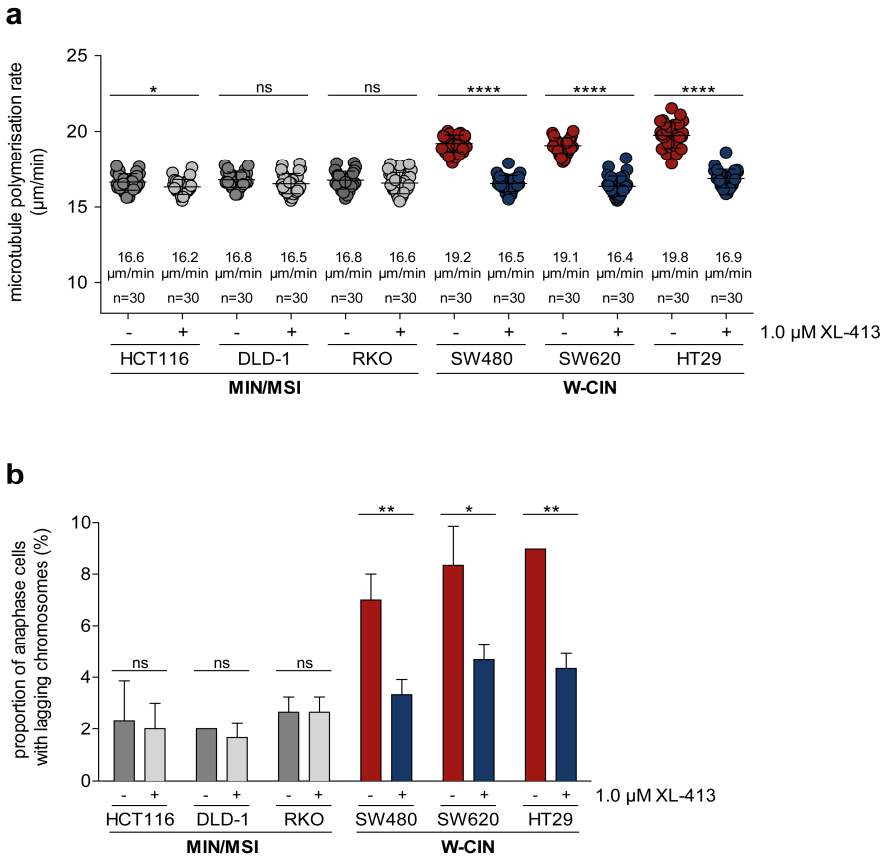

Figure 4.30: CDC7 inhibition reduces microtubule polymerisation rates and the incidence of lagging chromosomes in chromosomally instable colorectal cancer cells. **(a)** The indicated colorectal cancer cell lines, which were either characterised by MIN/MSI or W-CIN, were transfected with pEGFP-*EB3*. 16 hours prior to live-cell microscopy, cells were treated with 0.5 µM or 1.0 µM XL-413. Cells were accumulated in mitosis by incubation with 2.0 µM DME for 1-2 hours. Scatter dot plots illustrate average microtubule polymerisation rates (20 microtubules/cell, three independent experiments with n=30 mitotic cells in total, mean ± SD, unpaired two-tailed *t*-test). **(b)** The indicated cell lines were synchronised with a double thymidine block and subsequently released into the cell cycle for 8.5-9 hours. 24 hours prior to fixation, cells were exposed to 0.5 µM or 1.0 µM XL-413. The DNA, microtubules, and kinetochores were stained for fluorescence microscopy. Anaphase cells were analysed to quantify the occurrence of lagging chromosomes, which is shown in the bar diagram (three independent experiments with n=300 anaphase cells in total, mean ± SD, unpaired two-tailed *t*-test).

To check if abnormally increased origin firing might directly contribute to the aberrant mitotic phenotypes observed in colorectal cancer cell lines characterised by W-CIN, different colorectal cancer cell lines were treated with the CDC7 inhibitor XL-413. EB3-GFP tracking experiments revealed that the elevated microtubule growth rates in W-CIN cell lines (19.1 µm/min - 19.8 µm/min) were decreased to 16.4 µm/min - 16.9 µm/min by treatment with 1.0 µM XL-413 (Figure 4.30a). Accordingly, the incidence of lagging chromosomes in W-CIN cell lines was reduced from 7.0 % - 9.0 % to 3.3 % - 4.7 % after microtubule growth rates were decreased by exposure to 1.0 µM XL-413 (Figure 4.30b). In MIN/MSI cell lines, CDC7 inhibition by XL-413 hardly affected microtubule growth rates and the incidence of lagging chromosomes (Figure 4.30a, b). These results further support the hypothesis that deregulated origin firing during S phase impairs chromosome segregation in the following mitosis.

Altogether, the results presented here indicate that excessive CDC7-dependent origin firing upon increased CDK1 activity might contribute to the induction of increased mitotic microtubule polymerisation rates, chromosome missegregation, and W-CIN. However, further analyses are required to detect origin firing and replication fork progression, for example by DNA combing assays, and to elucidate the mechanisms leading from deregulated origin firing and/or replication stress to abnormally high microtubule polymerisation rates.

5 DISCUSSION

5.1 Increased CDK1 activity causes whole chromosomal instability by increasing microtubule growth rates in mitotic spindles

Recently, our lab has shown that increased mitotic microtubule polymerisation rates raise the incidence of lagging chromosomes leading to chromosome missegregation and W-CIN (Ertych *et al*., 2014). Cancer-relevant genetic alterations were analysed to find out if they contribute to the development of W-CIN by increasing microtubule growth rates. *TP53* loss or mutations belong to the most prevalent genetic lesions in human tumours including colorectal cancer (Kandoth *et al*., 2013; Muzny *et al*., 2012). In addition, several other cancer-relevant lesions lead to the loss of p53 function. For instance, mouse double-minute 2 (MDM2) is a ubiquitin ligase which targets p53 and, thus, promotes its proteasomal degradation (Honda *et al*., 1997; Kubbutat *et al*., 1997). In several tumour entities, the *MDM2* gene is overexpressed which is often associated with metastasis, therapy resistance, and poor prognosis (Rayburn *et al*., 2005). High MDM2 levels contribute to tumourigenesis and the development of chromosomal instability by both p53-dependent and p53-independent mechanisms (Eischen, 2016). Another possible route to p53 inactivation is its degradation mediated by the viral oncoprotein E6 after infection with the human papillomavirus types 16 and 18 (HPV-16/-18) (Scheffner *et al*., 1990), which can cause cervical cancer or head-and-neck cancer (Bosch *et al*., 2013). E6 promotes the interaction of p53 and the cellular ubiquitin ligase E6AP which finally results in p53's proteasomal degradation (Martinez-Zapien *et al*., 2016). However, loss of p53 alone is neither sufficient to increase microtubule growth rates nor to induce W-CIN and aneuploidy (Bunz *et al*., 2002; Ertych *et al*., 2014). These results could be confirmed in this study (Figure 4.1,Figure 4.4). Nonetheless, loss of *TP53* is strongly associated with W-CIN (Muzny *et al*., 2012). In cultured cells, it has been shown that chromosome missegregation and the proliferation of aneuploid cells are limited due to p53-induced cell cycle delay (Thompson and Compton, 2010). *Vice versa,* depletion of *TP53* resulted in tolerance of aneuploid karyotypes and the propagation of aneuploid cells. The p53 response might be triggered by gene dosage imbalances which arise due to aneuploidy (Thompson and Compton, 2010). Gene dosage alterations can also induce metabolic changes leading to an increased production of reactive oxygen species which trigger p53 signalling in an ATM-dependent manner (Li *et al*., 2010). Other groups suggested that p53 was activated upon DNA damage during cytokinesis in the presence of lagging chromosomes (Janssen *et al*., 2011) or upon

phosphorylation of H3.3 in misaligned chromosomes (Hinchcliffe *et al*., 2016). Thus, the growth impairment of aneuploid cells (Chunduri and Storchová, 2019; Williams *et al*., 2008) might be overcome by p53 inactivation in chromosomally instable cells. However, it has also been shown that lower rates of chromosome missegregation, which can be observed in tumours, do not necessarily trigger a strong p53 response (Santaguida *et al*., 2017). Previous findings from our lab revealed that the simultaneous loss of both *TP53* and *TP73* leads to increased microtubule polymerisation rates and W-CIN (Berger, 2016) which is in line with the results presented in this study (Figure 4.1,Figure 4.4). In contrast to *TP53*, *TP73* is rarely mutated in cancer but loss of its expression due to loss of its locus on chromosome arm 1p36 or promotor silencing is frequently detected (Corn *et al*., 1999; Kaghad *et al*., 1997; Martinez-Delgado *et al*., 2002; Puig *et al*., 2003). Interestingly, mice with heterozygous inactivating mutations of both *TP53* and *TP73* suffer from a higher tumour burden, develop more metastases, and have a reduced survival time in comparison with mice with a heterozygous inactivating mutation of only one transcription factor (Flores *et al*., 2005). This would be compatible with the presence of chromosomal instability in these mice, but it was not tested in this study. Our bioinformatic analyses showed that a small proportion of colorectal adenocarcinoma and breast cancer samples display *TP53* mutation in combination with reduced expression of *TP73* (Schmidt *et al*., 2021). Furthermore, overexpression of *ΔNp73*, which leads to the inactivation of both p53 and p73, is detected in various cancers (Di *et al*., 2013) and has been shown to promote the development of metastases (Steder *et al*., 2013). Additionally, our work showed that *ΔNp73* overexpression results in increased microtubule polymerisation rates, a higher incidence of lagging chromosomes, and W-CIN in otherwise chromosomally stable colorectal cancer cells (Berger, 2016; Schmidt *et al*., 2021). In conclusion, p53 and p73 seem to cooperate in their tumour suppressive function and in the maintenance of genomic stability and the inactivation of both transcription factors might contribute to the development of chromosomally instable tumours.

The gene *CDKN1A*, encoding for the cell cycle regulator $p21^{CIP1}$, is a well-known target of both p53 and p73 (Jost *et al*., 1997; Kaghad *et al*., 1997). In line with this, I could show that the restoration of *CDKN1A* expression rescued elevated microtubule polymerisation rates and the increased incidence of lagging chromosomes observed after *TP53*/*TP73* depletion (Figure 4.8). Furthermore, knockout of *CDKN1A* in an otherwise chromosomally stable colorectal cancer cell line mimics the phenotype observed after loss of *TP53* and *TP73* (Figure 4.5,Figure 4.6). This confirms previous

results from our group which were obtained after siRNA-mediated depletion of *CDKN1A* in HCT116 cells (Berger, 2016). It has previously been described that loss of *CDKN1A* causes mitotic defects including the occurrence of lagging chromosomes and a prolonged duration of mitosis (Kreis *et al*., 2014). The exact underlying mechanism remained unknown but it was proposed that increased CDK1 activity and decreased Aurora B activity in anaphase contribute to the mitotic defects observed upon *CDKN1A* loss (Kreis *et al*., 2014). Interestingly, our bioinformatic analyses of colorectal adenocarcinoma and breast cancer samples revealed that the expression of *CDKN1A* was reduced in cells with mutant *TP53* and this effect was even more pronounced after additional loss of *TP73*, although this additional lesion was only infrequently detected. Importantly, the decreased expression of *CDKN1A* was associated with a higher W-CIN score in these tumour samples (Schmidt *et al*., 2021). This in line with other studies demonstrating a correlation of reduced *CDKN1A* expression, CIN, and poor prognosis (Barboza *et al*., 2006; Ogino *et al*., 2006; Ohashi *et al*., 2020). The loss of $p21^{CIP1}$ is not necessarily a consequence of impaired p53/p73 signalling. The downregulation of *CDKN1A* expression and the inactivation of $p21^{CIP1}$ have also been described after overexpression of oncogenic *c-MYC* which is a relevant alteration in cancer cells (García-Gutiérrez *et al*., 2019). Additionally, *CDKN1A* silencing by long non-coding RNA is frequently observed in cancer (Morlando and Fatica, 2018; Yu *et al*., 2018). The tumour suppressive function of $p21^{CIP1}$ is mainly attributed to its role as cell cycle regulator and promoter of senescence and apoptosis (Abbas and Dutta, 2009). $p21^{CIP1}$ can inhibit both CDK1 and CDK2 and, thus, induce cell cycle arrest in G1 and G2 phase (Medema *et al*., 1998). In addition, $p21^{CIP1}$ can also inhibit PCNA which prevents DNA replication and, thus, contributes to its function as cell cycle regulator (Luo *et al*., 1995). However, the classification of $p21^{CIP1}$ as a tumour suppressor has been challenged by findings describing the overexpression of $p21^{CIP1}$ in some tumours. It has been proposed that the oncogenic function might occur due to $p21^{CIP1}$'s ability to suppress apoptosis and to promote the assembly of active CDK4/6-cyclin D complexes (Abbas and Dutta, 2009).

We assumed that the p53/p73-$p21^{CIP1}$ pathway promotes the maintenance of proper microtubule growth rates and chromosomal stability in the analysed colorectal cancer cells by regulating CDKs, especially the mitotic CDK1. This hypothesis is supported by the fact that the mitotic defects which were observed upon loss of the p53/p73-$p21^{CIP1}$ axis could be rescued by partial inhibition of its target CDK1 (Figure 4.10 -

4.12). This is in line with the findings by Kreis *et al.* (2014) demonstrating the rescue of chromosome segregation defects upon treatment with the CDK1 inhibitor RO-3306.

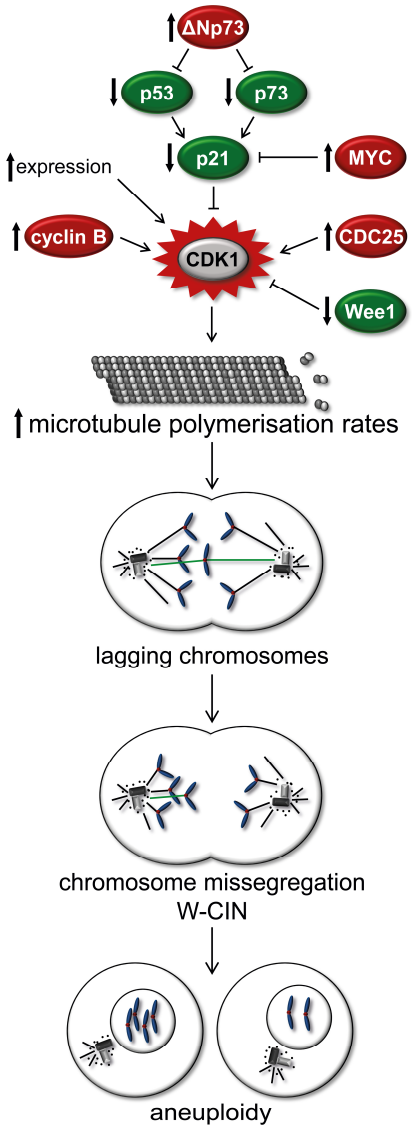

Figure 5.1: Increased CDK1 activity results in increased microtubule polymerisation rates, chromosome missegregation, W-CIN, and aneuploidy.
Several cancer-relevant alterations, which might lead to increased CDK1 activity, are illustrated. Increased CDK1 causes whole chromosomal instability by increasing microtubule polymerisation rates. Scheme adapted from (Schmidt *et al*., 2021).

Independent of p53/p73-p21^{CIP1} signalling, inhibition of CDK1's negative regulator Wee1 and expression of a constitutively active *CDK1* mutant resulted in increased microtubule growth rates and W-CIN (Figure 4.14 - 4.16) indicating that elevated CDK1 activity functions as key trigger for increased microtubule growth rates and W-CIN. Indeed, *CDK1* and *CCNB1/2* are frequently overexpressed in cancer which is associated with W-CIN and poor clinical outcome (Carter *et al*., 2006; Li *et al*., 2020). Interestingly, mild inhibition of CDK1 rescued the mitotic defects in several

chromosomally instable colorectal cancer cell lines (Figure 4.17) indicating that elevated CDK1 activity triggers increased microtubule polymerisation rates and chromosome missegregation in these cells. However, a clear correlation between W-CIN and decreased protein levels of p73, p53, or $p21^{CIP}$, or an increase in CDK1 levels or activity could not be detected in the analysed cell lines (Figure 4.18). Nonetheless, other pathways modulating CDK1 activity might be affected in these cell lines. Several cancer-associated alterations in CDK1 regulators have been described previously. For instance, the overexpression of the CDK1 activating phosphatase CDC25 was detected in some cancer entities (Sur and Agrawal, 2016). We would also expect downregulation of Wee1 as a possibility to increase CDK1 activity contributing to tumourigenesis and W-CIN. However, the overexpression of Wee1 was described for several cancers (Do *et al*., 2013). In these cells, elevated Wee1 activity is needed to delay mitotic entry in the presence of severe DNA damage and to generate additional time for DNA repair processes (Geenen and Schellens, 2017). Possible routes leading to increased CDK1 activity, thereby resulting in abnormally high microtubule polymerisation rates, chromosome segregation defects, and W-CIN, are illustrated in Figure 5.1.

The results presented in this study show that increased CDK1 activity is a trigger for abnormally high microtubule polymerisation rates in mitosis, chromosome missegregation, and W-CIN. Despite the strong link between increased microtubule polymerisation rates and W-CIN (Böhly *et al*., 2019; Ertych *et al*., 2014, 2016; Lüddecke *et al*., 2016), it is not entirely clear how increased microtubule growth rates induce chromosome missegregation. Previous analyses suggested that elevated microtubule polymerisation rates result in transient spindle misalignment which facilitates the formation of merotelic microtubule-kinetochore attachments and, thus, chromosome missegregation (Ertych *et al*., 2014). More recently, our lab has shown that increased microtubule polymerisation rates interfere with the cellular actin cortex which impairs proper positioning of the mitotic spindle (Schermuly, 2019). The increased formation of merotelic microtubule-kinetochore attachments has also been described as a consequence of multipolar spindle intermediates in cells with supernumerary centrosomes (Ganem *et al*., 2009). Additionally, the delayed or accelerated separation of centrosomes leads to transient spindle misorientation promoting the occurrence of merotelic microtubule-kinetochore attachments and chromosome missegregation (Nam and Van Deursen, 2014; Silkworth and Cimini, 2012). Interestingly, *CCNB2* overexpression in mice led to spindle misalignment, lagging chromosomes and chromosomal instability (Nam and Van Deursen, 2014).

This in line with our results showing elevated microtubule growth rates and chromosome missegregation upon increased CDK1 activity. Additionally, these findings support the hypothesis that transient spindle misalignment might mediate the generation of lagging chromosomes and chromosome missegregation upon increased microtubule polymerisation rates caused by abnormally high CDK1 activity.

5.2 Increased CDK1 activity in S phase is responsible for defects in the following mitosis

Strikingly, the results presented in this study suggest that increased mitotic microtubule polymerisation rates and chromosome missegregation were caused by elevated CDK1 activity in S phase and not during mitosis (Figure 4.20, Figure 4.21). This was surprising since CDK1 belongs to the major regulators of mitosis (Nigg, 2001) and, therefore, CDK1 was expected to directly act during mitosis. Since our lab has recently described that mild replication stress leads to higher microtubule polymerisation rates in mitosis, chromosome segregation defects, and W-CIN (Böhly *et al*., 2019), it was tempting to speculate that increased CDK1 activity in S phase might also interfere with DNA replication. This hypothesis was supported by the fact that the mitotic defects observed in cells with increased CDK1 activity could be rescued by nucleoside supplementation (Figure 4.26), which can suppress DNA replication stress (Bester *et al*., 2011), and by reduction of origin firing due to inhibition of CDC7 (Figure 4.27,Figure 4.28) or siRNA-mediated knockdown of either *CDC7* or *MCM2* (Figure 4.29) (Labib, 2010; Tsuji *et al*., 2006). However, the interpretation of these results is complicated by the interplay between replication stress and origin firing. It has been shown before that a decrease in replication fork velocity (replication stress) leads to the activation of additional origins as a compensatory mechanism (Ge *et al*., 2007; Woodward *et al*., 2006). *Vice versa*, excessive origin firing can lead to replication stress due to the rapid consumption of nucleotides and replication factors (Zhong *et al*., 2013).

It is well established that inhibition of ATR or its target CHK1 induces excessive origin firing in replicating cells (Couch *et al*., 2013; Moiseeva *et al*., 2017; Petermann *et al*., 2010; Syljuåsen *et al*., 2005). It has been demonstrated, at least for CHK1 inhibition, that origin firing is the primary defect which triggers a secondary response regarding replication speed (Rodriguez-Acebes *et al*., 2018). Moiseeva *et al.* (2019) proposed that inhibition of ATR-CHK1 signalling results in increased CDK1 activity leading to the dissociation of the RIF1-PP1 complex and excessive CDC7-dependent origin

firing (Figure 1.5). Therefore, I analysed the influence of ATR inhibition and *RIF1* depletion on microtubule polymerisation rates and chromosome segregation (Figure 4.23 -Figure 4.25). Indeed, the inhibition of ATR and the depletion of *RIF1* resulted in the same mitotic defects observed upon increased CDK1 activity. Additionally, reduction of origin firing by inhibition of CDC7 rescued both the abnormally high microtubule polymerisation rates and the higher incidence of lagging chromosomes. Along this line, CDK1 inhibition rescued the mitotic defects observed upon ATR inhibition but not after *RIF1* knockdown which supports the hypothesis that ATR inhibition increases CDK1 activity and that RIF1 is a target of CDK1.

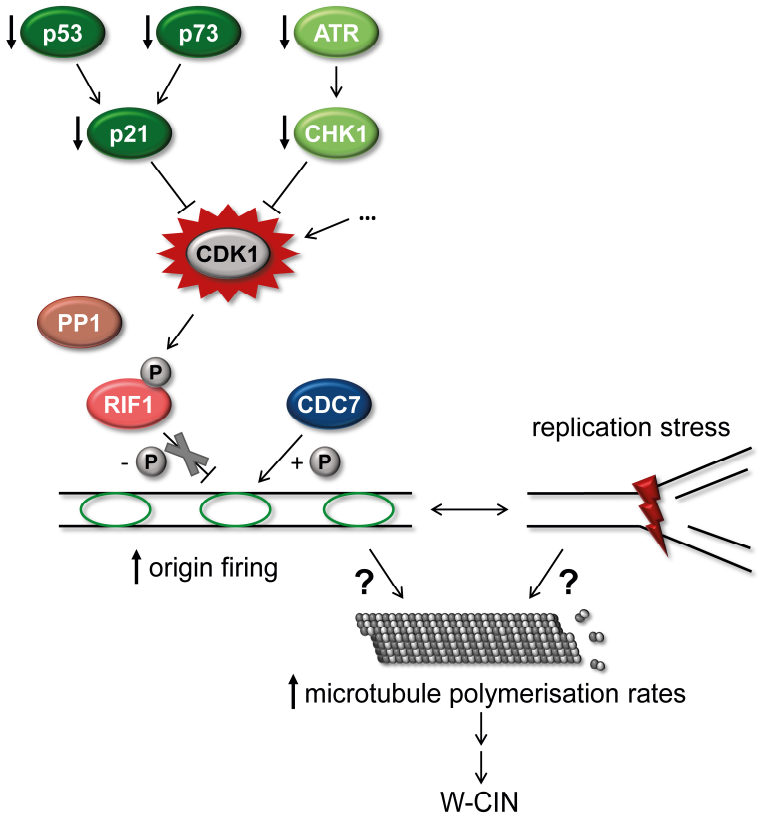

Figure 5.2: Model proposing the link between increased CDK1 activity, origin firing, and W-CIN.
Loss of p53/p73-p21^{CIP1} or ATR-CHK1 signalling leads to increased CDK1 activity. CDK1 phosphorylates RIF1 resulting in the dissociation of the phosphatase complex RIF1-PP1. CDC7-mediated phosphorylation of the replicative helicase contributes to excessive origin firing. Origin firing and/or replication stress trigger increased microtubule polymerisation rates and, consequently, W-CIN.

Interestingly, nucleoside supplementation rescued the mitotic defects induced by ATR inhibition, probably because increased origin firing might lead to slowed fork progression and replication stress (Rodriguez-Acebes *et al.*, 2018; Zhong *et al.*, 2013). Based on these results it can be proposed that increased CDK1 activity upon loss of the p53/p73-p21^{CIP1} axis, inhibition of ATR-CHK1 signalling, or other

mechanisms (Figure 5.1) causes the dissociation of the RIF1-PP1 phosphatase complex, and, consequently, increased CDC7-dependent origin firing. In turn, excessive origin firing can lead to a subsequent decrease in replication speed (Zhong *et al*., 2013). This interference of CDK1 with DNA replication results in increased mitotic microtubule polymerisation rates and, finally, W-CIN (Figure 5.2). To further confirm this hypothesis, it is necessary to detect origin firing and replication speed in cells with increased CDK1 activity, for example by DNA combing assays.

The link between increased origin firing, replication stress, and increased microtubule polymerisation rates resulting in W-CIN is currently not known. Recently, it has been shown that aphidicolin-induced replication stress leads to premature centriole disengagement, multipolar spindle intermediates in mitosis, and chromosome missegregation. Signalling cascades involving ATR, CDK1, and PLK1 contribute to the premature centriole disengagement. Additionally, increased stability of spindle microtubules, which favours the persistence of erroneous microtubule-kinetochore attachments, has been observed upon replication stress (Wilhelm *et al*., 2019). It is tempting to speculate that not only centriole separation could be modulated by replication stress induced signalling but also the activity and localisation of microtubule associated proteins including microtubule polymerases. A possible candidate might be the microtubule polymerase ch-TOG, which is frequently overexpressed in cancer (Charrasse *et al*., 1995). Interestingly, the protein levels of ch-TOG were slightly increased after depletion of *TP53* and *TP73* in HCT116. It would be interesting to elucidate if this increase might be mediated by increased origin firing and replication stress upon *TP53*/*TP73* loss.

Previous work from our lab showed that the loss of *BRCA1*, the loss of its positive regulator *CHK2*, or overexpression of its negative regulator *AURKA* induce increased microtubule polymerisation rates, chromosome missegregation, and W-CIN (Ertych *et al*., 2014, 2016). So far, this has been attributed to direct mitotic functions of CHK2-BRCA1 (Ertych *et al*., 2014, 2016; Stolz *et al*., 2010). It has been speculated that the loss of CHK2-BRCA1 might modulate the activity of microtubule-associated proteins at microtubule plus-tips or centrosomes. One promising candidate was the microtubule polymerase ch-TOG (Ertych *et al*., 2014, 2016) which is indeed upregulated in several cancers (Charrasse *et al*., 1995). However, CHK2 and BRCA1 are major regulators of the DNA damage response and DNA repair (Shaltiel *et al*., 2015; Zhang, 2013). In the light of the recent findings of our lab (this study, Böhly *et al*., 2019) the loss of BRCA1 and CHK2 might also result in impaired DNA replication

and DNA damage mediating increased microtubule polymerisation rates and W-CIN. This possibility remains to be tested.

It is of note that alterations in genes involved in the initiation of DNA replication are highly cancer-relevant and associated with the development of chromosomal instability. Recently, it has been described that the complex consisting of RIF1 and the phosphatase PP1 is necessary to protect stalled replication forks upon replication stress. Loss of RIF1-PP1 leads to fork degradation and S-CIN (Garzón *et al*., 2019; Mukherjee *et al*., 2019). The complexes MCM2-7 and GINS are major components of the replicative helicase (Bell and Kaguni, 2013; Moyer *et al*., 2006). The overexpression of the genes encoding for the six MCM subunits has been described in various cancer types (Das *et al*., 2014). Similarly, the MCM2-7 loading factors *CDC6* and *CDT1* as well as the subunits of the GINS complex are frequently overexpressed in cancer (Blow and Gillespie, 2008; Bu *et al*., 2020; Lian *et al*., 2018; Liontos *et al*., 2007). *CDT1* and *CDC6* overexpression promote re-licensing of origins and, consequently, re-replication leading to severe chromosomal aberrations (Blow and Gillespie, 2008; Liontos *et al*., 2007). Induction of chromosomal instability upon *CDT1* overexpression without detectable re-replication has also been described (Tatsumi *et al*., 2006). CDC7 overexpression is frequently detected in both cancer cell lines and primary tumours and is often correlated with p53 loss (Bonte *et al*., 2008). Interestingly, increased CDC7-dependent origin firing was also observed after expression of *TP53* carrying gain-of-function mutations in the DNA-binding domain (Datta *et al*., 2017). Together, increased origin firing seems to be significantly associated with chromosomal instability in human cancer. This is also supported by the fact that inhibition of CDC7 rescued elevated microtubule polymerisation rates and chromosome missegregation in three different chromosomally instable colorectal cancer cell lines (Figure 4.30).

5.3 Interplay between whole and structural chromosomal instability

The results presented in this study indicate that increased CDK1 activity in S phase leads to increased mitotic microtubule polymerisation rates, chromosome missegregation, and W-CIN (Figure 5.2). The mechanism might involve increased origin firing and replication stress, which can arise due to excessive origin firing (Zhong *et al*., 2013), which is in line with previous findings from our lab (Böhly *et al*., 2019). Interestingly, high CDK1 activity in S phase was also shown to cause severe DNA damage due to the aberrant activation of the endonuclease MUS81-SLX4 (Duda

et al., 2016). In most tumour cells, both structural chromosomal aberrations and aneuploidy can be detected (Sansregret *et al*., 2018). This also indicates an interplay in the mechanisms leading to these aberrations which is indeed supported by recent studies. Replication stress, which has long been known as a cause for S-CIN, is also involved in the missegregation of whole chromosomes during mitosis (Böhly *et al*., 2019; Burrell *et al*., 2013a). *Vice versa,* the presence of additional chromosomes has been shown to induce replication stress and structural chromosomal rearrangements (Passerini *et al*., 2016). Additionally, misaligned chromosomes might end up in the cleavage furrow of dividing cells which leads to DNA damage during cytokinesis (Janssen *et al*., 2011). Furthermore, missegregated chromosomes form micronuclei which are prone to additional DNA damage (Crasta *et al*., 2012; Zhang *et al*., 2015). Further elucidation of the mechanisms underlying both structural and whole chromosomal instability will lead to a better understanding of the generation of complex heterogeneous karyotypes observed in human tumour cell populations.

REFERENCES

Abbas, T., and Dutta, A. (2009). P21 in cancer: Intricate networks and multiple activities. Nat. Rev. Cancer *9*, 400–414.

Akhmanova, A., and Steinmetz, M.O. (2015). Control of microtubule organization and dynamics: Two ends in the limelight. Nat. Rev. Mol. Cell Biol. *16*, 711–726.

Antonin, W., and Neumann, H. (2016). Chromosome condensation and decondensation during mitosis. Curr. Opin. Cell Biol. *40*, 15–22.

Asbury, C.L. (2017). Anaphase a: Disassembling microtubules move chromosomes toward spindle poles. Biology (Basel). *6*, 1–32.

Bailey, S.G., Cragg, M.S., and Townsend, P.A. (2011). Family friction as Δnp73 antagonises p73 and p53. Int. J. Biochem. Cell Biol. *43*, 482–486.

Bakhoum, S.F., Thompson, S.L., Manning, A.L., and Compton, D.A. (2009a). Genome stability is ensured by temporal control of kinetochore-microtubule dynamics. Nat. Cell Biol. *11*, 27–35.

Bakhoum, S.F., Genovese, G., and Compton, D.A. (2009b). Deviant Kinetochore Microtubule Dynamics Underlie Chromosomal Instability. Curr. Biol. *19*, 1937–1942.

Baranovskiy, A.G., Babayeva, N.D., Suwa, Y., Gu, J., Pavlov, Y.I., and Tahirov, T.H. (2014). Structural basis for inhibition of DNA replication by aphidicolin. Nucleic Acids Res. *42*, 14013–14021.

Barber, T.D., McManus, K., Yuen, K.W.Y., Reis, M., Parmigiani, G., Shen, D., Barrett, I., Nouhi, Y., Spencer, F., Markowitz, S., *et al*. (2008). Chromatid cohesion defects may underlie chromosome instability in human colorectal cancers. Proc. Natl. Acad. Sci. U. S. A. *105*, 3443–3448.

Barboza, J.A., Liu, G., Ju, Z., El-Naggar, A.K., and Lozano, G. (2006). P21 delays tumor onset by preservation of chromosomal stability. Proc. Natl. Acad. Sci. U. S. A. *103*, 19842–19847.

Bastians, H. (2015). Causes of chromosomal instability. In Chromosomal Instability in Cancer Cells, (Springer International Publishing), pp. 95–113.

Bell, S.P., and Kaguni, J.M. (2013). Helicase loading at chromosomal origins of replication. Cold Spring Harb. Perspect. Biol. *5*, 1–20.

Berger, K. (2016). A Role For Microtubule Dynamics For The Induction Of Chromosomal Instability And Cell Migration And Invasion In Human Cancer Cells. PhD Thesis, Georg-August-University Göttingen. available at: https://ediss.uni-goettingen.de/handle/11858/00-1735-0000-0023-3E82-9?show=full.

Bester, A.C., Roniger, M., Oren, Y.S., Im, M.M., Sarni, D., Chaoat, M., Bensimon, A., Zamir, G., Shewach, D.S., and Kerem, B. (2011). Nucleotide deficiency promotes genomic instability in early stages of cancer development. Cell *145*, 435–446.

Bhabha, G., Johnson, G.T., Schroeder, C.M., and Vale, R.D. (2016). How Dynein Moves Along Microtubules. Trends Biochem. Sci. *41*, 94–105.

Blow, J.J., and Gillespie, P.J. (2008). Replication licensing and cancer - A fatal entanglement? Nat. Rev. Cancer *8*, 799–806.

Bodakuntla, S., Jijumon, A.S., Villablanca, C., Gonzalez-Billault, C., and Janke, C. (2019). Microtubule-Associated Proteins: Structuring the Cytoskeleton. Trends Cell Biol. *29*, 804–819.

Böhly, N., Kistner, M., and Bastians, H. (2019). Mild replication stress causes aneuploidy by deregulating microtubule dynamics in mitosis. Cell Cycle *18*, 2770–2783.

Bonte, D., Lindvall, C., Liu, H., Dykema, K., Furge, K., and Weinreich, M. (2008). Cdc7-Dbf4 kinase overexpression in multiple cancers and tumor cell lines is correlated with p53 inactivation. Neoplasia *10*, 920–931.

Booher, R.N., Holman, P.S., and Fattaey, A. (1997). Human Myt1 is a cell cycle-regulated kinase that inhibits Cdc2 but not Cdk2 activity. J. Biol. Chem. *272*, 22300–22306.

Bosch, F.X., Broker, T.R., Forman, D., Moscicki, A.B., Gillison, M.L., Doorbar, J., Stern, P.L., Stanley, M., Arbyn, M., Poljak, M., *et al*. (2013). Comprehensive control of human papillomavirus infections and related diseases. Vaccine *31*, F1–F31.

Brouhard, G.J., Stear, J.H., Noetzel, T.L., Al-Bassam, J., Kinoshita, K., Harrison, S.C., Howard, J., and Hyman, A.A. (2008). XMAP215 Is a Processive Microtubule Polymerase. Cell *132*, 79–88.

Brummelkamp, T.R., Bernards, R., and Agami, R. (2002). A system for stable expression of short interfering RNAs in mammalian cells. Science. *296*, 550–553.

Bu, F., Zhu, X., Yi, X., Luo, C., Lin, K., Zhu, J., Hu, C., Liu, Z., Zhao, J., Huang, C., *et al*. (2020). Expression profile of gins complex predicts the prognosis of pancreatic cancer patients. Onco. Targets. Ther. *13*, 11433–11444.

Bunz, F., Dutriaux, A., Lengauer, C., Waldman, T., Zhou, S., Brown, J.P., Sedivy, J.M., Kinzler, K.W., and Vogelstein, B. (1998). Requirement for p53 and p21 to sustain G2 arrest after DNA damage. Science. *282*, 1497–1501.

Bunz, F., Fauth, C., Speicher, M.R., Dutriaux, A., Sedivy, J.M., Kinzler, K.W., Vogelstein, B., and Lengauer, C. (2002). Targeted Inactivation of p53 in Human Cells Does Not Result in Aneuploidy. Cancer Res. *62*, 1129–1133.

Burgers, P.M.J., and Kunkel, T.A. (2017). Eukaryotic DNA replication fork. Annu. Rev. Biochem. *86*, 417–438.

Burrell, R.A., McClelland, S.E., Endesfelder, D., Groth, P., Weller, M.C., Shaikh, N., Domingo, E., Kanu, N., Dewhurst, S.M., Gronroos, E., *et al*. (2013a). Replication stress links structural and numerical cancer chromosomal instability. Nature *494*, 492–496.

Burrell, R.A., McGranahan, N., Bartek, J., and Swanton, C. (2013b). The causes and consequences of genetic heterogeneity in cancer evolution. Nature *501*, 338–345.

Byun, T.S., Pacek, M., Yee, M.C., Walter, J.C., and Cimprich, K.A. (2005). Functional uncoupling of MCM helicase and DNA polymerase activities activates the ATR-dependent checkpoint. Genes Dev. *19*, 1040–1052.

Carter, S.L., Eklund, A.C., Kohane, I.S., Harris, L.N., and Szallasi, Z. (2006). A signature of chromosomal instability inferred from gene expression profiles predicts clinical outcome in multiple human cancers. Nat. Genet. *38*, 1043–1048.

Charrasse, S., Mazel, M., Taviaux, S., Berta, P., Chow, T., and Larroque, C. (1995). Characterization of the cDNA and Pattern of Expression of a New Gene Over-Expressed in Human Hepatomas and Colonic Tumors. Eur. J. Biochem. *234*, 406–413.

Cheeseman, I.M., and Desai, A. (2008). Molecular architecture of the kinetochore-microtubule interface. Nat. Rev. Mol. Cell Biol. *9*, 33–46.

Cheffings, T.H., Burroughs, N.J., and Balasubramanian, M.K. (2016). Actomyosin Ring Formation and Tension Generation in Eukaryotic Cytokinesis. Curr. Biol. *26*, R719–R737.

Cheng, C.H., and Kuchta, R.D. (1993). DNA Polymerase ε: Aphidicolin Inhibition and the Relationship between Polymerase and Exonuclease Activity. Biochemistry *32*, 8568–8574.

Chunduri, N.K., and Storchová, Z. (2019). The diverse consequences of aneuploidy. Nat. Cell Biol. *21*, 54–62.

Cimini, D. (2008). Merotelic kinetochore orientation, aneuploidy, and cancer. Biochim. Biophys. Acta - Rev. Cancer *1786*, 32–40.

Cimini, D., Howell, B., Maddox, P., Khodjakov, A., Degrassi, F., and Salmon, E.D. (2001). Merotelic kinetochore orientation is a major mechanism of aneuploidy in mitotic mammalian tissue cells. J. Cell Biol. *152*, 517–527.

Cimprich, K.A., and Cortez, D. (2008). ATR: An essential regulator of genome integrity. Nat. Rev. Mol. Cell Biol. *9*, 616–627.

Cisyk, A.L., Penner-Goeke, S., Lichtensztejn, Z., Nugent, Z., Wightman, R.H., Singh, H., and McManus, K.J. (2015). Characterizing the Prevalence of Chromosome Instability in Interval Colorectal Cancer. Neoplasia *17*, 306–316.

Cooper, G.M. (2000). The Eukaryotic Cell Cycle. In The Cell: A Molecular Approach. 2nd Edition., (Sinauer Associates)

Corn, P.G., Kuerbitz, S.J., Van Noesel, M.M., Esteller, M., Compitello, N., Baylin, S.B., and Herman, J.G. (1999). Transcriptional silencing of the p73 gene in acute lymphoblastic leukemia and Burkitt's lymphoma is associated with 5' CpG island methylation. Cancer Res. *59*, 3352–3356.

Couch, F.B., Bansbach, C.E., Driscoll, R., Luzwick, J.W., Glick, G.G., Bétous, R., Carroll, C.M., Jung, S.Y., Qin, J., Cimprich, K.A., *et al*. (2013). ATR phosphorylates SMARCAL1 to prevent replication fork collapse. Genes Dev. *27*, 1610–1623.

Crasta, K., Ganem, N.J., Dagher, R., Lantermann, A.B., Ivanova, E. V., Pan, Y., Nezi, L., Protopopov, A., Chowdhury, D., and Pellman, D. (2012). DNA breaks and chromosome pulverization from errors in mitosis. Nature *482*, 53–58.

Das, M., Singh, S., Pradhan, S., and Narayan, G. (2014). MCM Paradox: Abundance of Eukaryotic Replicative Helicases and Genomic Integrity. Mol. Biol. Int. *2014*, 1–11.

Datta, A., Ghatak, D., Das, S., Banerjee, T., Paul, A., Butti, R., Gorain, M., Ghuwalewala, S., Roychowdhury, A., Alam, S.K., *et al*. (2017). p53 gain-of-function mutations increase Cdc7-dependent replication initiation. EMBO Rep. *18*, 2030–2050.

Debatisse, M., and Rosselli, F. (2019). A journey with common fragile sites: From S phase to telophase. Genes, Chromosom. Cancer *58*, 305–316.

Derry, W.B., Wilson, L., and Jordan, M.A. (1995). Substoichiometric Binding of Taxol Suppresses Microtubule Dynamics. Biochemistry *34*, 2203–2211.

Desai, A., and Mitchison, T.J. (1997). Microtubule polymerization dynamics. Annu. Rev. Cell Dev. Biol. *13*, 83–117.

Di, C., Yang, L., Zhang, H., Ma, X., Zhang, X., Sun, C., Li, H., Xu, S., An, L., Li, X., *et al*. (2013). Mechanisms, function and clinical applications of DNp73. Cell Cycle *12*, 1861–1867.

Dimitrov, A., Quesnoit, M., Moutel, S., Cantaloube, I., Poüs, C., and Perez, F. (2008). Detection of GTP-tubulin conformation in vivo reveals a role for GTP remnants in microtubule rescues. Science (80-.). *322*, 1353–1356.

Do, K., Doroshow, J.H., and Kummar, S. (2013). Wee1 kinase as a target for cancer therapy. Cell Cycle *12*, 3348–3353.

Duda, H., Arter, M., Gloggnitzer, J., Teloni, F., Wild, P., Blanco, M.G., Altmeyer, M., and Matos, J. (2016). A Mechanism for Controlled Breakage of Under-replicated Chromosomes during Mitosis. Dev. Cell *39*, 740–755.

Dunican, D.S., McWilliam, P., Tighe, O., Parle-McDermott, A., and Croke, D.T. (2002). Gene expression differences between the microsatellite instability (min) and chromosomal instability (cin) phenotypes in colorectal cancer revealed by high-density cdna array hybridization. Oncogene *21*, 3253–3257.

Eischen, C.M. (2016). Genome stability requires p53. Cold Spring Harb. Perspect. Med. *6*, 1–14.

Elbashir, S.M., Harborth, J., Lendeckel, W., Yalcin, A., Weber, K., and Tuschl, T. (2001). Duplexes of 21-nucleotide RNAs mediate RNA interference in cultured mammalian cells. Nature *411*, 494–498.

Ertych, N., Stolz, A., Stenzinger, A., Weichert, W., Kaulfuß, S., Burfeind, P., Aigner, A., Wordeman, L., and Bastians, H. (2014). Increased microtubule assembly rates influence chromosomal instability in colorectal cancer cells. Nat. Cell Biol. *16*, 779–791.

Ertych, N., Stolz, A., Valerius, O., Braus, G.H., and Bastians, O. (2016). CHK2-BRCA1 tumor-suppressor axis restrains oncogenic Aurora-A kinase to ensure proper mitotic microtubule assembly. Proc. Natl. Acad. Sci. U. S. A. *113*, 1817–1822.

Fisher, R.P., and Morgan, D.O. (1994). A novel cyclin associates with M015/CDK7 to form the CDK-activating kinase. Cell *78*, 713–724.

Flores, E.R., Sengupta, S., Miller, J.B., Newman, J.J., Bronson, R., Crowley, D., Yang, A., McKeon, F., and Jacks, T. (2005). Tumor predisposition in mice mutant for p63 and p73: Evidence for broader tumor suppressor functions for the p53 family. Cancer Cell *7*, 363–373.

Fodde, R., Kuipers, J., Rosenberg, C., Smits, R., Kielman, M., Gaspar, C., Van Es, J.H., Breukel, C., Wiegant, J., Giles, R.H., *et al*. (2001). Mutations in the APC tumour suppressor gene cause chromosomal instability. Nat. Cell Biol. *3*, 433–438.

Gaillard, H., García-Muse, T., and Aguilera, A. (2015). Replication stress and cancer. Nat. Rev. Cancer *15*, 276–280.

Ganem, N.J., Godinho, S.A., and Pellman, D. (2009). A mechanism linking extra centrosomes to chromosomal instability. Nature *460*, 278–282.

García-Gutiérrez, L., Delgado, M.D., and León, J. (2019). Myc oncogene contributions to release of cell cycle brakes. Genes (Basel). *10*, 1–29.

Gartner, M., Sunder-Plassmann, N., Seiler, J., Utz, M., Vernos, I., Surrey, T., and Giannis, A. (2005). Development and biological evaluation of potent and specific inhibitors of mitotic kinesin Eg5. ChemBioChem *6*, 1173–1177.

Garzón, J., Ursich, S., Lopes, M., Hiraga, S. ichiro, and Donaldson, A.D. (2019). Human RIF1-Protein Phosphatase 1 Prevents Degradation and Breakage of Nascent DNA on Replication Stalling. Cell Rep. *27*, 2558-2566.e4.

Gascoigne, K.E., and Cheeseman, I.M. (2011). Kinetochore assembly: If you build it, they will come. Curr. Opin. Cell Biol. *23*, 102–108.

Ge, X.Q., and Blow, J.J. (2010). Chk1 inhibits replication factory activation but allows dormant origin firing in existing factories. J. Cell Biol. *191*, 1285–1297.

Ge, X.Q., Jackson, D.A., and Blow, J.J. (2007). Dormant origins licensed by excess Mcm2-7 are required for human cells to survive replicative stress. Genes Dev. *21*, 3331–3341.

Geenen, J.J.J., and Schellens, J.H.M. (2017). Molecular pathways: Targeting the protein kinase Wee1 in cancer. Clin. Cancer Res. *23*, 4540–4544.

Gelot, C., Magdalou, I., and Lopez, B.S. (2015). Replication stress in mammalian cells and its consequences for mitosis. Genes (Basel). *6*, 267–298.

Glotzer, M. (2005). The molecular requirements for cytokinesis. Science (80-.). *307*, 1735–1739.

Godek, K.M., Kabeche, L., and Compton, D.A. (2015). Regulation of kinetochore-microtubule attachments through homeostatic control during mitosis. Nat. Rev. Mol. Cell Biol. *16*, 57–64.

Green, R.A., and Kaplan, K.B. (2003). Chromosome instability in colorectal tumor cells is associated with defects in microtubule plus-end attachments caused by a dominant mutation in APC. J. Cell Biol. *163*, 949–961.

Green, R.A., Paluch, E., and Oegema, K. (2012). Cytokinesis in Animal Cells. Annu. Rev. Cell Dev. Biol. *28*, 29–58.

Gregan, J., Polakova, S., Zhang, L., Tolić-Nørrelykke, I.M., and Cimini, D. (2011). Merotelic kinetochore attachment: Causes and effects. Trends Cell Biol. *21*, 374–381.

Gressner, O., Schilling, T., Lorenz, K., Schulze Schleithoff, E., Koch, A., Schulze-Bergkamen, H., Maria Lena, A., Candi, E., Terrinoni, A., Valeria Catani, M., *et al*. (2005). TAp63α induces apoptosis by activating signaling via death receptors and mitochondria. EMBO J. *24*, 2458–2471.

Grieco, D., and Serpico, A.F. (2020). Recent advances in understanding the role of Cdk1 in the Spindle Assembly Checkpoint. F1000Research *9*, 1–8.

Grob, T.J., Novak, U., Maisse, C., Barcaroli, D., Lüthi, A.U., Pirnia, F., Hügli, B., Graber, H.U., De Laurenzi, V., Fey, M.F., *et al*. (2001). Human ΔNp73 regulates a dominant negative feedback loop for TAp73 and p53. Cell Death Differ. *8*, 1213–1223.

Guo, X., Keyes, W.M., Papazoglu, C., Zuber, J., Li, W., Lowe, S.W., Vogel, H., and Alea, A. (2009). TAp63 induces senescence and suppresses tumorigenesis in vivo. Nat. Cell Biol. *11*, 1451–1457.

Hanahan, D., and Weinberg, R.A. (2011). Hallmarks of cancer: The next generation. Cell *144*, 646–674.

Harbour, J.W., Luo, R.X., Dei Santi, A., Postigo, A.A., and Dean, D.C. (1999). Cdk phosphorylation triggers sequential intramolecular interactions that progressively block Rb functions as cells move through G1. Cell *98*, 859–869.

Heald, R., and Khodjakov, A. (2015). Thirty years of search and capture: The complex simplicity of mitotic spindle assembly. J. Cell Biol. *211*, 1103–1111.

Heald, R., McLoughlin, M., and McKeon, F. (1993). Human wee1 maintains mitotic timing by protecting the nucleus from cytoplasmically activated cdc2 kinase. Cell *74*, 463–474.

Hinchcliffe, E.H., Day, C.A., Karanjeet, K.B., Fadness, S., Langfald, A., Vaughan, K.T., and Dong, Z. (2016). Chromosome missegregation during anaphase triggers p53 cell cycle arrest through histone H3.3 Ser31 phosphorylation. Nat. Cell Biol. *18*, 668–675.

Hirai, H., Iwasawa, Y., Okada, M., Arai, T., Nishibata, T., Kobayashi, M., Kimura, T., Kaneko, N., Ohtani, J., Yamanaka, K., *et al*. (2009). Small-molecule inhibition of Wee1 kinase by MK-1775 selectively sensitizes p53-deficient tumor cells to DNA-damaging agents. Mol. Cancer Ther. *8*, 2992–3000.

Hirokawa, N., Noda, Y., Tanaka, Y., and Niwa, S. (2009). Kinesin superfamily motor proteins and intracellular transport. Nat. Rev. Mol. Cell Biol. *10*, 682–696.

Hohmann, and Dehghani (2019). The Cytoskeleton—A Complex Interacting Meshwork. Cells *8*, 1–55.

Honda, R., Tanaka, H., and Yasuda, H. (1997). Oncoprotein MDM2 is a ubiquitin ligase E3 for tumor suppressor p53. FEBS Lett. *420*, 25–27.

Hunter, A.W., Caplow, M., Coy, D.L., Hancock, W.O., Diez, S., Wordeman, L., and Howard, J. (2003). The kinesin-related protein MCAK is a microtubule depolymerase that forms an ATP-hydrolyzing complex at microtubule ends. Mol. Cell *11*, 445–457.

Ikegami, S., Taguchi, T., Ohashi, M., Oguro, M., Nagano, H., and Mano, Y. (1978). Aphidicolin prevents mitotic cell division by interfering with the activity of DNA polymerase-α [18]. Nature *275*, 458–460.

Im, J.S., Ki, S.H., Farina, A., Jung, D.S., Hurwitz, J., and Lee, J.K. (2009). Assembly of the Cdc45-Mcm2-7-GINS complex in human cells requires the Ctf4/And-1, RecQL4, and Mcm10 proteins. Proc. Natl. Acad. Sci. U. S. A. *106*, 15628–15632.

Janssen, A., Kops, G.J.P.L., and Medema, R.H. (2009). Elevating the frequency of chromosome mis-segregation as a strategy to kill tumor cells. Proc. Natl. Acad. Sci. U. S. A. *106*, 19108–19113.

Janssen, A., Van Der Burg, M., Szuhai, K., Kops, G.J.P.L., and Medema, R.H. (2011). Chromosome segregation errors as a cause of DNA damage and structural chromosome aberrations. Science (80-.). *333*, 1895–1898.

Joerger, A.C., Rajagopalan, S., Natan, E., Veprintsev, D.B., Robinson, C. V., and Fersht, A.R. (2009). Structural evolution of p53, p63, and p73: Implication for heterotetramer formation. Proc. Natl. Acad. Sci. U. S. A. *106*, 17705–17710.

Jones, R.M., Mortusewicz, O., Afzal, I., Lorvellec, M., García, P., Helleday, T., and Petermann, E. (2013). Increased replication initiation and conflicts with transcription underlie Cyclin E-induced replication stress. Oncogene *32*, 3744–3753.

Jordan, M.A., Toso, R.J., Thrower, D., and Wilson, L. (1993). Mechanism of mitotic block and inhibition of cell proliferation by taxol at low concentrations. Proc. Natl. Acad. Sci. U. S. A. *90*, 9552–9556.

Jordan, M.A., Wendell, K., Gardiner, S., Brent Derry, W., Copp, H., and Wilson, L. (1996). Mitotic Block Induced in HeLa Cells by Low Concentrations of Paclitaxel (Taxol) Results in Abnormal Mitotic Exit and Apoptotic Cell Death. Cancer Res. *56*, 816–825.

Jost, C.A., Marin, M.C., and Kaelin, W.G. (1997). p73 is a human p53-related protein that can induce apoptosis. Nature *389*, 191–194.

Kaghad, M., Bonnet, H., Yang, A., Creancier, L., Biscan, J.C., Valent, A., Minty, A., Chalon, P., Lelias, J.M., Dumont, X., *et al*. (1997). Monoallelically expressed gene related to p53 at 1p36, a region frequently deleted in neuroblastoma and other human cancers. Cell *90*, 809–819.

Kandoth, C., McLellan, M.D., Vandin, F., Ye, K., Niu, B., Lu, C., Xie, M., Zhang, Q., McMichael, J.F., Wyczalkowski, M.A., *et al*. (2013). Mutational landscape and significance across 12 major cancer types. Nature *502*, 333–339.

Kirschner, M., and Mitchison, T. (1986). Beyond self-assembly: From microtubules to morphogenesis. Cell *45*, 329–342.

Knowlton, A.L., Lan, W., and Stukenberg, P.T. (2006). Aurora B Is Enriched at Merotelic Attachment Sites, Where It Regulates MCAK. Curr. Biol. *16*, 1705–1710.

Kollman, J.M., Merdes, A., Mourey, L., and Agard, D.A. (2011). Microtubule nucleation by γ-tubulin complexes. Nat. Rev. Mol. Cell Biol. *12*, 709–721.

Koltun, E.S., Tsuhako, A.L., Brown, D.S., Aay, N., Arcalas, A., Chan, V., Du, H., Engst, S., Ferguson, K., Franzini, M., *et al*. (2012). Discovery of XL413, a potent and selective CDC7 inhibitor. Bioorganic Med. Chem. Lett. *22*, 3727–3731.

Kops, G.J.P.L., Weaver, B.A.A., and Cleveland, D.W. (2005). On the road to cancer: Aneuploidy and the mitotic checkpoint. Nat. Rev. Cancer *5*, 773–785.

Kreis, N.N., Sanhaji, M., Rieger, M.A., Louwen, F., and Yuan, J. (2014). P21Waf1/Cip1 deficiency causes multiple mitotic defects in tumor cells. Oncogene *33*, 5716–5728.

Kreis, N.N., Louwen, F., and Yuan, J. (2019). The multifaceted p21 (Cip1/Waf1/CDKN1A) in cell differentiation, migration and cancer therapy. Cancers (Basel). *11*, 1–23.

Kubbutat, M.H.G., Jones, S.N., and Vousden, K.H. (1997). Regulation of p53 stability by Mdm2. Nature *387*, 299–303.

Labib, K. (2010). Howdo Cdc7 and cyclin-dependent kinases trigger the initiation of chromosome replication in eukaryotic cells? Genes Dev. *24*, 1208–1219.

Leman, A.R., and Noguchi, E. (2012). Local and global functions of Timeless and Tipin in replication fork protection. Cell Cycle *11*, 3945–3955.

Levine, A.J., and Oren, M. (2009). The first 30 years of p53: Growing ever more complex. Nat. Rev. Cancer *9*, 749–758.

Levrero, M., De Laurenzi, V., Costanzo, A., Sabatini, S., Gong, J., Wang, J.Y.J., and Melino, G. (2000). The p53/p63/p73 family of transcription factors: Overlapping and distinct functions. J. Cell Sci. *113*, 1661–1670.

Lewis, C.W., Jin, Z., Macdonald, D., Wei, W., Qian, X.J., Choi, W.S., He, R., Sun, X., and Chan, G. (2017). Prolonged mitotic arrest induced by Wee1 inhibition sensitizes breast cancer cells to paclitaxel. Oncotarget *8*, 73705–73722.

Li, D., Marchenko, N.D., Schulz, R., Fischer, V., Velasco-Hernandez, T., Talos, F., and Moll, U.M. (2011). Functional inactivation of endogenous MDM2 and CHIP by HSP90 causes aberrant stabilization of mutant p53 in human cancer cells. Mol. Cancer Res. *9*, 577–588.

Li, J., Wang, Y., Wang, X., and Yang, Q. (2020). CDK1 and CDC20 overexpression in patients with colorectal cancer are associated with poor prognosis: Evidence from integrated bioinformatics analysis. World J. Surg. Oncol. *18*, 1–11.

Li, M., Fang, X., Baker, D.J., Guo, L., Gao, X., Wei, Z., Han, S., Van Deursen, J.M., and Zhang, P. (2010). The ATM-p53 pathway suppresses aneuploidy-induced tumorigenesis. Proc. Natl. Acad. Sci. U. S. A. *107*, 14188–14193.

Lian, Y.F., Li, S.S., Huang, Y.L., Wei, H., Chen, D.M., Wang, J.L., and Huang, Y.H. (2018). Up-regulated and interrelated expressions of GINS subunits predict poor prognosis in hepatocellular carcinoma. Biosci. Rep. *38*, 1–10.

Liontos, M., Koutsami, M., Sideridou, M., Evangelou, K., Kletsas, D., Levy, B., Kotsinas, A., Nahum, O., Zoumpourlis, V., Kouloukoussa, M., *et al*. (2007). Deregulated overexpression of hCdt1 and hCdc6 promotes malignant behavior. Cancer Res. *67*, 10899–10909.

Loukopoulos, P., Shibata, T., Katoh, H., Kokubu, A., Sakamoto, M., Yamazaki, K., Kosuge, T., Kanai, Y., Hosoda, F., Imoto, I., *et al*. (2007). Genome-wide array-based comparative genomic hybridization analysis of pancreatic adenocarcinoma: Identification of genetic indicators that predict patient outcome. Cancer Sci. *98*, 392–400.

De Luca, M., Brunetto, L., Asteriti, I.A., Giubettini, M., Lavia, P., and Guarguaglini, G. (2008). Aurora-A and ch-TOG act in a common pathway in control of spindle pole integrity. Oncogene *27*, 6539–6549.

Lüddecke, S., Ertych, N., Stenzinger, A., Weichert, W., Beissbarth, T., Dyczkowski, J., Gaedcke, J., Valerius, O., Braus, G.H., Kschischo, M., *et al*. (2016). The putative oncogene CEP72 inhibits the mitotic function of BRCA1 and induces chromosomal instability. Oncogene *35*, 2398–2405.

Lundberg, A.S., and Weinberg, R.A. (1998). Functional Inactivation of the Retinoblastoma Protein Requires Sequential Modification by at Least Two Distinct Cyclin-cdk Complexes. Mol. Cell. Biol. *18*, 753–761.

Luo, Y., Hurwitz, J., and Massagué, J. (1995). Cell-cycle inhibition by independent CDK and PCNA binding domains in p21cip1. Nature *375*, 159–161.

Magdalou, I., Lopez, B.S., Pasero, P., and Lambert, S.A.E. (2014). The causes of replication stress and their consequences on genome stability and cell fate. Semin. Cell Dev. Biol. *30*, 154–164.

Malumbres, M., and Barbacid, M. (2001). To cycle or not to cycle: A critical decision in cancer. Nat. Rev. Cancer *1*, 222–231.

Malumbres, M., and Barbacid, M. (2005). Mammalian cyclin-dependent kinases. Trends Biochem. Sci. *30*, 630–641.

Malumbres, M., and Barbacid, M. (2009). Cell cycle, CDKs and cancer: A changing paradigm. Nat. Rev. Cancer *9*, 153–166.

Martín-Caballero, J., Flores, J.M., García-Palencia, P., and Serrano, M. (2001). Tumor Susceptibility of p21Waf1/Cip1-deficient Mice. Cancer Res. *61*, 6234–6238.

Martinez-Delgado, B., Melendez, B., Cuadros, M., Garcia, M.J., Nomdedeu, J., Rivas, C., Fernandez-Piqueras, J., and Benítez, J. (2002). Frequent inactivation of the p73 gene by abnormal methylation or LOH in non-Hodgkin's lymphomas. Int. J. Cancer *102*, 15–19.

Martinez-Zapien, D., Ruiz, F.X., Poirson, J., Mitschler, A., Ramirez, J., Forster, A., Cousido-Siah, A., Masson, M., Pol, S. Vande, Podjarny, A., *et al*. (2016). Structure of the E6/E6AP/p53 complex required for HPV-mediated degradation of p53. Nature *529*, 541–545.

Medema, R.H., Klompmaker, R., Smits, V.A.J., and Rijksen, G. (1998). p21(waf1) can block cells at two points in the cell cycle, but does not interfere with processive DNA-replication or stress-activated kinases. Oncogene *16*, 431–441.

Michel, L.S., Liberal, V., Chatterjee, A., Kirchwegger, R., Pasche, B., Gerald, W., Dobles, M., Sorger, P.K., Murty, V.V.V.S., and Benezra, R. (2001). MAD2 haplo-insufficiency causes premature anaphase and chromosome instability in mammalian cells. Nature *409*, 355–359.

Millar, J.B., Blevitt, J., Gerace, L., Sadhu, K., Featherstone, C., and Russell, P. (1991). p55CDC25 is a nuclear protein required for the initiation of mitosis in human cells. Proc. Natl. Acad. Sci. *88*, 10500–10504.

Mitchison, T., and Kirschner, M. (1984). Dynamic instability of microtubule growth. Nature *312*, 237–242.

Moiseeva, T.N., and Bakkenist, C.J. (2019). Dormant origin signaling during unperturbed replication. DNA Repair (Amst). *81*, 1–11.

Moiseeva, T., Hood, B., Schamus, S., O'Connor, M.J., Conrads, T.P., and Bakkenist, C.J. (2017). ATR kinase inhibition induces unscheduled origin firing through a Cdc7-dependent association between GINS and And-1. Nat. Commun. *8*, 1–11.

Moiseeva, T.N., Yin, Y., Calderon, M.J., Qian, C., Schamus-Haynes, S., Sugitani, N., Osmanbeyoglu, H.U., Rothenberg, E., Watkins, S.C., and Bakkenist, C.J. (2019). An ATR and CHK1 kinase signaling mechanism that limits origin firing during unperturbed DNA replication. Proc. Natl. Acad. Sci. U. S. A. *116*, 13374–13383.

Montagnoli, A., Valsasina, B., Croci, V., Menichincheri, M., Rainoldi, S., Marchesi, V., Tibolla, M., Tenca, P., Brotherton, D., Albanese, C., *et al*. (2008). A Cdc7 kinase inhibitor restricts initiation of DNA replication and has antitumor activity. Nat. Chem. Biol. *4*, 357–365.

Morlando, M., and Fatica, A. (2018). Alteration of epigenetic regulation by long noncoding RNAs in cancer. Int. J. Mol. Sci. *19*, 570–586.

Moyer, S.E., Lewis, P.W., and Botchan, M.R. (2006). Isolation of the Cdc45/Mcm2-7/GINS (CMG) complex, a candidate for the eukaryotic DNA replication fork helicase. Proc. Natl. Acad. Sci. U. S. A. *103*, 10236–10241.

Mukherjee, C., Tripathi, V., Manolika, E.M., Heijink, A.M., Ricci, G., Merzouk, S., de Boer, H.R., Demmers, J., van Vugt, M.A.T.M., and Ray Chaudhuri, A. (2019). RIF1 promotes replication fork protection and efficient restart to maintain genome stability. Nat. Commun. *10*, 1–16.

Muller, P.A.J., and Vousden, K.H. (2014). Mutant p53 in cancer: New functions and therapeutic opportunities. Cancer Cell *25*, 304–317.

Musacchio, A. (2015). The Molecular Biology of Spindle Assembly Checkpoint Signaling Dynamics. Curr. Biol. *25*, R1002–R1018.

Muzny, D.M., Bainbridge, M.N., Chang, K., Dinh, H.H., Drummond, J.A., Fowler, G., Kovar, C.L., Lewis, L.R., Morgan, M.B., Newsham, I.F., *et al*. (2012). Comprehensive molecular characterization of human colon and rectal cancer. Nature *487*, 330–337.

Nam, E.A., and Cortez, D. (2011). ATR signalling: More than meeting at the fork. Biochem. J. *436*, 527–536.

Nam, H.J., and Van Deursen, J.M. (2014). Cyclin B2 and p53 control proper timing of centrosome separation. Nat. Cell Biol. *16*, 535–546.

Nigg, E.A. (2001). Mitotic kinases as regulators of cell division and its checkpoints. Nat. Rev. Mol. Cell Biol. *2*, 21–32.

O'Donnell, M., and Kuriyan, J. (2006). Clamp loaders and replication initiation. Curr. Opin. Struct. Biol. *16*, 35–41.

O'Shaughnessy, B., and Thiyagarajan, S. (2018). Mechanisms of contractile ring tension production and constriction. Biophys. Rev. *10*, 1667–1681.

Ogino, S., Kawasaki, T., Kirkner, G.J., Ogawa, A., Dorfman, I., Loda, M., and Fuchs, C.S. (2006). Down-regulation of p21 (CDKNIA/CIPI) is inversely associated with microsatellite instability and CpG island methylator phenotype (CIMP) in colorectal cancer. J. Pathol. *210*, 147–154.

Ohashi, R., Angori, S., Batavia, A.A., Rupp, N.J., Ajioka, Y., Schraml, P., and Moch, H. (2020). Loss of CDKN1A mRNA and Protein Expression Are Independent Predictors of Poor Outcome in Chromophobe Renal Cell Carcinoma Patients. Cancers (Basel). *12*, 1–13.

Passerini, V., Ozeri-Galai, E., De Pagter, M.S., Donnelly, N., Schmalbrock, S., Kloosterman, W.P., Kerem, B., and Storchová, Z. (2016). The presence of extra chromosomes leads to genomic instability. Nat. Commun. *7*, 1–12.

Petermann, E., Woodcock, M., and Helleday, T. (2010). Chk1 promotes replication fork progression by controlling replication initiation. Proc. Natl. Acad. Sci. U. S. A. *107*, 16090–16095.

Petry, S. (2016). Mechanisms of Mitotic Spindle Assembly. Annu. Rev. Biochem. *85*, 659–683.

Pflaum, J., Schlosser, S., and Müller, M. (2014). P53 family and cellular stress responses in cancer. Front. Oncol. *4*, 1–15.

Pletts Goscin, L., and Byrnes, J.J. (1982). DNA Polymerase δ: One Polypeptide, Two Activities. Biochemistry *21*, 2513–2518.

Puig, P., Capodieci, P., Drobnjak, M., Verbel, D., Prives, C., Cordon-Cardo, C., and Di Como, C.J. (2003). p73 Expression in Human Normal and Tumor Tissues: Loss of p73α Expression Is Associated with Tumor Progression in Bladder Cancer. Clin. Cancer Res. *9*, 5642–5651.

Queralt, E., and Uhlmann, F. (2008). Cdk-counteracting phosphatases unlock mitotic exit. Curr. Opin. Cell Biol. *20*, 661–668.

Rayburn, E., Zhang, R., He, J., and Wang, H. (2005). MDM2 and Human Malignancies: Expression, Clinical Pathology, Prognostic Markers, and Implications for Chemotherapy. Curr. Cancer Drug Targets *5*, 27–41.

Rodriguez-Acebes, S., Mourón, S., and Méndez, J. (2018). Uncoupling fork speed and origin activity to identify the primary cause of replicative stress phenotypes. J. Biol. Chem. *293*, 12855–12861.

Roostalu, J., and Surrey, T. (2017). Microtubule nucleation: Beyond the template. Nat. Rev. Mol. Cell Biol. *18*, 702–710.

Sansregret, L., Vanhaesebroeck, B., and Swanton, C. (2018). Determinants and clinical implications of chromosomal instability in cancer. Nat. Rev. Clin. Oncol. *15*, 139–150.

Santaguida, S., Richardson, A., Iyer, D.R., M'Saad, O., Zasadil, L., Knouse, K.A., Wong, Y.L., Rhind, N., Desai, A., and Amon, A. (2017). Chromosome Mis-segregation Generates Cell-Cycle-Arrested Cells with Complex Karyotypes that Are Eliminated by the Immune System. Dev. Cell *41*, 638-651.e5.

Satyanarayana, A., and Kaldis, P. (2009). Mammalian cell-cycle regulation: Several cdks, numerous cyclins and diverse compensatory mechanisms. Oncogene *28*, 2925–2939.

Scheffner, M., Werness, B.A., Huibregtse, J.M., Levine, A.J., and Howley, P.M. (1990). The E6 oncoprotein encoded by human papillomavirus types 16 and 18 promotes the degradation of p53. Cell *63*, 1129–1136.

Schermuly, N. (2019). Regulation Of Spindle Orientation By A Mitotic Actin Pathway In Chromosomally Unstable Cancer Cells. PhD Thesis, Georg-August-Universität Göttingen. available at: https://ediss.uni-goettingen.de/handle/21.11130/00-1735-0000-0005-14F2-3.

Schmidt, A.K., Pudelko, K., Boekenkamp, J.E., Berger, K., Kschischo, M., and Bastians, H. (2021). The p53/p73 - p21CIP1 tumor suppressor axis guards against chromosomal instability by restraining CDK1 in human cancer cells. Oncogene *40*, 436–451.

Schmidt, M., Lu, Y., Liu, B., Fang, M., Mendelsohn, J., and Fan, Z. (2000). Differential modulation of paclitaxel-mediated apoptosis by p21(Waf1) and p27(Kip1). Oncogene *19*, 2423–2429.

Scholey, J.M., Civelekoglu-Scholey, G., and Brust-Mascher, I. (2016). Anaphase B. Biology (Basel). *5*, 1–30.

Seibert, M., Krüger, M., Watson, N.A., Sen, O., Daum, J.R., Slotman, J.A., Braun, T., Houtsmuller, A.B., Gorbsky, G.J., Jacob, R., *et al*. (2019). CDK1-mediated phosphorylation at H2B serine 6 is required for mitotic chromosome segregation. J. Cell Biol. *218*, 1164–1181.

Shaltiel, I.A., Krenning, L., Bruinsma, W., and Medema, R.H. (2015). The same, only different - DNA damage checkpoints and their reversal throughout the cell cycle. J. Cell Sci. *128*, 607–620.

Shen, K.C., Heng, H., Wang, Y., Lu, S., Liu, G., Deng, C.X., Brooks, S.C., and Wang, Y.A. (2005). ATM and p21 cooperate to suppress aneuploidy and subsequent tumor development. Cancer Res. *65*, 8747–8753.

Siddiqui, K., On, K.F., and Diffley, J.F.X. (2013). Regulating DNA replication in Eukarya. Cold Spring Harb. Perspect. Biol. *5*, 1–20.

Silkworth, W.T., and Cimini, D. (2012). Transient defects of mitotic spindle geometry and chromosome segregation errors. Cell Div. *7*, 1–8.

Solomon, D.A., Kim, J.S., Bondaruk, J., Shariat, S.F., Wang, Z.F., Elkahloun, A.G., Ozawa, T., Gerard, J., Zhuang, D., Zhang, S., *et al*. (2013). Frequent truncating mutations of STAG2 in bladder cancer. Nat. Genet. *45*, 1428–1430.

Srinivasan, S. V., Dominguez-Sola, D., Wang, L.C., Hyrien, O., and Gautier, J. (2013). Cdc45 Is a Critical Effector of Myc-Dependent DNA Replication Stress. Cell Rep. *3*, 1629–1639.

Steder, M., Alla, V., Meier, C., Spitschak, A., Pahnke, J., Fürst, K., Kowtharapu, B.S., Engelmann, D., Petigk, J., Egberts, F., *et al*. (2013). DNp73 Exerts Function in Metastasis Initiation by Disconnecting the Inhibitory Role of EPLIN on IGF1R-AKT/STAT3 Signaling. Cancer Cell *24*, 512–527.

Stepanova, T., Slemmer, J., Hoogenraad, C.C., Lansbergen, G., Dortland, B., De Zeeuw, C.I., Grosveld, F., Van Cappellen, G., Akhmanova, A., and Galjart, N. (2003). Visualization of microtubule growth in cultured neurons via the use of EB3-GFP (end-binding protein 3-green fluorescent protein). J. Neurosci. *23*, 2655–2664.

Stolz, A., Ertych, N., Kienitz, A., Vogel, C., Schneider, V., Fritz, B., Jacob, R., Dittmar, G., Weichert, W., Petersen, I., *et al*. (2010). The CHK2-BRCA1 tumour suppressor pathway ensures chromosomal stability in human somatic cells. Nat. Cell Biol. *12*, 492–499.

Strausfeld, U., Labbé, J.C., Fesquet, D., Cavadore, J.C., Picard, A., Sadhu, K., Russell, P., and Dorée, M. (1991). Dephosphorylation and activation of a p34cdc2/cyclin B complex in vitro by human CDC25 protein. Nature *351*, 242–245.

Sumara, I., Vorlaufer, E., Gieffers, C., Peters, B.H., and Peters, J.M. (2000). Characterization of vertebrate cohesin complexes and their regulation in prophase. J. Cell Biol. *151*, 749–761.

Sur, S., and Agrawal, D.K. (2016). Phosphatases and kinases regulating CDC25 activity in the cell cycle: clinical implications of CDC25 overexpression and potential treatment strategies. Mol. Cell. Biochem. *416*, 33–46.

Syljuåsen, R.G., Claus, †, Sørensen, S., Lasse, † ‡, Hansen, T., Fugger, K., Lundin, C., Johansson, F., Helleday, T., Sehested, M., *et al*. (2005). Inhibition of Human Chk1 Causes Increased Initiation of DNA Replication, Phosphorylation of ATR Targets, and DNA Breakage. Mol. Cell. Biol. *25*, 3553–3562.

Tan, C.H., Gasic, I., Huber-Reggi, S.P., Dudka, D., Barisic, M., Maiato, H., and Meraldi, P. (2015). The equatorial position of the metaphase plate ensures symmetric cell divisions. Elife *4*, 1–22.

Tanenbaum, M.E., and Medema, R.H. (2010). Mechanisms of Centrosome Separation and Bipolar Spindle Assembly. Dev. Cell *19*, 797–806.

Tang, Y.C., and Amon, A. (2013). Gene copy-number alterations: A cost-benefit analysis. Cell *152*, 394–405.

Tang, Y.C., Williams, B.R., Siegel, J.J., and Amon, A. (2011). Identification of aneuploidy-selective antiproliferation compounds. Cell *144*, 499–512.

Tassan, J.P., Jaquenoud, M., Fry, A.M., Frutiger, S., Hughes, G.J., and Nigg, E.A. (1995). In vitro assembly of a functional human CDK7-cyclin H complex requires MAT1, a novel 36 kDa RING finger protein. EMBO J. *14*, 5608–5617.

Tatsumi, Y., Sugimoto, N., Yugawa, T., Narisawa-Saito, M., Kiyono, T., and Fujita, M. (2006). Deregulation of Cdt1 induces chromosomal damage without rereplication and leads to chromosomal instability. J. Cell Sci. *119*, 3128–3140.

Thawani, A., Kadzik, R.S., and Petry, S. (2018). XMAP215 is a microtubule nucleation factor that functions synergistically with the γ-tubulin ring complex. Nat. Cell Biol. *20*, 575–585.

Thompson, S.L., and Compton, D.A. (2010). Proliferation of aneuploid human cells is limited by a p53-dependent mechanism. J. Cell Biol. *188*, 369–381.

Thompson, S.L., Bakhoum, S.F., and Compton, D.A. (2010). Mechanisms of Chromosomal Instability. Curr. Biol. *20*, R285–R295.

Toledo, L.I., Murga, M., Zur, R., Soria, R., Rodriguez, A., Martinez, S., Oyarzabal, J., Pastor, J., Bischoff, J.R., and Fernandez-Capetillo, O. (2011). A cell-based screen identifies ATR inhibitors with synthetic lethal properties for cancer-associated mutations. Nat. Struct. Mol. Biol. *18*, 721–727.

Tsuji, T., Ficarro, S.B., and Jiang, W. (2006). Essential role of phosphorylation of MCM2 by Cdc7/Dbf4 in the initiation of DNA replication in mammalian cells. Mol. Biol. Cell *17*, 4459–4472.

Vassilev, L.T., Tovar, C., Chen, S., Knezevic, D., Zhao, X., Sun, H., Heimbrook, D.C., and Chen, L. (2006). Selective small-molecule inhibitor reveals critical mitotic functions of human CDK1. Proc. Natl. Acad. Sci. U. S. A. *103*, 10660–10665.

Vermeulen, K., Van Bockstaele, D.R., and Berneman, Z.N. (2003). The cell cycle: A review of regulation, deregulation and therapeutic targets in cancer. Cell Prolif. *36*, 131–149.

Voter, W.A., and Erickson, H.P. (1984). The kinetics of microtubule assembly. Evidence for a two-stage nucleation mechanism. J. Biol. Chem. *259*, 10430–10438.

Waizenegger, I.C., Hauf, S., Meinke, A., and Peters, J.M. (2000). Two distinct pathways remove mammalian cohesin from chromosome arms in prophase and from centromeres in anaphase. Cell *103*, 399–410.

Wang, H., Zhao, A., Chen, L., Zhong, X., Liao, J., Gao, M., Cai, M., Lee, D.H., Li, J., Chowdhury, D., *et al*. (2009). Human RIF1 encodes an anti-apoptotic factor required for DNA repair. Carcinogenesis *30*, 1314–1319.

Wengner, A.M., Siemeister, G., Koppitz, M., Schulze, V., Kosemund, D., Klar, U., Stoeckigt, D., Neuhaus, R., Lienau, P., Bader, B., *et al*. (2016). Novel Mps1 kinase inhibitors with potent antitumor activity. Mol. Cancer Ther. *15*, 583–592.

Wilhelm, T., Olziersky, A.M., Harry, D., De Sousa, F., Vassal, H., Eskat, A., and Meraldi, P. (2019). Mild replication stress causes chromosome mis-segregation via premature centriole disengagement. Nat. Commun. *10*, 1–14.

Williams, B.R., Prabhu, V.R., Hunter, K.E., Glazier, C.M., Whittaker, C.A., Housman, D.E., and Amon, A. (2008). Aneuploidy affects proliferation and spontaneous immortalization in mammalian cells. Science (80-.). *322*, 703–709.

Woodward, A.M., Göhler, T., Luciani, M.G., Oehlmann, M., Ge, X., Gartner, A., Jackson, D.A., and Blow, J.J. (2006). Excess Mcm2-7 license dormant origins of replication that can be used under conditions of replicative stress. J. Cell Biol. *173*, 673–683.

Yang, A., Kaghad, M., Wang, Y., Gillett, E., Fleming, M.D., Dötsch, V., Andrews, N.C., Caput, D., and McKeon, F. (1998). p63, a p53 homolog at 3q27-29, encodes multiple products with transactivating, death-inducing, and dominant-negative activities. Mol. Cell *2*, 305–316.

Yang, A., Schweitzer, R., Sun, D., Kaghad, M., Walker, N., Bronson, R.T., Tabin, C., Sharpe, A., Caput, D., Crum, C., *et al*. (1999). p63 is essential for regenerative proliferation in limb, craniofacial and epithelial development. Nature *398*, 714–718.

Yang, A., Walker, N., Bronson, R., Kaghad, M., Oosterwegel, M., Bonnin, J., Vagner, C., Bonnet, H., Dikkes, P., Sharpe, A., *et al*. (2000). p73-Deficient mice have neurological, pheromonal and inflammatory defects but lack spontaneous tumours. Nature *404*, 99–103.

Yu, Y., Zhang, M., Wang, N., Li, Q., Yang, J., Yan, S., He, X., Ji, G., and Miao, L. (2018). Epigenetic silencing of tumor suppressor gene CDKN1A by oncogenic long non-coding RNA SNHG1 in cholangiocarcinoma. Cell Death Dis. *9*, 1–13.

Zeman, M.K., and Cimprich, K.A. (2014). Causes and consequences of replication stress. Nat. Cell Biol. *16*, 2–9.

Zhang, J. (2013). The role of BRCA1 in homologous recombination repair in response to replication stress: Significance in tumorigenesis and cancer therapy. Cell Biosci. *3*, 1–14.

Zhang, C.Z., Spektor, A., Cornils, H., Francis, J.M., Jackson, E.K., Liu, S., Meyerson, M., and Pellman, D. (2015). Chromothripsis from DNA damage in micronuclei. Nature *522*, 179–184.

Zhong, Y., Nellimootti, T., Peace, J.M., Knott, S.R.V., Villwock, S.K., Yee, J.M., Jancuska, J.M., Rege, S., Tecklenburg, M., Sclafani, R.A., *et al*. (2013). The level of origin firing inversely affects the rate of replication fork progression. J. Cell Biol. *201*, 373–383.

Zhu, J., Jiang, J., Zhou, W., and Chen, X. (1998). The Potential Tumor Suppressor p73 Differentially Regulates Cellular p53 Target Genes. Cancer Res. *58*, 5061–5065.

ACKNOWLEDGEMENTS - DANKSAGUNG

In the following, I want to thank everyone who contributed to this thesis and supported me during the last four years.

At first, I want to express my sincere gratitude to my supervisor Prof. Dr. Holger Bastians for the opportunity to work on this interesting research project. Thank you for the patient guidance, support, and helpful advice during the last years.

I also want to thank Dr. Ruth Geiss-Friedlander and Prof. Dr. Heidi Hahn, who supported me with valuable advice as members of my thesis committee.

Additionally, I thank Prof. Dr. Heike Krebber for the opportunity to use laboratories and equipment.

I am very grateful to all the former and current members of the Bastians lab for the great working atmosphere, vivid discussions, good ideas, motivating words, and many cheerful moments during and after work. Especially, I want to thank Karo, Elina, and Nadine, not only for the constant support at work but also for the wonderful time we have spent together outside the lab. In addition, I thank Karo for proofreading parts of this thesis.

Außerdem möchte ich mich von Herzen bei meinem Freund Christian bedanken, für das Korrekturlesen dieser Arbeit aber vor allem für die fortwährende Unterstützung. Danke, dass du mich stets ermutigt, mich immer wieder aufgemuntert und zum Lachen gebracht hast.

Der größte Dank gebührt meiner Familie, allen voran meinen Eltern. Danke, dass ihr mich immer unterstützt und an mich glaubt.